

American University in Cairo

## AUC Knowledge Fountain

---

Theses and Dissertations

Student Research

---

6-1-2015

### Design of tailor-made polymers with intrinsic micro-porosity for the “environmentally friendly” separation and storage of natural and industrial gas mixtures

Worood Adel El-mehalmey

Follow this and additional works at: <https://fount.aucegypt.edu/etds>

---

#### Recommended Citation

##### APA Citation

El-mehalmey, W. (2015). *Design of tailor-made polymers with intrinsic micro-porosity for the “environmentally friendly” separation and storage of natural and industrial gas mixtures* [Master's Thesis, the American University in Cairo]. AUC Knowledge Fountain.

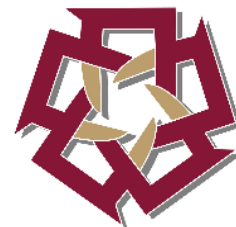
<https://fount.aucegypt.edu/etds/87>

##### MLA Citation

El-mehalmey, Worood Adel. *Design of tailor-made polymers with intrinsic micro-porosity for the “environmentally friendly” separation and storage of natural and industrial gas mixtures*. 2015. American University in Cairo, Master's Thesis. *AUC Knowledge Fountain*.

<https://fount.aucegypt.edu/etds/87>

This Master's Thesis is brought to you for free and open access by the Student Research at AUC Knowledge Fountain. It has been accepted for inclusion in Theses and Dissertations by an authorized administrator of AUC Knowledge Fountain. For more information, please contact [thesisadmin@aucegypt.edu](mailto:thesisadmin@aucegypt.edu).



AMERICAN UNIVERSITY IN CAIRO  
SCHOOL OF SCIENCE AND ENGINEERING

Design of tailor-made polymers with intrinsic micro-  
porosity for the “environmentally friendly” separation and  
storage of natural and industrial gas mixtures

---

A Thesis Submitted to

Masters of Science in Nanotechnology Program

In partial fulfilment of the requirements for

The degree of Master of Science

By:

**Worood Adel El-Mehalmey**

Under the supervision of:

**Prof. Tarek Madkour** (*Advisor*)

Department of Chemistry, The American University in Cairo

**Dr. Rasha Azzam** (*Co-advisor*)

Department of chemistry, Helwan University

5/24/2015

## *Acknowledgements:*

---

I can not find words to express my immense gratitude to my research advisor and mentor, Dr. Tarek Madkour. This thesis would not have been possible without his continuous guidance and unconditional help and support. Since day one, I was deeply indebted to his exceptional planning and research skills that were incredibly helpful throughout the research project. His dedication, enthusiasm and passion about research made me very much like research and appreciate its value. As a teacher, he is always incomparably generous with his knowledge, time and effort. During the hardest times of this research, his encouragement, understanding, patience and motivation gave me confidence. I consider it an honor to have been able to work with him as he transformed this educational experience into a time for personal growth as well. He always believed in me and my work which made me believe in myself as well.

I would also like to express my sincere thanks and appreciation to Dr. Rasha Azzam my co-advisor for her great help and guidance in the organic synthesis field. She held my hand through my first steps into research and lab work. She and Dr. Tarek always treated me as a daughter, I felt so comfortable working under their supervision and I consider them my second family. I love you and I thank you for all your efforts.

I can not find words to express my thanks to all the professors who enriched me with their great knowledge during the master's courses especially Dr. Adham Ramadan who has played a significant role in upgrading my skills in all research aspects. I also grateful to Dr. Hanadi Salem not only for opening my eyes to different scientific perspectives but also for the great advices she gave to me. She has always been there for me.

I also would like to thank my Zewail city family, Poussy Ali, Ramy Alkady, Mohamed El-Metwally and Sara Ahmed, for their great support. I cannot forget to thank Dr. Mohamed Alkordi for his great guidance with the ASAP 2020, without his facilities and expertise it would have been impossible to finish this work and for suggesting the use of these polymers as CO<sub>2</sub> capturing systems. He really changed by mind set without even noticing. He made me realize that a good researcher has to pay attention to every small detail as well as to look at the overall picture.

I was very lucky having so many good people surrounding me during my masters. My words can not express how much I am thankful and grateful having my great four musketeers Ruaa, Yomna, Alshaimaa and Nada, without you I would have given up so long time ago. I really love you and you are my sisters. You always wished me luck and you supported me even when you were facing some obstacles in your own research. The moment you knew that I reached this step, I saw the happiness in your eyes and no other words can express it. This journey has proven to me that the greatness is not only in the goal you want to achieve but also in the people you meet during the journey.

I would like also to thank my dearest friends Salma, Israa, Sara, Ghada and Samar for providing me with all what I need to finish my work and you were always keen on making the environment so comfortable. You believed in me and my work and I really wish you all great success and happiness, you do deserve it and more. I can not also forget to thank Ahmed Hamdy for his continuous support.

I can not forget Ramadan, Amr, Abdelaziz and Ahmed without their great help in providing me with small needed glass ware and other things, I would not have achieved the bigger goal. I consider them the unknown soldiers.

At last but not least I would like to thank my dear family for their unconditional love, prayers, support and guidance, I would not have reached this without you all in my life. They always accept my mood swings and depression moments. Thank you my dear father, mother, sister Ghosoun, brother Abdelrahaman, brother in law Mostafa and the beautiful new family member Malika.

## *List of Abbreviations:*

---

BET: Brunauer, Emmett and Teller

CHCl<sub>3</sub>: Chloroform

CO<sub>2</sub>: Carbon dioxide

DMAC: N,N-dimethylacetamide

DMF: Dimethyl formamide

DMSO: Dimethyl Sulfoxide

DMTA: Dynamic Mechanical Thermal Analysis

D<sub>0</sub>: Diffusion Coefficient

DSC: Differential Thermal Calorimetry

FFV: Fractional Free Volume

FTIR: Fourier Transform Infrared

GCC: Global Climate Change

GHG: Greenhouse gases

GPC: Gel Permeation Chromatography

H<sub>2</sub>: Hydrogen

IPPC: Intergovernmental Panel Climate Change

IUPAC: International Union of Pure and Applied Chemistry

M<sub>n</sub>: Number average molecular weight

MOFs: Metal Organic Frameworks

M<sub>w</sub>: Weight average molecular weight

NH<sub>4</sub>OH: Ammonium Hydroxide

NMP: N-methyl-2-pyrrolidone

NMR: Nuclear Magnetic Resonance

p/p<sup>0</sup>: Relative pressure

PAA: Polyamic acid

PIMs: Polymers of intrinsic micro-porosity

PIs: Polyimides

PTMSP: Poly[1-(trimethylsilyl)-1-propyne]

PXRD: Powder X-ray Diffraction

RDF: Radial Distribution Function

S/V<sub>T</sub>: Surface Area to Volume Ratio

TGA: Thermogravimetric Analysis

THF: Tetrahydrofuran

TMS: Tetramethylsilane

## *Abstract:*

---

More than 80% of the worldwide commercial energy supply is based on fossil fuels. The heavy use of fossil fuels has resulted in large amounts of greenhouse gas emissions especially carbon dioxide (CO<sub>2</sub>) and depletion of the fossil fuel resources. Searching for alternative sources for energy such as hydrogen (H<sub>2</sub>) gas is a crucial step but requires excellent storage systems. Similarly, CO<sub>2</sub> high level of production requires good capture and storage systems as well.

Nanoporous polymers have found great application in the area of natural gas separation. Depending on the size and volume of the pores, the efficiency of the nanoporous polymers may vary. In as much, it is envisaged that these highly interesting polymers could also be used for capturing and storing CO<sub>2</sub> and H<sub>2</sub> gases for various applications. The high porosity in the micro and nano size scale rendered these polymers to possess massive surface area making these polymers remarkably suitable for capturing and storing various gases. In this study, a range of nanoporous polyimide polymers were synthesized using a two-step poly-condensation reactions of bis (carboxylic anhydride) with various aromatic diamines designed to investigate the effect of the polymeric microstructures on the conformational characteristics and consequently on the pore sizes and pore size distribution for gas storage application. The polymerization reactions resulted in various polymers of intrinsic micro-porosity (PIMs), which are known to comprise rigid backbone due to their lack of rotational freedom along the polymeric backbone and thus diminishing the ability of these chains to pack space efficiently and thus leading to the formation of intrinsic micro-pores. The polymers exhibited high surface area as determined by nitrogen adsorption and high thermal stability as determined by TGA. The high surface area was further validated using molecular simulation techniques. Structural modifications of the diamines have resulted into a variety of nanoporous polymeric structures. The chemical structures were confirmed using FTIR, NMR and GPC techniques. BET isotherms of the resultant polymers were carried out to evaluate their physical characteristics. The simulation results showed that the fractional free volume and the Connolly surface of the PIMs had greater values resulting from the nanoporosity of the rigid chains in agreement with the experimental findings and giving rise to a fundamental understanding of the influence of the polymeric structures on the ultimate intrinsic microporosity.

## Table of Contents:

<i>Acknowledgments</i> .....	i
<i>List of Abbreviations</i> .....	iii
<i>Abstract</i> .....	v
<i>Table of Contents</i> .....	vi
<i>List of Figures</i> .....	x
<i>List of Tables</i> .....	xiii
<b>Chapter 1: <u>Introduction</u></b> .....	1
<b>1. Introduction:</b> .....	2
<b>1.1. Motivation:</b> .....	2
<b>1.2. Conventional Method for Gas Storage and Separation:</b> .....	4
<b>1.2.1. Cryogenic Distillation:</b> .....	4
<b>1.2.2. Membranes:</b> .....	5
<b>A. Porous Materials for Gas Separation:</b> .....	5
<b>A.1. Crystalline Porous Materials:</b> .....	6
<b>A.1.1. Zeolites:</b> .....	6
<b>A.1.2. Metal-Organic Frameworks (MOFs):</b> .....	6
<b>A.2. Amorphous Porous Materials:</b> .....	7
<b>A.2.1. Activate Carbons:</b> .....	7
<b>A.2.2. Polymers of Intrinsic Micro-porosity (PIMs):</b> .....	7
<b>B. Polyimides:</b> .....	8
<b>B.1. Polyimides Structure:</b> .....	8
<b>B.2. Polyimides Properties:</b> .....	9
<b>B.3. Polyimides Synthesis:</b> .....	9
<b>C. Gas Separation Mechanisms through Porous Polymeric Membranes:</b> .....	11



1.3. Thesis Scope and Objectives: .....	12
Chapter 2: <u>Literature Review</u> .....	14
2. Literature Review:.....	15
2.1. Extrinsic Micro-Porous Structures: .....	15
2.2. Intrinsic Micro-Porous Structures: .....	16
2.2.1. Structure-Property Relationships of Polymers of Intrinsic Micro-Porosity.....	18
A. Solubility: .....	26
B. Thermal Stability: .....	27
C. Mechanical Properties: .....	28
D. Surface Area: .....	28
2.2.2. Gas Separation Application of Polymers of Intrinsic Micro-Porosity:.....	29
2.2.3. Molecular Simulation of Polymers of Intrinsic Micro-Porosity:.....	31
Chapter 3: <u>Materials, Synthesis and Characterization</u> .....	34
3. Materials, Synthesis and Characterization:.....	35
3.1. Materials: .....	35
3.1.1. Purchased Materials and Subsequent Purification: .....	35
3.1.2. Synthesized Materials for Nanoporous Polymerization:.....	36
A. Synthesis of 4, 5-Dichlorophthalic anhydride: .....	36
B. Synthesis of 4, 5-Dichlorophthalimide: .....	36
C. Synthesis of 4, 5-Dichlorophthalamide: .....	37
D. Synthesis of 4, 5-Dichlorophthalonitrile: .....	37
E. Synthesis of 3,3,3',3'- tetra-methyl- 2,2',3,3'- tetrahydro-1,1' spirobi [cyclopenta[b] dibenzo[b,e] [1,4] dioxine]-7,7',8,8'-tetracarbonitrile: (Bisphthalonitrile) .....	38
F. Synthesis of 3,3,3',3'- tetramethyl- 2,2',3,3'- tetrahydro- 1,1'-spirobi [cyclopenta[b] dibenzo[b,e] [1,4] dioxine]-7,7',8,8'-tetracarboxylic acid: .....	38

<b>G.</b>	<b>Synthesis of Dianhydride Monomer:</b> .....	39
<b>3.2.</b>	<b>Synthesis of Polymers of Intrinsic Microporosity based on Polyimides Structures (PIMs-PIs):</b> .....	40
<b>3.2.1.</b>	<b>PIM-PI-01</b> .....	40
<b>3.2.2.</b>	<b>PIM-PI-02</b> .....	41
<b>3.2.3.</b>	<b>PIM-PI-03</b> .....	42
<b>3.2.4.</b>	<b>PIM-PI-04</b> .....	42
<b>3.2.5.</b>	<b>PIM-PI-05</b> .....	43
<b>3.2.6.</b>	<b>PIM-PI-06</b> .....	44
<b>3.3.</b>	<b>Characterization Techniques:</b> .....	45
<b>3.3.1.</b>	<b>Fourier Transform Infrared Spectroscopy (FTIR):</b> .....	45
<b>3.3.2.</b>	<b>Nuclear Magnetic Resonance Spectroscopy (NMR):</b> .....	45
<b>3.3.3.</b>	<b>Elemental Analysis (CHNS/O):</b> .....	46
<b>3.3.4.</b>	<b>Powder X-Ray Diffraction (PXRD):</b> .....	46
<b>3.3.5.</b>	<b>Gel Permeation Chromatography (GPC):</b> .....	47
<b>3.3.6.</b>	<b>Thermal Gravimetric Analysis (TGA):</b> .....	47
<b>3.3.7.</b>	<b>Nitrogen Adsorption Analysis (BET):</b> .....	48
<b>3.3.8.</b>	<b>Carbon Dioxide Adsorption Analysis:</b> .....	49
Chapter 4:	<b><u>Results and Discussion</u></b> .....	50
<b>4.</b>	<b>Results and Discussion</b> .....	51
<b>4.1.</b>	<b>Structural Analysis of the Synthesized PIMs-PIs:</b> .....	51
<b>4.1.1.</b>	<b>Fourier Transform Infrared Spectroscopy (FTIR):</b> .....	53
<b>4.1.2.</b>	<b>Nuclear Magnetic Resonance Spectroscopy (NMR):</b> .....	55
<b>4.1.3.</b>	<b>Elemental Analysis (CHNS):</b> .....	55
<b>4.1.4.</b>	<b>Gel Permeation Chromatography (GPC):</b> .....	56

4.1.5.	<b>Powder X-ray Diffraction (PXRD):</b> .....	57
4.2.	<b>Performance Analysis of the Synthesized PIMs-PIs:</b> .....	58
4.2.1.	<b>Thermogravimetric Analysis (TGA):</b> .....	59
4.2.2.	<b>Nitrogen Adsorption Analysis:</b> .....	60
4.2.3.	<b>Carbon Dioxide Analysis:</b> .....	68
<b>Chapter 5: <u>Molecular Simulation of Polymers of Intrinsic Microporosity based on Polyimides Structures (PIMs-PIs)</u></b> .....		72
5.	<b>Molecular Simulation of Polymers of Intrinsic MicroPorosity Based on Polyimides Structures (PIMs-PIs):</b> .....	73
5.1.	<b>Modeling and Simulation Protocol:</b> .....	73
5.1.1.	<b>Molecular Dynamics Simulation Protocols:</b> .....	73
5.1.2.	<b>Evaluation of the Fractional Free Volume (FFV) and Connolly Surface Area to Volume Ratio (<math>S/V_T</math>):</b> .....	74
5.1.3.	<b>Determination of the mean-square displacement and the self-diffusion coefficients:</b> .....	75
5.2.	<b>Assessment of the Nano-Porosity of the Simulated PIM-PIs:</b> .....	75
5.2.1.	<b>Evaluation of the Fractional Free Volume (FFV) and the Connolly Surface Area to volume Ratio (<math>S/V_T</math>):</b> .....	76
5.2.2.	<b>Evaluation of the Diffusion Coefficients:</b> .....	77
<b>Chapter 6: <u>Conclusion and Future Perspectives</u></b> .....		84
6.	<b>Conclusion and Future Perspectives:</b> .....	85
6.1.	<b>Conclusion:</b> .....	85
6.2.	<b>Future Perspectives:</b> .....	86
References:	.....	87

## *List of Figures:*

---

<b>Figure 1.1</b> The tremendous increase in carbon dioxide emissions during the last 50 years	3
<b>Figure 1.2</b> Depletion of fossil fuels within the coming few decades.	4
<b>Figure 1.3</b> Heterocyclic imide repeat unit.	8
<b>Figure 1.4</b> The classical method for polyimide synthesis.	10
<b>Figure 1.5</b> Modes of possible separation in porous membranes.	11
<b>Figure 2.1</b> The synthesis for Phthalocyanine Framework.	16
<b>Figure 2.2</b> Polymers of intrinsic micro-porosity based on dibenzodioxin formation.	19
<b>Figure 2.3</b> Polymers of intrinsic micro-porosity based on imide formation.	23
<b>Figure 2.4</b> Structure of the repeat unit of a) PIM-PI-OH-2 and b) PIM-PI-OH-3.	27
<b>Figure 2.5</b> Thermogravimetric analysis of a) PIM-PI-OH-2 (----), Copol-OH(1-2) (—— ) b) PIM-PI-OH-3.	28
<b>Figure 2.6</b> Robeson's plots of (a) CO <sub>2</sub> /N <sub>2</sub> , (b) CO <sub>2</sub> /CH <sub>4</sub> and (c) O <sub>2</sub> /N <sub>2</sub> selectivity versus the permeability of the fastest gas.	30
<b>Figure 2.7</b> The PIM's structure that have been used in Madkour's study.	31
<b>Figure 2.8</b> Simulation cell for PIM polymer with propane.	32
<b>Figure 3.1</b> Fourier Transform Infrared Spectroscopy, Center of Materials Science, Zewail City.	45
<b>Figure 3.2</b> (a) The Elemental Analyzer Flash 2000 (b) Sensitive Balance, at Center of Materials Science, Zewail City.	46
<b>Figure 3.3</b> Powder X-Ray Diffractometer, at the Chemistry Department, AUC.	47

<b>Figure 3.4</b> TA Instruments, TGA Q50, Center of Materials Science, Zewail City.	48
<b>Figure 3.5</b> Micromeritics ASAP 2020 Surface Area and Porosimetry Analyzer, Center of Materials Science, Zewail City.	48
<b>Figure 4.1</b> The Synthesis of the Dianhydride Monomer.	53
<b>Figure 4.2</b> The FTIR spectra of tetracarboxylic acid (—) and dianhydride monomer (—).	53
<b>Figure 4.3</b> The FTIR spectra of the PIMs-PIs (blues) and the dianhydride monomer (—).	54
<b>Figure 4.4</b> Powder X-ray Diffraction analysis for PIM-PIs.	58
<b>Figure 4.5</b> Thermaogravimetric Analysis for PIM-PIs.	59
<b>Figure 4.6</b> The N <sub>2</sub> isotherm for PIM-PI-01.	61
<b>Figure 4.7</b> The N <sub>2</sub> isotherm for PIM-PI-02.	62
<b>Figure 4.8</b> The N <sub>2</sub> isotherm for PIM-PI-03.	63
<b>Figure 4.9</b> The N <sub>2</sub> isotherm for PIM-PI-04.	64
<b>Figure 4.10</b> The N <sub>2</sub> isotherm for PIM-PI-05.	64
<b>Figure 4.11</b> The N <sub>2</sub> isotherm for PIM-PI-06.	65
<b>Figure 4.12</b> CO <sub>2</sub> Adsorption for PIM-PI-01.	68
<b>Figure 4.13</b> CO <sub>2</sub> Adsorption for PIM-PI-02.	68
<b>Figure 4.14</b> CO <sub>2</sub> Adsorption for PIM-PI-03.	69
<b>Figure 4.15</b> CO <sub>2</sub> Adsorption for PIM-PI-04.	69
<b>Figure 4.16</b> CO <sub>2</sub> Adsorption for PIM-PI-05.	69

<b>Figure 4.17</b> CO <sub>2</sub> Adsorption for PIM-PI-06.	70
<b>Figure 4.18</b> Heat of Adsorption for PIM-PI-01, PIM-PI-02, PIM-PI-03 and PIM-PI-05.	71
<b>Figure 4.19</b> Heat of Adsorption for PIM-PI-04 and PIM-PI-6.	71
<b>Figure 5.1</b> The Simulation Cells Containing both PIM-PI-04 and CO <sub>2</sub> gas.	74
<b>Figure 5.2.</b> The extent of Connolly Surface area in (a) porous PIM-PI-04, (b) non-porous Polyamide.	76
<b>Figure 5.3</b> Mean Square Displacement of PIM-PI-04 with CO <sub>2</sub> .	78
<b>Figure 5.4.</b> Mean Square Displacement of PIM-PI-05 with CO <sub>2</sub> .	78
<b>Figure 5.5.</b> Mean Square Displacement of PIM-PI-04 with H <sub>2</sub> .	79
<b>Figure 5.6.</b> Mean Square Displacement of PIM-PI-05with H <sub>2</sub> .	79
<b>Figure 5.7</b> Mean Square Displacement of PIM-PI-06 with CO <sub>2</sub> .	81
<b>Figure 5.8</b> Mean Square Displacement of PIM-PI-06 with H <sub>2</sub> .	81
<b>Figure 5.9</b> The molecular simulation model for (a) PIM-PI-04 and (b) PIM-PI-05.	82
<b>Figure 5.10</b> Radial Distribution Function of PIM-PI-04, 05, and 06.	82

## *List of Tables:*

---

<b>Table 2.1</b> PIMs based on dibenzodioxin formation using 5, 5', 6, 6'-tetrahydroxy-3, 3, 3', 3'-tetramethylspirobisindane monomer.	17
<b>Table 2.2</b> PIMs based on dibenzodioxin formation using 1, 1'-binaphthalene -2, 2', 3'3'-tetrol monomer.	19
<b>Table 2.3</b> PIMs based on dibenzodioxin formation using 9, 10-dimethyl-2, 3, 9, 10-ethanoanthracene-2, 3, 6, 7-tetrol monomer.	20
<b>Table 2.4</b> PIMs based on dibenzodioxin formation using 4, 4'-(9H-fluorene-9, 9-diyl) bis (benzene-1, 2-diol) monomer.	21
<b>Table 2.5</b> PIMs based on dibenzodioxin formation using tetrafluoro-terephthalonitrile monomer.	22
<b>Table 2.6</b> PIMs based on imide formation using 9,9,9',9'-tetramethyl-8,8',9,9'-tetrahydro-7,7'-spirobi[cyclopenta[b]furo[3,4- <i>i</i> ]dibenzo[ <i>b,e</i> ][1,4]dioxine-1,1',3,3'(4 <i>aH</i> ,5 <i>a'H</i> ,10 <i>a'H</i> ,11 <i>aH</i> )-tetraone monomer .	24
<b>Table 2.7</b> PIMs based on imide formation using benzo[1,2 <i>c</i> :4,5- <i>c'</i> ]difuran-1,3,5,7-tetraone monomer.	25
<b>Table 2.8</b> PIMs based on imide formation using 5, 5'-(perfluoropropane-2, 2-diyl) bis (isobenzofuran-1, 3-dione) monomer.	26
<b>Table 2.9</b> The decomposition points for different PIM-PIs.	27
<b>Table 4.1</b> The Synthesis of PIM-PIs.	52
<b>Table 4.2</b> Comparing the percentages of C, H, N and O calculated (Expected) to those obtained (Found) using Elemental Analyzer (Flash 2000, CHNS/O).	56
<b>Table 4.3</b> Gel Permeation Chromatography (GPC) Analysis in tetra-hydro-furan (THF).	57

<b>Table 5.1.</b> Self-Diffusion Coefficients ( $D_0$ ) of PIM-PI-04, 05 and 06 and Diffusion Coefficients of $\text{CO}_2$ ( $D_{\text{CO}_2}$ ) and $\text{H}_2$ ( $D_{\text{H}_2}$ ) gases.	61
<b>Table 5.2.</b> Total Volume, Free Volume, Connolly Surface, Surface Area to Free Volume Ratio and Surface Area to Total Volume Ratio of PIM-PI-04, 05 and 06.	66
<b>Table 6.1</b> The BET Surface Areas and Pore Volume of PIM-PIs.	77
<b>Table 6.2</b> The Pore Size Distribution (PSD) For The Synthesized PIM-PIs.	80



# Chapter 1:

## Introduction

## ***1. Introduction:***

---

### ***1.1. Motivation:***

---

More than 80% of the worldwide commercial energy supply is based on fossil fuels. Coal accounts for 25.3% of the energy; 35% for oil and 20.7% for natural gas. These energy sources are used to produce heat, mechanical energy and electrical power. The heavy use of fossil fuels (coal, petroleum and natural gas) as all energy source has led to two major drawbacks. The first is related to the environment mainly due to the high emissions of greenhouse gases (GHG), especially carbon dioxide (CO<sub>2</sub>). These emissions have been identified as the major contributor to global warming and climate change. Studies indicate that climate change is irreversible and may last for up to 1000 years even after the emissions have stopped. Measures must be taken to reduce CO<sub>2</sub> emissions and consequently restrain global warming [1–4]. The second is related to the scarcity of fossil fuel resources. Eliminating the dependency on fossil fuels as a sole source of energy and searching for alternative sources such as hydrogen (H<sub>2</sub>) is considered nowadays a crucial step. Consequently, H<sub>2</sub> gas production as a renewable source of energy can be considered a two-sided weapon against the drawbacks of fossil fuels [5,6].

Conventionally, gases are separated using cryogenic distillation. It is an energy intensive process as well as a damaging one to the environment since it involves the consumption of large amount of fossil fuel to generate the required energy for the liquefaction and distillation processes [1,2,7]. Additionally, purity of products separated by cryogenic separation might be relatively low, which also highlight the urgent need for gas separation and storage using cost-effective techniques that consumes relatively less energy [1].

CO<sub>2</sub> concentrations in the earth's atmosphere have been increased tremendously over the last 50 years as shown in *Figure 1.1*. Although the role of CO<sub>2</sub> in animal respiration and photosynthesis has been known since the 18<sup>th</sup> century, its role in other areas was of little interest until 1900. The processes by which CO<sub>2</sub> is absorbed or released by the global carbon system determine the amount that will remain in the atmosphere. Recent scientific analysis suggests that the observable changes in atmospheric CO<sub>2</sub> concentrations that are being recorded could have major effects on the earth's climate, the growth and development of all green plants, as well as many other less easily defined natural processes and human endeavors. Carbon dioxide is nearly

transparent to solar radiation, but it absorbs some of the outgoing long-wave radiation from the earth, creating a so-called "greenhouse effect." Different calculations of "green-house" warming indicate that doubling the CO<sub>2</sub> content of the air could result in a globally averaged temperature increase of the lower atmosphere of several degrees centigrade [7–9].

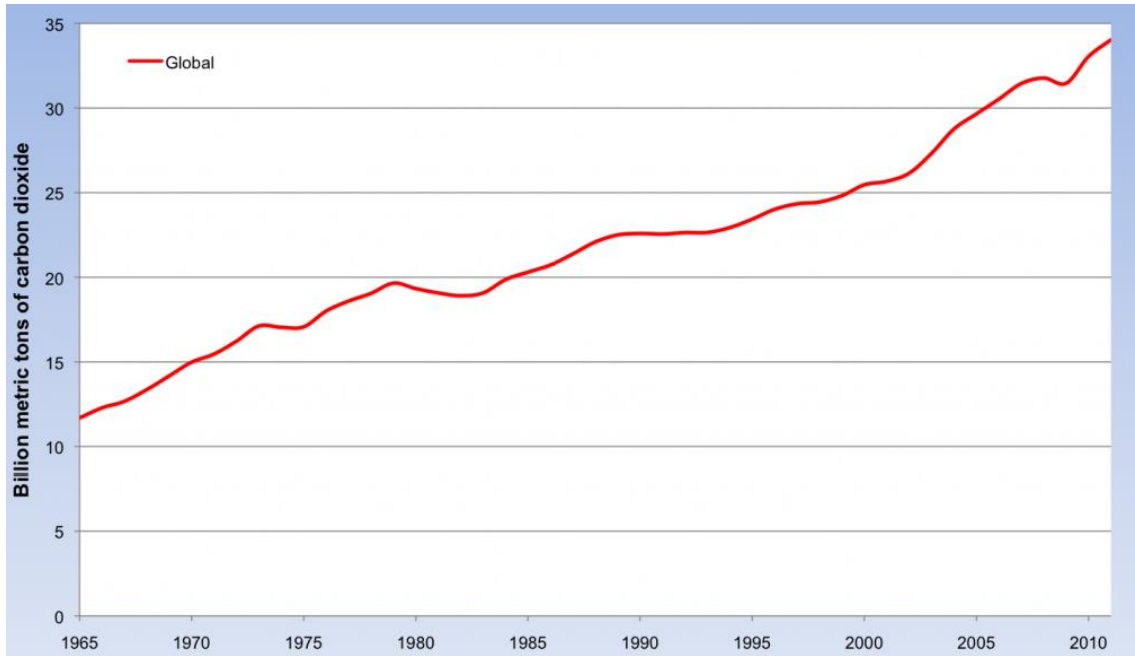


*Figure 1.1* The tremendous increase in carbon dioxide emissions during the last 50 years [10].

In 2007 the Intergovernmental panel climate change (IPPC) claimed that immediate actions are required to alleviate the global climate change (GCC). Human Environments will be threaten in various ways as consequences for the damaging of the ecosystems. GCC is believed to be due to the increasing levels of greenhouse gases, predominantly in the industrialized countries due to population growth and the western lifestyle [2,8].

In recent years, concerns about the observable depletion of energy and materials, as well as limits to the ecosystem's adaptation capability (e.g. climatic change) have been raised. All fossil fuels are finite and non-renewable on a human scale as shown in *Figure 1.2*. Consequently, renewable energy is the appropriate substitute for the fossil fuels decline. H<sub>2</sub> is recently considered as a potential solution for the 21<sup>st</sup> century, as it is capable of assisting in problems of environmental emissions, sustainability and energy security. H<sub>2</sub> is capable of being a substituent for fossil fuels in various applications such as furnaces and engines. As it can efficiently store and deliver energy. Moreover, fuel cells can be used to convert H<sub>2</sub> directly into electricity, which

can be used directly to operate automobiles. It produces water when being combusted with oxygen, therefore  $H_2$  is considered as an attractive environmentally friendly fuel. Additionally, the steam produced from the combustion has further applications in numerous industrial processes and space heating [6,11–14].

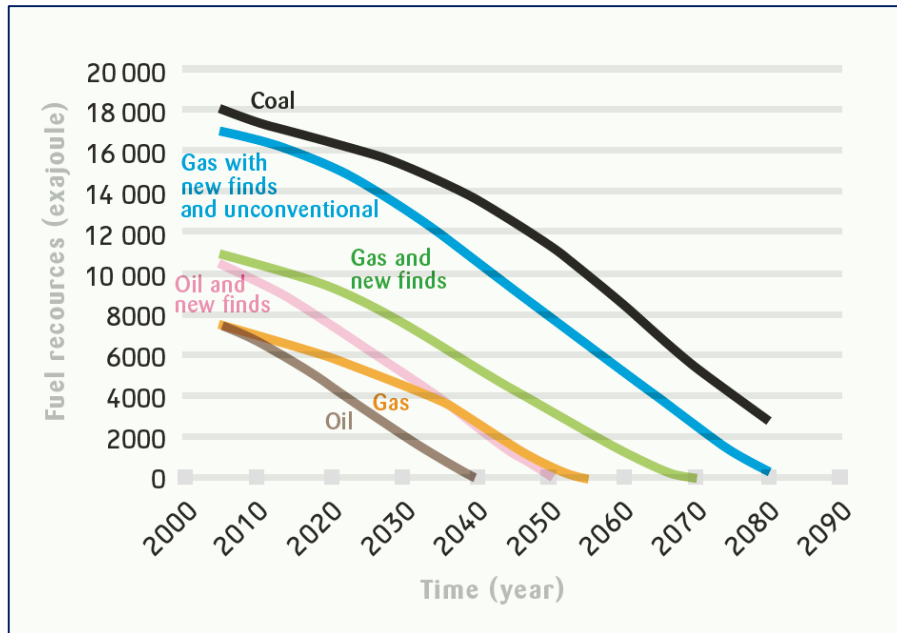


Figure 1.2 Depletion of fossil fuels within the coming few decades [15].

## 1.2. Conventional Method for Gas Storage and Separation:

### 1.2.1. Cryogenic Distillation:

Normally, separation of gases is carried out by a physical process known as “*cryogenic distillation*”. It is a process of cooling a gas mixture to induce a phase change for effective separation. It involves the separation of gases based upon the different boiling points and volatilities, which is an energy intensive processes as well as damaging ones to the environment since it involves the consumption of large amount of fossil fuel to generate the required energy for the liquefaction and distillation processes [1,2,9,16]. Hence, there is an urgent need for gas separation by a novel cost-effective material that consumes lower energy.

### *1.2.2. Membranes:*

---

Membranes for selective separation are commonly synthesized from natural or synthetic polymers including wool, rubber, and cellulose or polyimide, etc. Polymeric membranes can be glassy or rubbery, and fabricated into flat asymmetric or thin-composite sheets, tubules, or hollow fibers. In general, in the case of membrane-based separations, exploitation of the differences between the chemical, electronic, or physical properties of the species involved in the separation is required. For instance, a membrane may serve to separate based upon size, solubility, rate of diffusion or some combination of these properties [17].

In a porous membrane, the difference between the rates of which the molecular species diffuse through pores dictates the extent of separation. The term “porous membrane” encompasses a range of membranes, each having a given nominal pore size or average pore size in its distribution of pore sizes. Only those porous membranes having the smallest pore sizes will be considered here, as they have relevance to applications involving gas separation processes. In general, a major disadvantage of porous membranes for gas separation is the difficulty associated with the fabrication of membranes with a narrow pore size distribution. Another drawback is the potential of water and other vapor condensing in the small pores leading to pore blocking and inhibiting gas transport through the membrane [18].

#### *A. Porous Materials for Gas Separation:*

---

Porous materials are inter-molecular connected structures with porosity in at least one dimension. The International Union of Pure and Applied Chemistry (IUPAC) defined porosity as possessing cavities, or channels with high depth. IUPAC classifies porous materials according to their pores and channels width into; micro-porous (< 2nm), meso-porous (2-50nm), and macro-porous (> 50nm) [18,19]. They are also classified by the nature of their structure into either crystalline (e.g. zeolites or Metal-Organic-Frameworks) where the dimensions of the pores are determined by the crystal frame-work, therefore there is very little or no distribution of pore size, or amorphous (e.g. activated carbons and polymers) where the structure does not have long-range order and therefore can possess broad pore size distribution.

## ***A.1. Crystalline Porous Materials:***

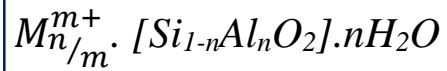
---

Crystalline porous materials are desirable due to their ordered molecular structure. They are potential candidates for applications based on size control such as molecular separations. However, they lack the ability of retaining their porosity upon solvent removal and collapse to form a denser phase that may be either crystalline or amorphous.

### ***A.1.1. Zeolites:***

---

Zeolite is a highly ordered inorganic micro-porous material. The crystalline substance is characterized by  $TO_2$  tetrahedral framework (T= Si, Al) connected to the neighboring tetrahedrals through oxygen atoms. It is characterized with a relatively high surface area between 300-600  $m^2g^{-1}$ ; the zeolite composition can be described as follows [20,21]:



The well-defined structure and chemistry of zeolites allows them to be used to study the chemistry of hydrogen binding to a variety of metal cation centres. Other applications include heterogeneous catalysis, use as catalyst supports, water softening, and as additives in detergents.

### ***A.1.2. Metal-Organic Frameworks:***

---

Metal organic frameworks (MOFs) are a class of crystalline organic-inorganic hybrid compounds formed by coordination of metal clusters or ions with organic linkers, in which bivalent or trivalent aromatic carboxylic acids or N-containing aromatics are commonly used to form frameworks with zinc, copper, chromium, aluminum, zirconium, and other elements. MOFs have high surface areas and high pore volumes in uniformly sized pores as well as high metal content. Because they can be tailored in structure and functionality for particular applications, metal-organic frameworks have a great potential in such areas as chemical catalysis, gas separation, and molecular recognition [18,22,23].

## *A.2. Amorphous Porous Materials:*

---

An alternative strategy for producing porous materials is to design molecules that are unable to pack effectively in the solid state, irrespective of molecular orientation or processing conditions. In principle, this provides a number of advantages over porous molecular crystals and might overcome the problem of porosity loss in crystals on de-solvation.

### *A.2.1. Activated Carbons:*

---

An activated carbon is a predominantly amorphous solid that can possess an extraordinary large internal surface area and pore volume that is responsible for its adsorptive properties. It has been exploited in many different liquid- and gas-phase applications. They are produced by the carbonization of different natural or synthetic materials followed by chemical and/or physical activation. During carbonization, porosity is created from the random arrangement of planar hexagonal graphene sheets that are cross-linked by non-graphitised aliphatic units to create a polymer network that cannot fill space efficiently. The spaces between the twisted network of defective carbon layers of activated carbon constitute the micro-porous, meso-porous and macro-porous structures offering a large internal surface area up to 2500m<sup>2</sup>/g [21,24,25].

### *A.2.2. Polymers of Intrinsic Micro-Porosity: (PIMs)*

---

PIMs are another class of porous materials that was first reported by Mckweon and are of interest due to their ease of synthesis, wide potential applications and high thermal and chemical stability. Intrinsic micro-porosity is a continuous network of interconnected intermolecular voids, which is a direct consequence of the macro-molecules shape and rigidity. Generally, polymers lack micro-porosity since they possess enough conformational and rotational freedom to pack space efficiently. However, PIMs are composed of highly rigid and contorted macro-molecules which cannot pack space-efficiently, leaving molecular-sized interconnected voids. The rigidity is caused by the presence of fused rings along the polymeric backbone whereas the contorted structures arise from the incorporation of non-planar sites of contortion. Several well-established classes of polymers can possess intrinsic micro-porosity such as polyacetylenes,

fluorinated polymers and polyimides, which will be the focus of this work due to its exceptional advantages in gas separation application [5,21,26–31].

## ***B. Polyimides:***

---

Polyimides (PIs) are a class of thermally stable polymers that are often based on stiff aromatic backbones. When this interesting class of polymers is produced with intrinsic micro-porosity, it can lead to an effective and stable membranes for gas separation and storage. Polyimides were first prepared by Bogert and Renshaw in 1908, and they were then widely used and rapidly developed in the 1960s. Polyimides have received great attention as they are very useful for many high-tech applications [31]. The chemistry of polyimides is in itself a vast area with a large variety of available monomers as well as several known methodologies for their synthesis and preparation.

### ***B.1. Polyimides Structure:***

---

Polyimides are step wise or poly-condensation polymers derived from both aliphatic or aromatic dianhydrides and diamines, or their derivatives, and contain a heterocyclic imide linkage in the repeat unit, as shown in *Figure 1.3*.

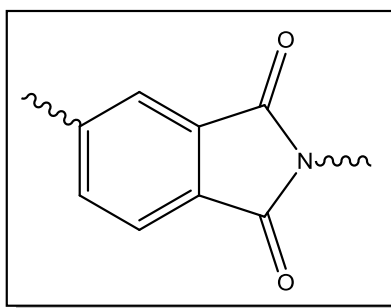


*Figure 1.3* Heterocyclic imide repeat unit.



## ***B.2. Polyimides Properties:***

---

Since the synthesis of the first high molecular weight aromatic polyimides, interest in this class of polymers has been growing steadily due to their thermo-oxidative stability, unique electrical properties, high radiation and solvent resistance, and high mechanical strength. Fully aromatic polyimides have rigid chains and strong inter-chain interactions, which result in the polymers having poor solubility and non-melting characteristics. The development of polymeric materials suitable for multi-purpose technological applications requires an ability to manipulate the morphological features of a given polymer to render the desired functional properties. Polyimides are high-performance polymers that have applications ranging from aerospace to microelectronics [32,33].

## ***B.3. Polyimides Synthesis:***

---

The “two-step” method is the most frequently used method for polyimide synthesis. It involves the use of a poly-amic acid (PAA) precursor, which is cyclized to form the imide linkage, known as the “classical” method. Other pathways could be used for polyimide synthesis have been elucidated by various researchers through the past years. Generally, as shown in *Figure 1.4* the poly-amic acid is formed when a di-functional amine and a di-functional anhydride mutually react in a polar aprotic solvent such as N-methyl-2-pyrrolidone (NMP), N,N-dimethylacetamide (DMAc), N,N-dimethylformamide (DMF) and dimethyl sulfoxide (DMSO) [30,32–34]. This reversible nucleophilic substitution reaction takes place when the amine group attacks one of the carbonyl carbons in the anhydride moiety and displaces carboxylate functionality. This is followed by proton transfer. It was found that there is a direct relation between the dianhydride reactivity and electron affinity ( $E_a$ ), the higher the electron affinity of dianhydride, the faster the reactivity with the nucleophile. The presence of electron withdrawing or donating groups will greatly influence the electron affinity of the anhydride carbonyl groups. However, the diamine reactivity with phthalic anhydride is correlated to the basicity  $pK_a$ , i.e. the greater the basicity of the diamine groups, the faster it will react with the dianhydride. A diamine bridged by a withdrawing group shows decreased nucleophilicity. Therefore, the lower the reactivity between the diamine and dianhydride groups during the PAA formation, the lower molecular weight obtained and vice versa, with fixed reaction time. It is already apparent that the

rate of PAA formation is largely dependent on diamine basicity and anhydride electron affinity. However, reaction rate is also a function of the solvent [30,31].

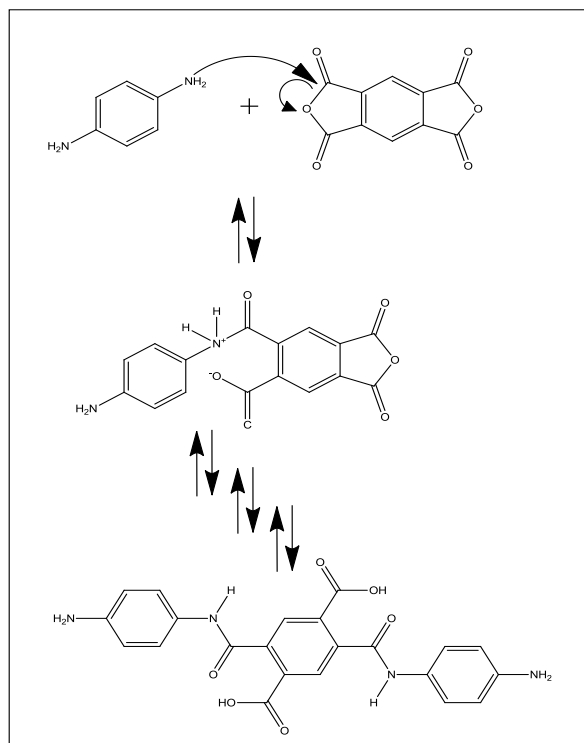


Figure 1.4 The classical method for polyimide synthesis.

To produce PAA with a precise molecular weight, it is essential to completely eliminate water from the monomers and the solvents used in the reaction. This is usually attained by cautiously drying the monomers and distilling the solvents. As in the existence of water the dianhydride will hydrolyze giving the diacid which reacts with slower rate as compared to the dianhydride with a given amine. Water will also promote the reverse reaction, which is hydrolytic scission of the amide link. PAA Cyclization will also produce water and may result in chain hydrolysis. Different methods have been used to facilitate the cyclization of PAA and the removal of water. It can be reached by either heating the PAA in solution, or adding a dehydrating reagents [35].

### *C. Gas Separation Mechanisms through Porous Polymeric Membranes:*

---

Membranes for selective separation are commonly synthesized from natural or synthetic polymers. They can be either brittle or flexible, and fabricated into flat asymmetric or thin-composite sheets, tubules, or hollow fibers. Membrane-based separation is based on the differences in physical and/or chemical interactions between gases and the membrane material, which can be modified to allow some components to pass preferentially through the membrane based on size (kinetic) and/or affinity (thermodynamics). There are several modes of separation possible in porous membranes as shown in *Figure 1.5*, i.e., solution-diffusion, Knudsen diffusion, and molecular sieving [35–38]. These are formally defined by gas permeability and selectivity which are inversely related. Therefore, the goal of any study related to the membranes is to form one with high permeability and selectivity, In addition to adequate strength and life time.

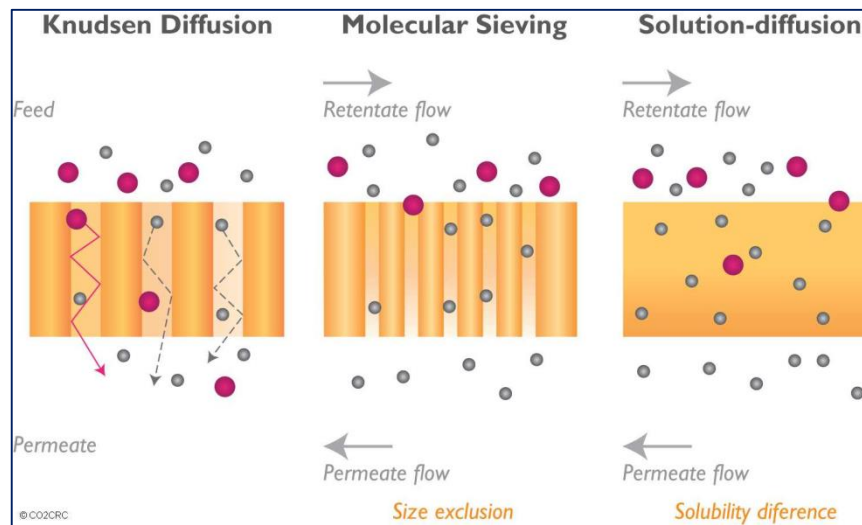


*Figure 1.5* Modes of separation possible in porous membranes [39].

The first to use the term “solution-diffusion mechanism” was Graham [9] in 1866. He postulated that the penetrant leaves the external phase by dissolving in the membrane. It then undergoes molecular diffusion in the membrane, driven towards the downstream face by a concentration or pressure gradient. It is principally takes place in membranes with pore size greater than the mean free path of the diffusing molecules [35,36].

Knudsen's diffusion occurs in a porous membrane, whose pore sizes are smaller than the mean free path of the gas molecules. The mean free path is the average distance a particle travels between collisions. The larger the particles or the denser the gas, the more frequent the collisions are and the shorter the mean free path. In Knudsen diffusion gas molecules interact with the pore walls much more frequently than colliding with one another which allows lighter molecules to preferentially diffuse through pores. Knudsen's diffusion principally takes place in membranes with a pore diameter in the range of 50-100Å. Finally, the molecular sieving mode occurs in porous membrane, whose pore sizes are equal to both the mean free path and the diameter of the gas molecules, in which different gas molecules are separated due to their size differences. Gas molecules with diameters equal or smaller than the pore size will normally pass, and those with larger diameters are excluded and prevented from passing through the membrane pores [35, 38,40].

### *1.3. Thesis Scope and Objectives:*

---

Recently, considerable efforts have been made in the synthesis of novel micro-porous materials which possess high internal surface areas and therefore have applications in modern technologies such as hydrogen storage, CO<sub>2</sub> capture and gas separations. The main objective of this thesis is to synthesize six different polymers of intrinsic micro-porosity for separation and storage of different gases that are known to be either hazardous to the environment or efficient for energy production. The main activities were carried out were: (i) poly-condensation synthesizing of various polyimides of different structures, (ii) characterizing of the different synthesized polymers through different techniques, (iii) examining several properties of the different synthesized polymers which are required for gas separation and storage application e.g. porosity, thermal stability and selective gas adsorption/desorption ability, (iv) using newly developed computational modeling techniques to investigate the influence of certain diamine groups on the conformation of the polymers and how this will finally affect the porosity and selective gas adsorption/desorption ability, and (v) comparing the simulated results of the synthesized polymers with the experimental results obtained from its characterization.

The synthesis of different polymers is accompanied by a complete characterization of their chemical structure by Fourier transform infrared spectroscopy (FTIR), nuclear magnetic

resonance (NMR) and elemental analyzer (CHNS& O). The achieved molecular weights and degree of polymerization are detected using gel permeation chromatography (GPC). BET techniques were used so as to study the properties essential for polymers used for gas separation and storage, including surface area, porosity, thermal stability and selective gas adsorption/desorption ability.

## Chapter 2:

### Literature Review

## *2. Literature Review:*

---

As mentioned previously micro-porous materials are those characterized with interconnected pores. Accordingly they can be applied in heterogeneous catalysis, adsorption, separation, and gas storage [41]. Micro-porous materials are normally classified according to the nature of the structure into either crystalline materials such as zeolites or amorphous materials such as activated carbon. Additionally, they can be also classified into extrinsic micro-porous and intrinsic micro-porous structures.

### *2.1. Extrinsic Micro-porous Structures:*

---

These are the structures that are not porous by nature, however they are forced to form pores during synthesis. Extrinsic micro-porosity arises from the template effect of the solvent molecules trapped within the structure as it forms [29]. It was achieved by Yaghi et al. in the formation of crystalline structure known as metal organic frameworks (MOFs) by placing the precursors in the suitable solvent and at a suitable temperature leading to a porous crystalline structure with its void space filled with solvent molecules. After the completion of the synthesis, the solvent molecules were removed by either the application of heat or vacuum [42,43]. They were found to be porous and possess both high nitrogen (N<sub>2</sub>) adsorption at 77 K and surface areas as determined by the Brunauer-Emmet-Teller (BET) method which was typically used since 1977 [44,45].

It was generally believed that crystalline materials are essentially most favored to produce porous structures. However, Tsyurupa et al. were able to successfully synthesize porous amorphous activated carbons such as hyper-cross-linked polymers (HCP) by using the solvent as a template, which was followed by removing the solvent molecules to reveal HPCs with permanent porosity and high surface areas [46–48]. High BET surface areas up to 2000 m<sup>2</sup> g<sup>-1</sup> were achieved by Germain et al. with a broad distribution of pore sizes that ranges from micro-pores, meso-pores and macro-pores [49–52]. The main drawback of the extrinsic micro-porosity is that it can be distorted upon structure rearrangement over time through the application of pressure and temperature for the solvent removal [29].

## 2.2. Intrinsic Micro-Porous Structure:

Masuda et al. paved the way to the term “intrinsic micro-porosity” in 1983 when they introduced poly[1-(trimethylsilyl)-1-propyne] (PTMSP) [53], which had the most astounding O<sub>2</sub> penetrability among all known polymers at that time. PTMSP is still utilized as a kind of perspective for recently produced high free volume polymers. The exceptionally high permeability in PTMSP is due to the rigid structure that hinders its efficient space filling, thus resulting in intermolecular voids. This idea was left till reignited again in 1990s when McKeown produced porous phthalocyanine materials. McKeown and co-workers were able in 1998 to synthesize a networked polymer consisting of phthalocyanine fused together with Spiro-cyclic group in order to produce a highly porous material [54]. They attempted numerous synthetic routes to end with the suitable polymerization reaction for synthesizing the Spiro-cyclic phthalocyanine framework [55]. It was found that the easiest route for its synthesis is by using a Spiro-cyclic bisphthalonitrile. As shown in Figure 2.1, the 4, 5- dichlorophthalonitrile reacts with 5, 5', 6, 6'-tetrahydroxy-3, 3, 3', 3'-tetramethylspirobisindane to give the required Bisphthalonitrile [52]. Eventually, this procedure resulted in frameworks with noteworthy micro-porosity as confirmed by nitrogen adsorption measurements from which apparent BET surface areas of more than 750m<sup>2</sup>g<sup>-1</sup> were calculated [56–58]. Additionally, these frameworks were observed to be characterized with valuable catalytic activity in oxidations reactions [59,60]. During those years wide range of micro-porous network polymers were synthesized and studied as potential hydrogen storage materials [60–65] and as heterogeneous catalysts [22,29,52,66,67].

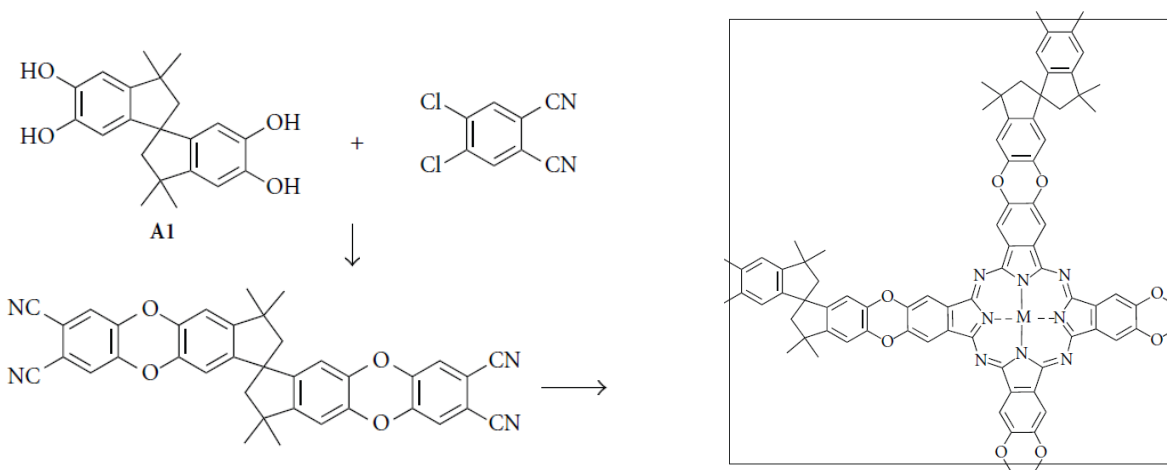
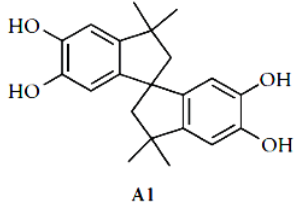
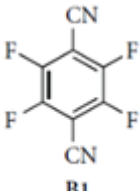


Figure 2.1 The synthesis for Phthalocyanine Framework [52].



The term “intrinsic micro-porosity” was introduced by McKeown in 2001 after the synthesis of porous soluble polymers through exploiting the idea of having a rigid component within the structure, in order to form interconnected pores. By applying this idea, they overcome the main drawback occurred with the extrinsic micro-porosity which is the loss of porosity after the removal of the solvent. Those polymers were known then with the term “polymers of intrinsic micro-porosity” (PIMs). Generally, polymers have sufficient conformational adaptability that permits them to readjust their shape so as to maximize their cohesive interactions between neighboring chains in order to pack space efficiently after the removal of the solvent molecules. However, PIMs lack this rotational flexibility along the polymer backbone, which guarantees that the macromolecular components are incapable of readjusting their conformity and that their highly contorted shape is maintained through the synthesis process. PIM-1 was synthesized through the reaction of 5, 5', 6, 6'-tetrahydroxy-3, 3, 3', 3'-tetramethylspirobisindane (A1) with tetrafluoro-terephthalonitrile (B1) and it was characterized with very high apparent average molecular mass as determined by GPC. The polymers were characterized by nitrogen adsorption at 77 K, and a considerably large BET surface areas of around 800m<sup>2</sup> g<sup>-1</sup> were determined as shown in Table 2.1. It was realized then that a covalent network was not necessary for obtaining micro-porosity in these polymers [21,66].

*Table 2.1* PIMs based on dibenzodioxin formation using 5, 5', 6, 6'-tetrahydroxy-3, 3, 3', 3'-tetramethylspirobisindane monomer.

<i>Monomer 1</i>	 A1			
<i>Monomer 2</i>	<i>Polymer Name</i>	<i>Solubility</i>	<i>Surface Area; BET (m<sup>2</sup> g<sup>-1</sup>)</i>	<i>Ref.</i>
 B1	PIM-1	THF and CHCl <sub>3</sub>	760-850	[68,78]

<p style="text-align: center;"><b>B2</b></p>	PIM-2	THF	600	[68]
<p style="text-align: center;"><b>B3</b></p>	PIM-3	THF	560	[68]
<p style="text-align: center;"><b>B4</b></p>	PIM-7	CHCl <sub>3</sub>	680	[70]
<p style="text-align: center;"><b>B5</b></p>	PIM-9	CHCl <sub>3</sub>	661	[70]

### *2.2.1. Structure-Property Relationships of Polymers of Intrinsic Micro-Porosity:*

PIMs' structures have been manipulated to reach desired properties in terms of porosity [61,68–74], solubility [75–77], thermal [69] and mechanical [79,80] properties. Most of the PIMs that have been synthesized, are composed of either dibenzodioxin or imide repeat units. In both strategies, at least one of the monomers has the contortion site, which provokes the formation of the interconnected pores and the other monomer could either has another contortion site or being aromatic in order to provide stiff backbone to the synthesized polymers. As shown

in Figure 2.2 in the dibenzodioxin formation process, one of the monomers is functionalized with hydroxyl groups and the other has a halogen group, at which the acid of the halogen is formed leaving the benzodioxin group. Those PIMs created through these procedures are presented in Tables 2.1, 2.2, 2.3, 2.4, and 2.5 accompanied by their solubility and porosity properties. However, the imide formation process depends on the presence of dianhydride monomer and diamine monomer, at which the oxygen group present in the dianhydride monomer is replaced with the nitrogen on the diamine as shown in Figure 2.3. PIMs created using this method are presented in Tables 2.6, 2.7, and 2.8 accompanied by their solubility and porosity properties.

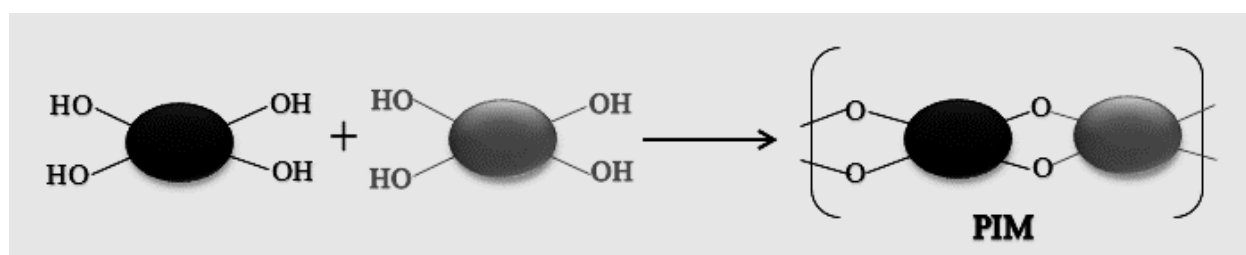


Figure 2.2 Polymers of intrinsic micro-porosity based on dibenzodioxin formation.

Table 2.2 PIMs based on dibenzodioxin formation using 1, 1'-binaphthalene -2, 2', 3,3'-tetrol monomer.

<i>Monomer 1</i>	 A2			
<i>Monomer 2</i>	<i>Polymer Name</i>	<i>Solubility</i>	<i>Surface Area; BET (m<sup>2</sup>g<sup>-1</sup>)</i>	<i>Ref.</i>
 B1	PIM-4	THF	440	[68]

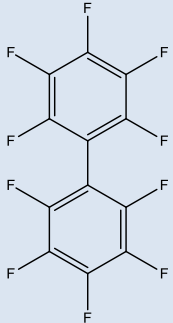
 <p style="text-align: center;"><b>B2</b></p>	PIM-5	THF	520	[68]
--	-------	-----	-----	------

Table 2.3 PIMs based on dibenzodioxin formation using 9, 10-dimethyl-2, 3, 9, 10-ethanoanthracene-2, 3, 6, 7-tetrol monomer.

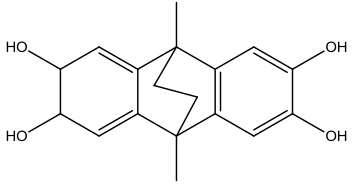
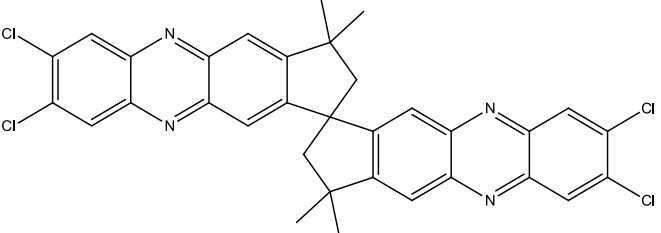
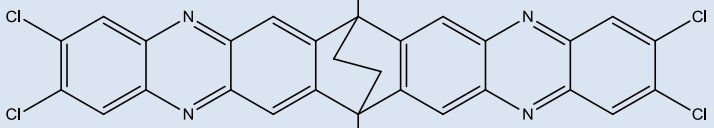
<i>Monomer 1</i>	 <p style="text-align: center;"><b>A4</b></p>			
<i>Monomer 2</i>	<i>Polymer Name</i>	<i>Solubility</i>	<i>Surface Area; BET (m<sup>2</sup>g<sup>-1</sup>)</i>	<i>Ref.</i>
 <p style="text-align: center;"><b>B4</b></p>	PIM-8	CHCl <sub>3</sub>	677	[70]
 <p style="text-align: center;"><b>B5</b></p>	PIM-10	m-cresol	680	[70]

Table 2.4 PIMs based on dibenzodioxin formation using 4, 4'-(9H-fluorene-9, 9-diyl) bis (benzene-1, 2-diol) monomer.

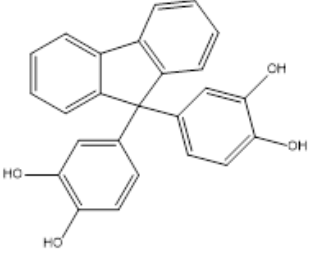
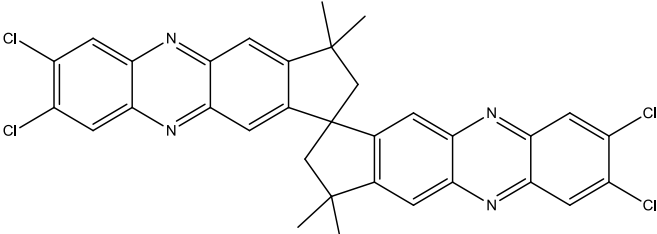
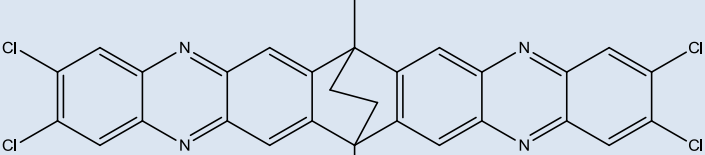
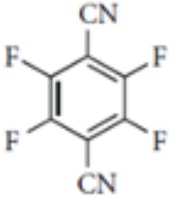
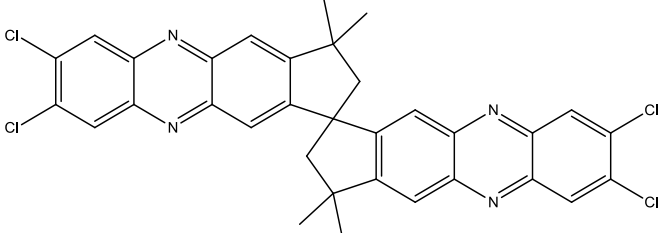
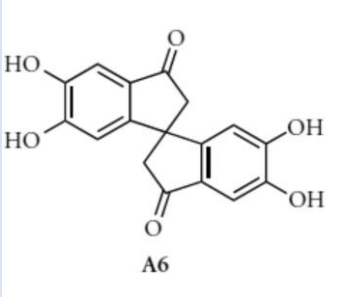
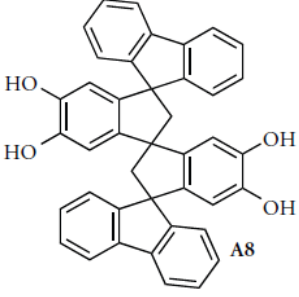
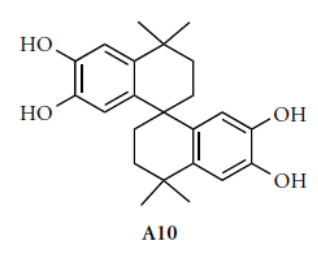
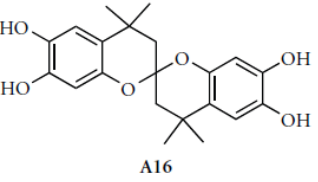
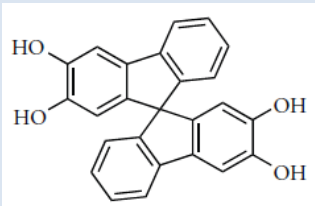
<p><i>Monomer 1</i></p>	 <p><b>A5</b></p>			
<p><i>Monomer 2</i></p>	<p><i>Polymer Name</i></p>	<p><i>Solubility</i></p>	<p><i>Surface Area; BET (m<sup>2</sup>g<sup>-1</sup>)</i></p>	<p><i>Ref.</i></p>
 <p><b>B4</b></p>	<p>Cardo-PIM-1</p>	<p>CHCl<sub>3</sub></p>	<p>621</p>	<p>[70]</p>
 <p><b>B5</b></p>	<p>Cardo-PIM-2</p>	<p>Partially soluble in CHCl<sub>3</sub></p>	<p>580</p>	<p>[70]</p>

Table 2.5 PIMs based on dibenzodioxin formation using tetrafluoro-terephthalonitrile monomer.

<p><i>Monomer 1</i></p>	 <p><b>B1</b></p>
-------------------------	--

<i>Monomer 2</i>	<i>Polymer Name</i>	<i>Solubility</i>	<i>Surface Area; BET (m<sup>2</sup>g<sup>-1</sup>)</i>	<i>Ref.</i>
 <p style="text-align: center;"><b>A4</b></p>	PIM-CO-100	Not Soluble	630	[79]
 <p style="text-align: center;"><b>A6</b></p>		Quinoline	501	[71]
 <p style="text-align: center;"><b>A8</b></p>		THF	895	[71]
 <p style="text-align: center;"><b>A10</b></p>		THF	432	[82]
 <p style="text-align: center;"><b>A16</b></p>	PIM-CO15	Quinoline	518	[83]

 <p style="text-align: center;">A18</p>	PIM-SBF	CHCl <sub>3</sub>	803	[73]
--	---------	-------------------	-----	------

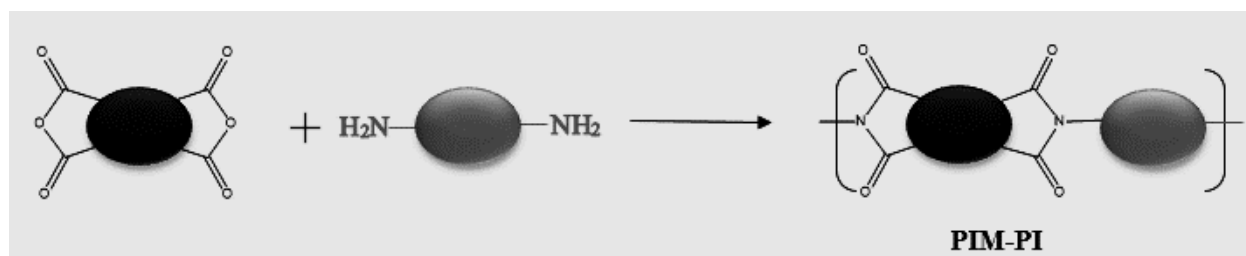
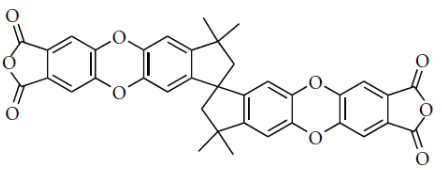
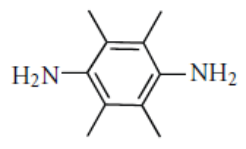


Figure 2.3 Polymers of intrinsic micro-porosity based on imide formation.

Table 2.6 PIMs based on imide formation using 9,9,9',9'-tetramethyl-8,8',9,9'-tetrahydro-7,7'-spirobi[cyclopenta[*b*]furo[3,4-*i*]dibenzo[*b,e*][1,4]dioxine-1,1',3,3'(4*aH*,5*a'H*,10*a'H*,11*aH*)-tetraone monomer .

<p style="text-align: center;"><i>Monomer 1</i></p>	 <p style="text-align: center;">Cl</p>			
<p style="text-align: center;"><i>Monomer 2</i></p>	<p style="text-align: center;"><i>Polymer Name</i></p>	<p style="text-align: center;"><i>Solubility</i></p>	<p style="text-align: center;"><i>Surface area; BET (m<sup>2</sup>g<sup>-1</sup>)</i></p>	<p style="text-align: center;"><i>Ref.</i></p>
 <p style="text-align: center;">D1</p>	PIM-PI-1	CHCl <sub>3</sub>	680	[84,85]

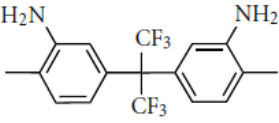
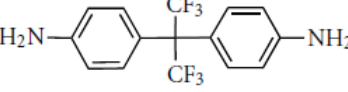
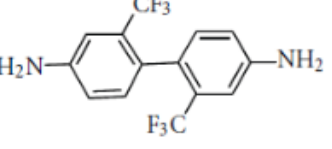
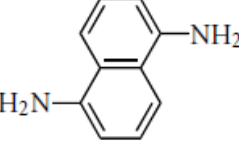
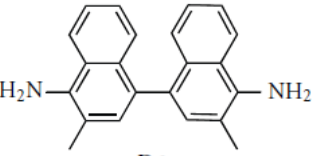
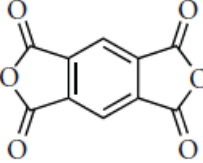
 <p style="text-align: center;">D2</p>	PIM-PI-2	CHCl <sub>3</sub>	500	[85]
 <p style="text-align: center;">D3</p>	PIM-PI-3	CHCl <sub>3</sub>	471	[84,85]
 <p style="text-align: center;">D4</p>	PIM-PI-4	CHCl <sub>3</sub>	486	[85]
 <p style="text-align: center;">D5</p>	PIM-PI-7	CHCl <sub>3</sub>	485	[85]
 <p style="text-align: center;">D6</p>	PIM-PI-8	CHCl <sub>3</sub>	683	[84,85]

Table 2.7 PIMs based on imide formation using benzo[1,2c:4,5-c']difuran-1,3,5,7-tetraone monomer.

<b>Monomer 1</b>	 <p style="text-align: center;">C2</p>
------------------	---



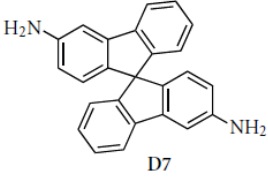
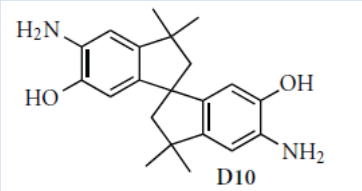
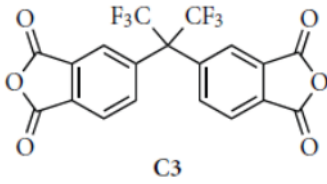
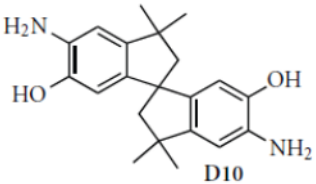
<i>Monomer 2</i>	<i>Polymer Name</i>	<i>Solubility</i>	<i>Surface area; BET (m<sup>2</sup>g<sup>-1</sup>)</i>	<i>Ref.</i>
 D7	P4	CHCl <sub>3</sub>	551	[86]
 D10	PIM-6FDA-OH	THF	225	[87]

Table 2.8 PIMs based on imide formation using 5, 5'-(perfluoropropane-2, 2-diyl) bis (isobenzofuran-1, 3-dione) monomer.

<i>Monomer 1</i>	 C3			
<i>Monomer 2</i>	<i>Polymer Name</i>	<i>Solubility</i>	<i>Surface area; BET (m<sup>2</sup>g<sup>-1</sup>)</i>	<i>Ref.</i>
 D10	PIM-PMDA-OH	THF	190	[87]

### *A. Solubility:*

---

The high solubility of PIMs in organic solvents is one of their specific properties and as shown in Tables 2.1-2.8. Ladder polymers are mostly insoluble [77] and regularly long alkyl chains units are essential for solubility. Though, PIMs' rigid and contorted molecular structures reduce the intermolecular interactions through controlling the extent of contact among polymer chains. In addition to the flexibility, the spirobisindane unit might also help in improving the polymers solubility [78]. It is observed that the PIM synthesized using ethanoanthracene monomer (A4) and tetrafluoro-terephthalonitrile (B1) monomers is insoluble [79], which have contributed to the high rigidity of the ethanoanthracene unit. This may have been also due to the two dimensional contortion of the polymer chain thus permitting the polar nitrile groups to interact and causing the increase in the polymer cohesion, in contrast to soluble PIMs which create random coils in three dimensions.

### *B. Thermal Stability:*

---

One of the reasons for the great interest in PIMs is their high thermal stability. For example, thermal analysis of PIM-1, including differential thermal Calorimetry (DSC) and thermal dynamic mechanical analysis (DMTA), exhibited no glass transition temperature or other thermal transition below its decomposition at around 450°C [69]. Moreover, PIMs made of polyimides were also thermally analyzed using thermal gravimetric analysis (TGA) and they were found to possess high decomposition points as shown in Table 2.9. In 2014, Shamsipur et al. synthesized PIM-PI-OH-2 and PIM-PI-OH-3 as shown in Figure 2.4, and they were thermally analyzed using TGA as shown in Figure 2.5. PIM-PI-OH-2 was characterized by lower decomposition point than expected; therefore a derivative (Copol-OH-(1-2)) was prepared at which two anhydride polymers were used instead of one with the diamine monomer. The derivative was found to be thermally more stable. The PIM-PI-OH-3 possessed high decomposition point which was highly near to that of Copol-OH-(1-2) [88].

*Table 2.9* The decomposition points for different PIM-PIs.

<i>Polymer Name</i>	<i>Decomposition Point</i>	<i>Ref.</i>
<b>PIM-PI-1</b>	~ 465°C	[84]
<b>PIM-PI-2</b>	~ 485°C	
<b>PIM-PI-3</b>	~ 480°C	
<b>PIM-PI-4</b>	~ 485°C	
<b>PIM-PI-7</b>	~ 492°C	
<b>PIM-PI-8</b>	~ 480°C	

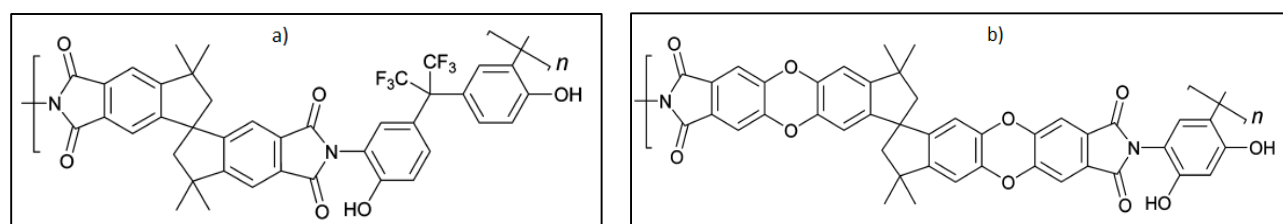


Figure 2.4 Structure of the repeat unit of a) PIM-PI-OH-2 and b) PIM-PI-OH-3 [88].

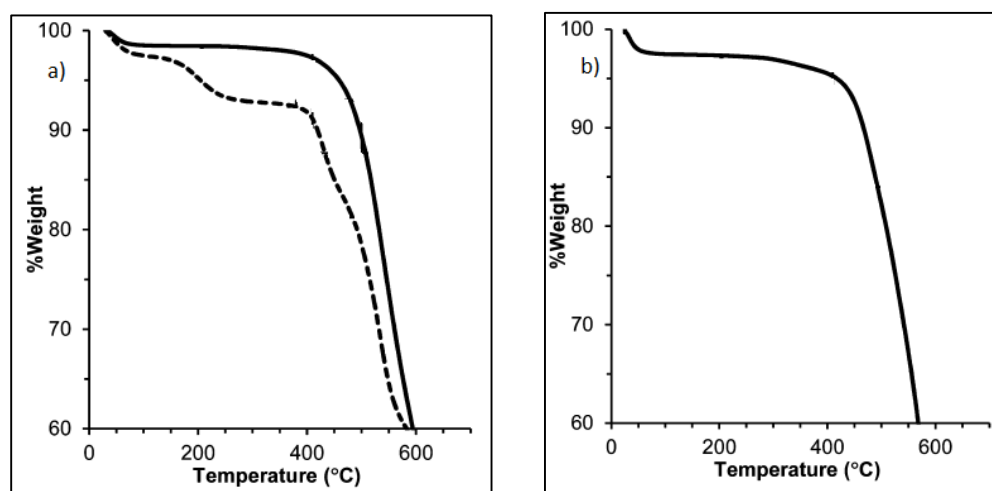


Figure 2.5 Thermal gravimetric analysis of a) PIM-PI-OH-2 (----), Copol-OH(1-2) (—) b) PIM-PI-OH-3 [88].

### *C. Mechanical Properties:*

---

Most of the synthesized PIMs were expected to form films to be used in different applications and tested mechanically. Some of the PIMs prepared by Shamsipur et al. were tested and Young's modulus exceeded 1 GPa [69] and that the samples ruptured just above 1% deformation, indicating the relative toughness of the PIMs ( $\epsilon = 6.6 \pm 3.2\%$ ). Therefore, further optimization of these materials was necessary to enhance their mechanical properties. PIM-1 possessed a tensile storage modulus of approximately 1GPa, a tensile strength of 45–47MPa, and a strain of 10%-11% at breakage which is considered a great improvement of the demarked 1% deformation [80,81].

### *D. Surface Area:*

---

Values for the apparent BET surface area of PIMs are given in Tables 2.1-2.8. The value of PIM-1 is within the range of 720–875m<sup>2</sup> g<sup>-1</sup> [61,68,72]. Only a few PIMs possessed higher apparent surface area than PIM-1, and these are prepared from monomers containing highly rigid aromatic substituents such as A8, A18, and B16 [71,73]. It was observed that PIMs based on more flexible structures, such as those derived from the tetrahydronaphthalene unit such as A10 and B1, were significantly less micro-porous than the equivalent spirobisindane-based polymers [89]. In general, it is difficult to predict the effect on micro-porosity by adding substituents to a PIM. For some rigid substituents, such as fused fluorenes (e.g., A8), some modest enhancement has been noted [71] but in it is observed that the substituents fill the micro-porosity resulted from the polymeric chains packing. The apparent surface area was significantly reduced in PIM-1 through the substitution of nitrile groups with carboxylic acid, thioamide, or tetrazole groups. This might be attributed to the increase in cohesion interactions between polymeric segments which subsequently improved the packing efficiency of the polymer [74–76].

### *2.2.2. Gas Separation Application of Polymers of intrinsic microporosity:*

---

Recently, required features for specific application have been the driver behind synthesizing PIMs with versatile structures. Different PIMs have been studied for various applications such as gas separation, organics adsorption and catalysis. However, in this section only PIMs that have been studied for gas separation will be discussed as related to the thesis scope. The huge interest in using membranes derived from polymers in gas separation, paved the path for the polymers' gas permeability investigation field. The polymeric membranes are desired to possess both high permeability and selectivity [90]. Solution-diffusion model is usually used to express the permeation of gases through polymeric membranes. Permeation selectivity could be either due to high solubility or high diffusivity. Rubbery polymers such as polydimethylsiloxane-PDMS exhibit large free volume which attributes to the voids present between the polymeric chains. In this case the permeability is relatively high, however the selectivity is low. On the contrary, the glassy polymers exhibit low permeability and high selectivity, this is due to the small free volume between the polymeric chains resulting in size selective permeability. The smaller gas molecules will diffuse more rapidly than the larger ones. Therefore, the glassy polymers are the ones used for gas separation applications. On the contrary, PTMSP is a glassy polymer that possessed high permeability and low selectivity towards gases. [91]. This trade-off relationship has been quantified by Robeson's upper bound through having a double logarithmic plots of selectivity against permeability in 1991[92]. He revised these upper Bound plots in 2008 for CO<sub>2</sub>/N<sub>2</sub>, CO<sub>2</sub>/CH<sub>4</sub> and O<sub>2</sub>/N<sub>2</sub> shown in Figure 2.6

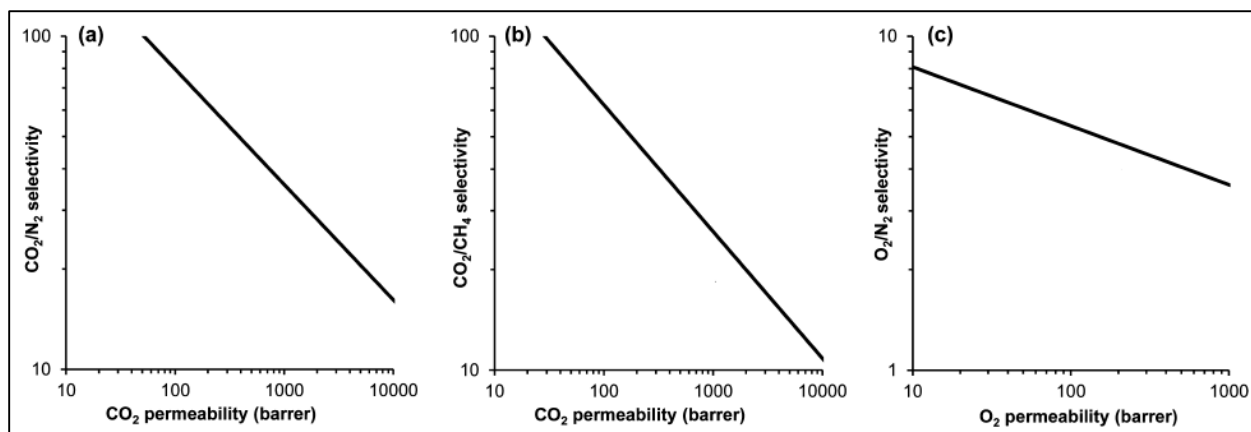


Figure 2.6 Robeson's plots of (a) CO<sub>2</sub>/N<sub>2</sub>, (b) CO<sub>2</sub>/CH<sub>4</sub> and (c) O<sub>2</sub>/N<sub>2</sub> selectivity versus the permeability of the fastest gas [93].

PIM-1 and PIM-7 were reported to possess good properties for producing gas separation membranes having both high permeability and good selectivity that places them well above the Robeson's upper-bound for many gas pairs. For O<sub>2</sub>/N<sub>2</sub> separation study, Polymers PIM-1 and PIM-7 show substantially higher selectivity than other polymers of similar permeability, the solubility values of these membranes are extraordinarily high but solubility selectivity is relatively small, O<sub>2</sub>/N<sub>2</sub> separation for the PIMs is dominated by the diffusivity selectivity (smaller gas molecules diffuse faster) as expected for glassy polymers. PIMs also lie above or near the upper bound line for several other commercially important gas combinations, including CO<sub>2</sub>/CH<sub>4</sub>, H<sub>2</sub>/N<sub>2</sub> and H<sub>2</sub>/CH<sub>4</sub>. The improved permeability and selectivity data of PIM membranes over the original Robeson's line (1991) has attributed to a revision of the upper bound in 2008. The microporosity of PIMs provides a high capacity for gas uptake, might be the reason behind their high apparent gases solubility. It has been noticed that polymers with rigid molecular structures usually lie on or close to Robeson's upper bound line [94].


Ghanem et al. studied the gas transport characteristics of PIM-polyimides (PIM-PIs) synthesized from 9,9,9',9'-tetramethyl-8,8',9,9'-tetrahydro-7,7'-spirobi[cyclopenta[*b*]furo[3,4-*i*]dibenzo[*b,e*][1,4]dioxine-1,1',3,3'(4*aH*,5*a'H*,10*a'H*,11*aH*)-tetraone (C1) with a variety of diamine units, showing that the permeability could be altered by changing the structure of the diamine to give higher or lower rotation freedom around the imide group. PIM-PI-1 and PIM-PI-8 which had methyl groups beside the amine group, showed both an exceptional permeability

and selectivity [83,84]. Additionally, Rogan et al developed PIM-PI-9 and PIM-PI-10 and they exhibited high permeability compared to previously synthesized polyimides [95].

In 2014, Shamsipur et al. prepared PIM-PIs from spiro center containing dianhydrides monomer with two different diamines: 2, 2-bis (3-amino-4-hydroxyphenyl) hexafluoropropane (bisAPAF) and 4, 6-diaminoresorcinol (DAR). The thermally treated poly-benzoxazole (PBO) polymers at 450 °C under N<sub>2</sub> for an hour, showed an increased permeability as compared to the previously synthesized. A polymer based on DAR (PIM-PBO-3) revealed a CO<sub>2</sub>/N<sub>2</sub> selectivity of higher than that obtained from polymers based on bisAPAF with the same dianhydride (PIM-PBO-1) [88].

### *2.2.3. Molecular Simulation of Polymers of Intrinsic Micro-Porosity:*

---

In addition to the practical synthetic routes that have been used in order to investigate the properties of PIMs and their ability to perform in certain application, limited number of molecular simulations have been performed to study different PIMs [96,97]. In 2012, Madkour has constructed a molecular representation of different PIM-PIs and different penetrant gas molecules and evaluated them for their permeability and selectivity characteristics using molecular dynamics simulation modules in Materials Studio  simulation package available from Accelrys, Inc., UK. The simulation study was used to investigate the self-diffusion of the various components of natural gas such as methane, ethane, propane and butane through PIM-PIs membranes [96]. Figure 2.7 illustrates the molecular structure of the PIM-PI, employed in this study.

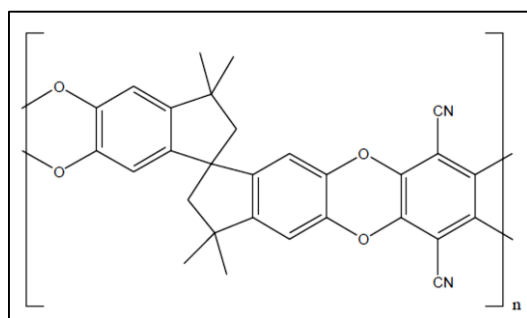
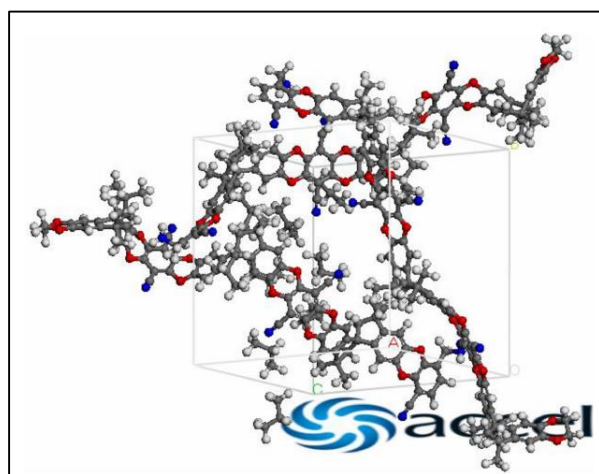


Figure 2.7 The PIM's structure that have been used in Madkour's study [96].

The MS amorphous cell module was used to construct the four individual simulation cells consisting of 3 PIM chains of  $1,600 \text{ g mol}^{-1}$  each along with 10 penetrant molecules representing each one of the four gases under study, respectively. Figure 2.8 represents one of the simulation cells used to study the self-diffusion of propane through the PIM polymer. The simulation cells in the four case studies were all cubic cells having densities  $1.0 \text{ g/cc}$ . The cells were all constructed using COMPASS forcefield assigned charges and Ewald summation method. After the construction was completed, the simulation cell was minimized using the MS Discover module till complete convergence. Once the simulation cells were minimized, they were all subjected to molecular dynamics runs using NVT ensemble for 300 ps with 1 fs time step at the temperature of 298K. Full trajectories were saved every 100 steps. During the simulation, the temperature was controlled using Anderson thermostat [96].



*Figure 2.8* Simulation cell for PIM polymer with propane [96].

The polyimide membranes demonstrated the capacity of making nano-scale channels inside the polymeric matrix throughout the molecular mobility of the polymeric chains through which specific gas molecules can penetrate the membrane surface. The gases investigated in this study are hydrocarbon based materials of similar basic chemical structures. The self-diffusion coefficients of the gas molecules were consequently used to define the permeability of the different gases through the membranes as the solubility of the gas molecules in the polymeric substances were supposed to be constant. Methane showed an outstandingly high self-diffusion coefficient obtained from the use of Einstein relation to the created molecular dynamics trajectories. All other gases had similar values for the self-diffusion coefficients, which show the



capability of the methane molecules to enter the polymeric membrane in a higher speed likely due to the matching between its molecular size and the size of the interconnected nano-channels within the membranes. The results also showed that the polymer molecules had lower self-diffusion coefficients than the gas due to the large size of the polymeric segments [96].

# Chapter 3:

## Materials, Synthesis and Characterization

### *3. Materials, Synthesis and Characterization:*

---

#### *3.1. Materials:*

---

##### *3.1.1. Purchased Materials and Subsequent Purification:*

---

The starting material 4, 5-dichlorophthalic acid (99%), potassium carbonate (ACS reagent,  $\geq 99.0\%$ ), and potassium hydroxide, diamines: (i) 4,4'-oxydianiline (97%), (ii) 4,4'-ethylenedianiline (technical,  $\geq 95\%$  (NT)), (iii) 1,5- diamionaphthalene (97%), (iv) 1,8-diamionaphthalene (99%), (v) 2,2'-biphenyldiamine ( $\geq 96.5\%$  (GC)) , and (vi) benzidine ( $\geq 98.0\%$  (N)) were all purchased from Sigma Aldrich. 5,5',6,6'-tetrahydroxy-3,3,3',3'-tetramethyl-1,1'-spirobisindane (97%) was purchased from Alfa Aesar, Germany. The above chemicals were used as received without any further purification.

Various reagents and solvents were also purchased such as Formamide (purum,  $\geq 98.0\%$  (T)), 33% ammonium hydroxide (33%  $\text{NH}_4\text{OH}$ ), thionyl chloride, N,N-dimethylformamide (DMF), ethanol, hydrochloric acid, acetic acid, acetic anhydride, toluene, anhydrous toluene, m-cresol, quinolone, methanol, chloroform ( $\text{CH}_3\text{Cl}$ ). All of the reagents and solvents were used as received except for the ammonium hydroxide and N, N-dimethylformamide.

Anhydrous DMF was used for the synthesis of both 4, 5-dichlorophthalonitrile and Bisphthalonitrile. The DMF was dried using molecular sieves (4A, 1-2mm (0.04-0.08in) beads), which was purchased from Alfa Aesar, Germany. First, 10% wt. /vol. of molecular sieves were weighed and then left in vacuum oven at  $100^\circ\text{C}$ , under 200 mbar vacuum pressures for 24 hours. After the completion of the drying, the molecular sieves were added to the DMF and stored in conical flask under nitrogen gas and finally left in the refrigerator.

To prepare the 25%  $\text{NH}_4\text{OH}$  concentration; for the synthesis of 4, 5-dichlorophthalamide from the 33% purchased one 606 milliliters of the 33%  $\text{NH}_4\text{OH}$  was added to 194 milliliters distilled water. The prepared concentration was stored in autoclaved bottle for further usage.

### *3.1.2. Synthesized Materials for Nano-Porous Polymerization:*

---

Due to the local unavailability, several reactants essential for the novel polymeric preparation had to be prepared in the lab and according to the procedures offered by Wohrle et.al. [98], and Ghanem et.al [85].

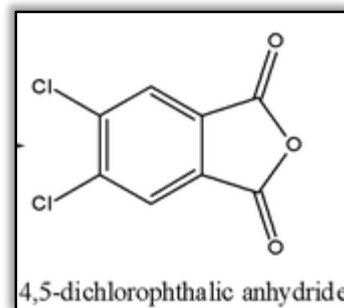
#### *A. Synthesis of 4, 5- Dichlorophthalic anhydride:*

---

In a rounded bottom flask 100 milliliters of acetic anhydride and 55 grams of 4, 5- dichlorophthalic acid (234 mmoles) were heated under reflux for five hours. The reaction mixture was cooled to room temperature, filtered, washed with 90 milliliters petroleum ether (30 milliliters per washing) and dried under vacuum. 44.5 grams (88% Yield) of white to gray crystals have been obtained.

Melting Point: 187°C

FTIR: 2990 and 3080  $\text{cm}^{-1}$  (C-H), 1750  $\text{cm}^{-1}$  (C=O)

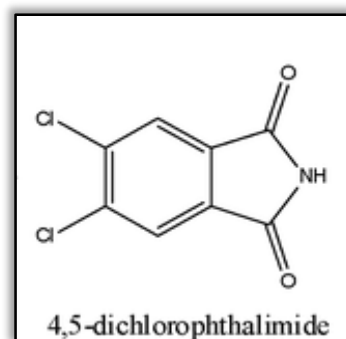


#### *B. Synthesis of 4, 5- Dichlorophthalimide:*

---

4, 5-dichlorophthalimide was also synthesized from the prepared anhydride. In a rounded bottom flask, 40 grams of 4, 5- Dichlorophthalic anhydride (184 mmoles) were suspended in 80 milliliters of formamide and heated under reflux for three hours. After the reaction was complete, the reaction mixture was allowed to cool down to room temperature, filtered under vacuum and washed with distilled water. 31.2 grams (78% Yield) of yellow powder has been obtained.

Melting Point: 196°C

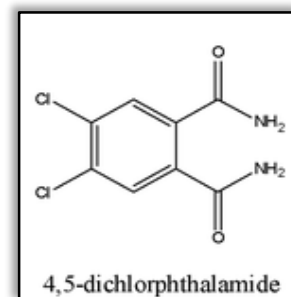


### C. Synthesis of 4, 5- Dichlorophthalamide:

The 4, 5-dichlorophthalamide has been synthesized from the imide through the following procedures. In a conical flask, 28.1 grams of 4, 5- Dichlorophthalimide (130 mmoles) were suspended in 180 milliliters of the prepared 24 % ammonium hydroxide and stirred at room temperature for 24 hours. After the 24 hours, additional 60 milliliters of 24% ammonium hydroxide were added and left to stir at room temperature for another 24 hours. The contents in the flask were filtered, washed with distilled water and dried under vacuum. 11.5 grams (38% Yield) of white solid has been obtained.

Melting Point: 246°C

FTIR: 3400, 3280 and 3175  $\text{cm}^{-1}$  (N-H), 1820 and 1750  $\text{cm}^{-1}$  (C=O)

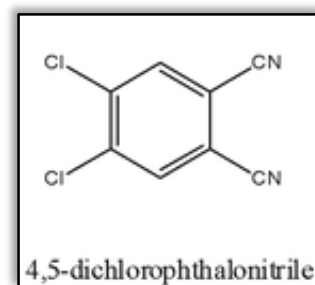


### D. Synthesis of 4, 5- Dichlorophthalonitrile:

4, 5-dichlorophthalonitrile has been synthesized from the amide following the next steps. A conical flask containing 60 milliliters of the prepared dry dimethyl formamide was placed in ice. 40 milliliters of thionyl chloride were added slowly. After the complete addition of thionyl chloride, the reaction was left at 0°C and stirred for 2 hours. This was followed by the addition of 18 grams of 4, 5- Dichlorophthalamide (72.2 mmoles) at 0°C and left to stir for another 5 hours. After 5 hours, the reaction was warmed to room temperature and left to stir for further 24 hours. The flask contents were then poured into ice-cold water and filtered under vacuum. Yellow powder was obtained and was re-crystallized from methanol. 9.8 grams (65% Yield) of yellow crystals has been obtained.

Melting Point: 184°C

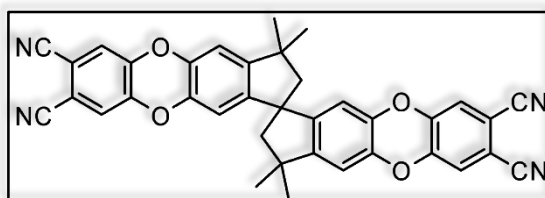
FTIR: 3050 and 3010  $\text{cm}^{-1}$  (C-H), 2240  $\text{cm}^{-1}$  (C-N)



***E. Synthesis of 3,3,3',3'-tetramethyl-2,2',3,3'-tetrahydro-1,1'-spirobi [cyclopenta[b] dibenzo[b,e] [1,4] dioxine]-7,7',8,8'-tetracarbonitrile: (Bisphthalonitrile)***

---

The synthesis of 3,3,3',3'-tetramethyl-2,2',3,3'-tetrahydro-1,1'-spirobi [cyclopenta [b]dibenzo[b,e][1,4]dioxine]-7,7',8,8'-tetracarbonitrile was achieved by the following procedures. In three neck rounded bottom flask 15 grams of 4,5- Dichlorophthalonitrile (76 mmoles) were added to 12 grams of 3,3,3',3'-Tetramethyl-1,1'-spirobiindane-5,5',6,6'-tetrol (35 mmoles) and left to stir under nitrogen. Then 150 milliliters of dry dimethyl formamide and 30 grams of potassium carbonate were added slowly to the solids and left in water bath at 80°C for 3 hours. After the reaction was completed, the contents were filtered, washed, dried and finally recrystallized from methanol and then dichloromethane. 16 grams (80% Yield) of powder has been obtained.



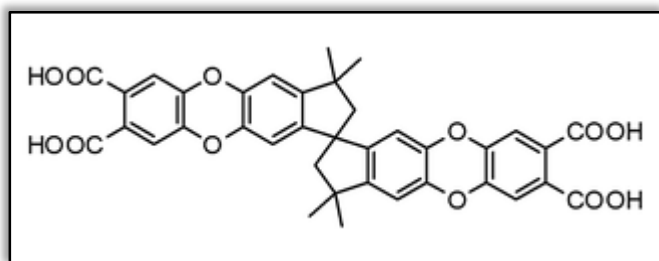
FTIR: 3086 and 3016  $\text{cm}^{-1}$  (C-H, aromatic), 2950 and 2850  $\text{cm}^{-1}$  (C-H, aliphatic), 2240  $\text{cm}^{-1}$  (C-N)

***F. Synthesis of 3,3,3',3'-tetramethyl-2,2',3,3'-tetrahydro-1,1'-spirobi [cyclopenta[b] dibenzo[b,e] [1,4] dioxine]-7,7',8,8'-tetracarboxylic acid:***

---

The 3,3,3',3'-tetramethyl-2,2',3,3'-tetrahydro-1,1'-spirobi [cyclopenta [b] dibenzo [b,e][1,4]dioxine]-7,7',8,8'-tetracarboxylic acid has been synthesized from the tetra-carbonitrile according to the following steps. In a conical flask a solution of 28.2 grams of potassium hydroxide (500 mmoles) in 280 milliliters of ethanol-water mixture (1:1 volume) was stirred and heated under reflux for 20 hours with 14.7 grams of (C) (25 mmoles). The resulting solution was hot-filtered to remove any insoluble particles. After cooling, the filtrate was acidified by

concentrated hydrochloric acid. The resulting precipitate was filtered, washed with cold water (1000 mL) and dried under vacuum. 15.8 grams (95% Yield) of white powder has been obtained.

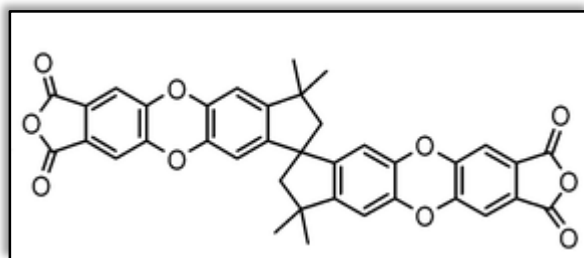


FTIR: 3400  $\text{cm}^{-1}$  (O-H), 3086 and 3016  $\text{cm}^{-1}$  (C-H, aromatic), 2950 and 2850  $\text{cm}^{-1}$  (C-H, aliphatic), 1700  $\text{cm}^{-1}$  (C=O)

### *G. Synthesis of Dianhydride Monomer:*

---

The synthesis of the dianhydride monomer, which is essential for the polymerization, was synthesized as follows: In three neck rounded bottom flask 13.46 grams of (D) (20 mmoles) was added to 105 milliliters of acetic anhydride. The mixture was heated under reflux and nitrogen atmosphere for 24 h. On cooling, the powder was collected by filtration, washed with acetic acid and toluene, and dried at 80° C under vacuum. 6.3 grams (49% Yield) producing pale yellow powder and as reported [85].



FTIR: 3059  $\text{cm}^{-1}$  (C-H aromatic), 2952  $\text{cm}^{-1}$  (C-H aliphatic), 1840 and 1760  $\text{cm}^{-1}$  (C=O)

This finally is the basic monomer that will be allowed to condense with the various purchased diamines for the final synthesis of the sought novel polymers of intrinsic microporosity based on polyimides structures, designated as PIM-PI-01-06.

### ***3.2. Synthesis of Polymers of Intrinsic Microporosity Based on Polyimides Structures (PIM-PIs):***

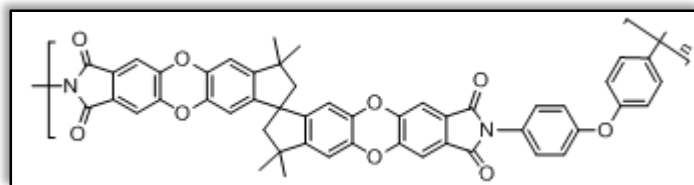
---

The two-step polycondensation reaction for the synthesis of the polymers was carried out as follow: to a 50 mL three neck rounded bottom flask; equipped with a Dean-Stark trap, nitrogen inlet, and reflux condenser, 1.15 grams (1.83mmoles) of the dianhydride monomer and (1.83mmoles) of the diamine, 10 milliliters of m-cresol, and 0.1 milliliters of quinoline and 2 milliliters of anhydrous toluene were added. After the reaction mixture had been stirred at room temperature for 1/2 hour, the temperature was raised gradually to 200° C and was then kept at that temperature for further 5 hours. During this time water was removed from the reaction mixture by azeotropic distillation. The resulting viscous solution was cooled and diluted with 20 milliliters of chloroform and then added drop wise to a vigorously stirred 600 milliliters of methanol. The resulting solid precipitate was collected by filtration, and dried under vacuum [85]. The same procedure was used to prepare all other six PIM-PIs under investigation in this work. In general, all the polymers were prepared using one common anhydride monomer reacted with a different diamine in each case.

#### ***3.2.1. PIM-PI-01:***

---

PIM-PI-01 is based on the reaction of the anhydride monomer with 4, 4'-oxydianiline diamine monomer.



*Color:* off-white

*Yield:* 55%

*FTIR:* 3030 cm<sup>-1</sup> (C-H aromatic), 2952 cm<sup>-1</sup> (C-H aliphatic), 1780 and 1750 cm<sup>-1</sup> (C=O)

*<sup>1</sup>H-NMR:* (CDCl<sub>3</sub>, δppm): 1.33 (6H, s, 2CH<sub>3</sub>), 1.39 (6H, s, 2CH<sub>3</sub>), 2.19 (2H, d, J= 13.5Hz, CH<sub>2</sub>), 2.35 (2H, d, J= 13.5, CH<sub>2</sub>), 6.39 (2H, s, Ar), 6.73 (2H, s, Ar), 7.00-7.54 (10H, m, Ar)



$^{13}\text{C-NMR}$ : ( $\text{CDCl}_3$ ,  $\delta\text{ppm}$ ): 30.09, 31.45 (4 $\text{CH}_3$ ), 43.53 (2 $\text{CH}_2$ ), 57.23 (2C), 59.11 (1C), 112.02, 119.48, 119.65, 127.13, 127.73, 128.19, 140.46, 140.58, 146.35, 147.40, 149.03, 156.43, 166.27 (Aromatic C)

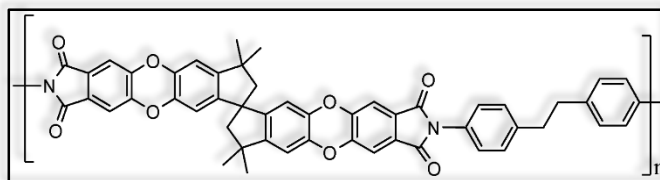
$\text{CHNS}$ :  $\text{C}_{50}\text{H}_{34}\text{N}_2\text{O}_9$  (Repeat Unit); C, 74.34%, H, 4.37%, N, 3.47%. Found: C, 72.65%, H, 4.15%, N, 4.57%

$\text{GPC}$ :  $M_n = 2495.9$ ,  $M_w = 12176$ ,  $M_w/M_n = 4.9$

$\text{XRD}$ : Amorphous

### 3.2.2. PIM-PI-02:

PIM-PI-02 is based on the reaction of the anhydride monomer with 4, 4'-ethylenedianiline diamine monomer.



*Color*: Pale Yellow

*Yield*: 38%

$\text{FTIR}$ : 3030 (C-H aromatic), 2952 (C-H aliphatic), 1780 and 1750 (C=O)

$^1\text{H-NMR}$ : ( $\text{CDCl}_3$ ,  $\delta\text{ppm}$ ): 1.33 (6H, s, 2 $\text{CH}_3$ ), 1.39 (6H, s, 2 $\text{CH}_3$ ), 2.19 (2H, d,  $J = 13.5\text{Hz}$ ,  $\text{CH}_2$ ), 2.35 (2H, d,  $J = 13.5$ ,  $\text{CH}_2$ ), 2.99 (4H, s, 2 $\text{CH}_2$ ), 6.39 (2H, s, Ar), 6.73 (2H, s, Ar), 7.03-7.39 (10H, m, Ar)

$^{13}\text{C-NMR}$ : ( $\text{CDCl}_3$ ,  $\delta\text{ppm}$ ): 30.20, 31.55 (4 $\text{CH}_3$ ), 37.50 (2 $\text{CH}_2$ ), 43.53 (2 $\text{CH}_2$ ), 57.23 (2C), 59.11 (1C), 110.23, 111.98, 126.53, 127.82, 129.18, 129.74, 133.23, 140.49, 140.60, 141.66, 146.34, 147.33, 149.00, 166.31 (Aromatic C)

$\text{CHNS}$ :  $\text{C}_{52}\text{H}_{39}\text{N}_2\text{O}_8$  (Repeat Unit), C, 76.18%, H, 4.79%, N, 3.42%. Found: C, 75.60%, H, 4.65%, N, 4.20%

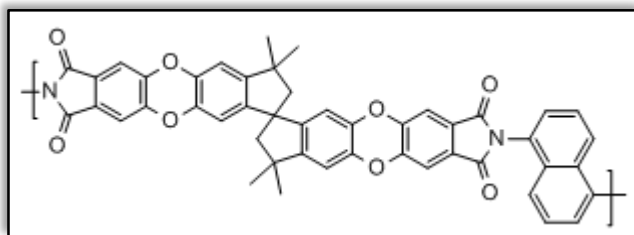
$\text{GPC}$ : Not available

$\text{XRD}$ : Amorphous

### 3.2.3. PIM-PI-03:

---

PIM-PI-03 is based on the reaction of the anhydride monomer with 1, 5-diaminonaphthalene diamine monomer.



*Color:* Green

*Yield:* 36%

*FTIR:* 3030 (C-H aromatic), 2952 (C-H aliphatic), 1780 and 1750 (C=O)

*<sup>1</sup>H-NMR:* (CDCl<sub>3</sub>, δppm): 1.27 (6H, s, 2CH<sub>3</sub>), 1.33 (6H, s, 2CH<sub>3</sub>), 2.12 (2H, d, J= 13.2Hz, CH<sub>2</sub>), 2.29 (2H, d, J= 13.5, CH<sub>2</sub>), 6.35 (2H, s, Ar), 6.69 (2H, s, Ar), 7.27-7.67 (10H, m, Ar)

*<sup>13</sup>C-NMR:* (CDCl<sub>3</sub>, δppm): 30.20, 31.45 (4CH<sub>3</sub>), 43.56 (2CH<sub>2</sub>), 57.27 (2C), 59.08 (1C), 110.31, 112.29, 124.56, 127.97, 129.08, 131.61, 140.46, 140.47, 140.58, 146.41, 147.55, 149.09, 166.56 (Aromatic C)

*CHNS:* C<sub>49</sub>H<sub>36</sub>N<sub>2</sub>O<sub>8</sub> (Repeat Unit), C, 75.37%, H, 4.65%, N, 3.59%. Found: C, 72.71%, 4.35%, 3.86%

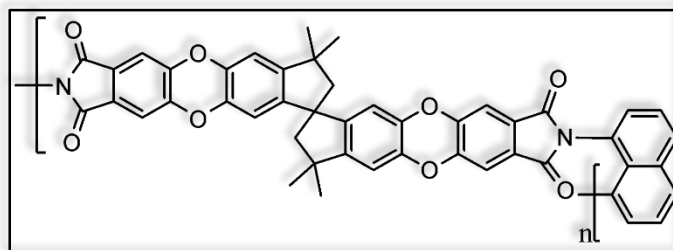
*GPC:* M<sub>n</sub>= 3726, M<sub>w</sub>= 13091, M<sub>w</sub>/M<sub>n</sub>= 3.5

*XRD:* Amorphous

### 3.2.4. PIM-PI-04:

---

PIM-PI-04 is based on the reaction of the anhydride monomer with 1, 8-diaminonaphthalene diamine monomer.



*Color:* Yellow

*Yield:* 86%

*FTIR:* 3030 (C-H aromatic), 2952 (C-H aliphatic), 1780 and 1750 (C=O)

*<sup>1</sup>H-NMR:* (CDCl<sub>3</sub>, δppm): 1.28 (6H, s, 2CH<sub>3</sub>), 1.36 (6H, s, 2CH<sub>3</sub>), 2.19 (2H, d, J= 6 Hz, CH<sub>2</sub>), 2.37 (2H, d, J= 6, CH<sub>2</sub>), 6.43 (2H, s, Ar), 6.76 (2H, s, Ar), 7.10-7.74 (10H, m, Ar)

*<sup>13</sup>C-NMR:* (CDCl<sub>3</sub>, δppm): Not Available

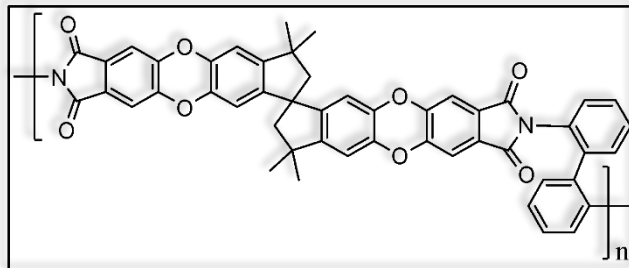
*CHNS:* C<sub>48</sub>H<sub>33</sub>N<sub>2</sub>O<sub>8</sub> (Repeat Unit), C, 75.28%, H, 4.34%, N, 3.66%. Found: C, 67.11%, H, 3.62%, N, 3.75%

*GPC:* M<sub>n</sub>= 3726, M<sub>w</sub>= 13091, M<sub>w</sub>/M<sub>n</sub>= 3.5

*XRD:* Amorphous

### ***3.2.5. PIM-PI-05:***

PIM-PI-05 is based on the reaction of the anhydride monomer with 2, 2'-biphenyldiamine diamine monomer.



*Color:* Green

*Yield:* 76%

*FTIR:* 3030 (C-H aromatic), 2952 (C-H aliphatic), 1780 and 1750 (C=O)

*<sup>1</sup>H-NMR:* 1.33 (6H, s, 2CH<sub>3</sub>), 1.39 (6H, s, 2CH<sub>3</sub>), 2.19 (2H, d, J= 13.5Hz, CH<sub>2</sub>), 2.35 (2H, d, J= 13.5, CH<sub>2</sub>), 6.39 (2H, s, Ar), 6.73 (2H, s, Ar), 7.00-9.04 (10H, m, Ar)

*<sup>13</sup>C-NMR:* (CDCl<sub>3</sub>, δppm): 30.26, 31.59 (4CH<sub>3</sub>), 43.48 (2CH<sub>2</sub>), 57.16 (2C), 59.15 (1C), 109.93, 111.93, 116.16, 121.37, 127.27, 128.52, 128.49, 132.92, 136.32, 139.75, 140.65, 146.33, 147.22, 166.27 (Aromatic C)

*CHNS:* C<sub>50</sub>H<sub>35</sub>N<sub>2</sub>O<sub>8</sub> (Repeat Unit), C, 75.84%, H, 4.46%, N, 3.54%. Found: C, 78.87%, H, 4.60%, N, 3.66%

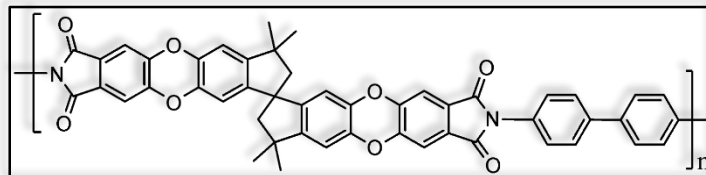
GPC:  $M_n = 3490.2$ ,  $M_w = 32574$ ,  $M_w/M_n = 9.3$

XRD: Amorphous

### 3.2.6. PIM-PI-06:

---

PIM-PI-0 is based on the reaction of the anhydride monomer with benzidine diamine monomer.



Color: Yellow

Yield: 82%

FTIR: 3030 (C-H aromatic), 2952 (C-H aliphatic), 1780 and 1750 (C=O)

$^1\text{H-NMR}$ : ( $\text{CDCl}_3$ ,  $\delta$ ppm): 1.33 (6H, s, 2CH<sub>3</sub>), 1.39 (6H, s, 2CH<sub>3</sub>), 2.19 (2H, d, J= 13.5Hz, CH<sub>2</sub>), 2.35 (2H, d, J= 13.5, CH<sub>2</sub>), 6.40 (2H, s, Ar), 6.74 (2H, s, Ar), 7.10-7.8 (10H, m, Ar)

$^{13}\text{C-NMR}$ : ( $\text{CDCl}_3$ ,  $\delta$ ppm): 30.06, 31.57 (4CH<sub>3</sub>), 43.53 (2CH<sub>2</sub>), 57.25 (2C), 59.11 (1C), 112.06, 126.68, 127.78, 127.97, 131.28, 140.09, 140.48, 140.59, 146.37, 147.47, 149.05, 166.21 (Aromatic C)

CHNS: C<sub>50</sub>H<sub>35</sub>N<sub>2</sub>O<sub>8</sub> (Repeat Unit), C, 75.84%, H, 4.46%, N, 3.54%. Found: C, 75.09%, H, 4.51%, N, 3.41%

GPC: Not Available

XRD: Amorphous

### *3.3. Characterization Techniques:*

---

Different characterization Techniques have been used to determine both the chemical and physical properties of the synthesized PIM-PIs. In this section complete presentation for the techniques used and their parameters will be discussed.

#### *3.3.1. Fourier Transform Infrared Spectroscopy (FTIR):*

---

Thermo-Scientific, Nicole iS10 FTIR at the Center of Materials Science, Zewail City shown in Figure 3.1 was used to reveal and confirm the chemical structures of the prepared materials. First, the infrared source was allowed to collect the background peaks, and then few milligrams of grinded powder were added to the surface of the diamond to be collected. All the synthesized chemicals were analyzed in the wavelength range from 400-4000  $\text{cm}^{-1}$  wavenumber.



*Figure 3.1* Fourier Transform Infrared Spectroscopy, the Center of Materials Science, Zewail City.

#### *3.3.2. Nuclear Magnetic Resonance Spectroscopy (NMR):*

---

Few milligrams of the synthesized polymers were dissolved in  $\text{CH}_3\text{Cl}$  and sent to the Institute of Chemical Warfare to be analyzed for obtaining  $^1\text{H}$ -NMR at 400 MHz and  $^{13}\text{C}$ -NMR spectra at 100 MHz. All chemical shifts are reported as parts per million ( $\delta$ ) using tetramethylsilane (TMS) as internal standard.

### ***3.3.3. Elemental Analysis (CHNS/O):***

---

Thermo-Scientific, FLASH 2000 CHNS/O analyzer at the Center of Materials Science, Zewail city shown in Figure 3.2 were employed to calculate the percentages of carbon, hydrogen, nitrogen and oxygen. About 3 milligrams of each polymer in specific capsule were weighed on the sensitive balance, and placed into the auto-sampler, in case of C, H and N a tin capsule was used. The sample was combusted in the left furnace at 950°C in order to calculate the carbon, hydrogen and nitrogen percentages. The carrier gas was helium, with flow rate 140ml/min. The percentages of C, H, and N calculated for each polymer was compared to that expected theoretically.

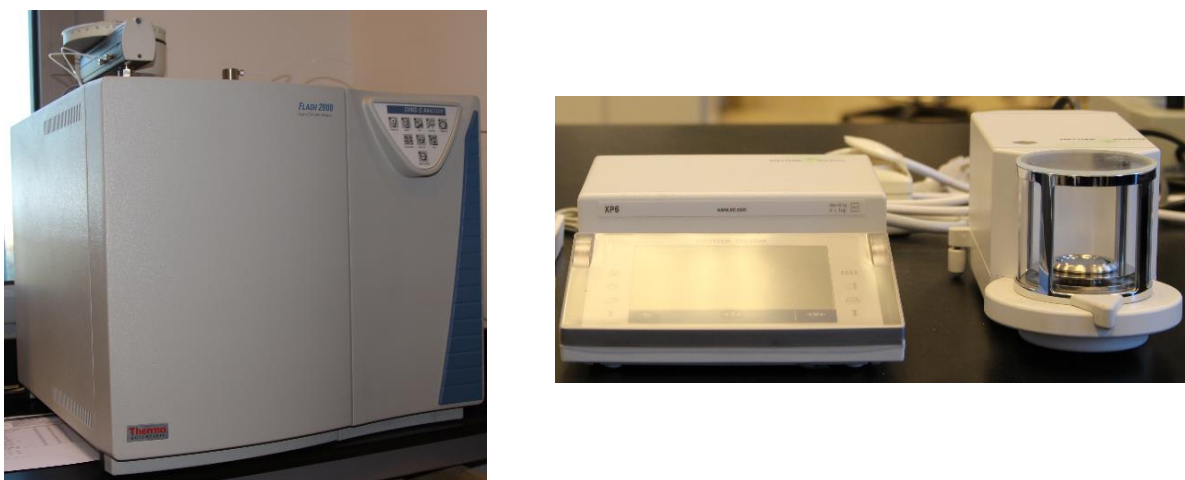


*Figure 3.2 (a) The Elemental Analyzer Flash 2000 (b) Sensitive Balance, at the Center of Materials Science, Zewail City.*

### ***3.3.4. Powder X-ray Diffraction (XRD):***

---

Powder x-ray diffraction (PXRD) patterns of the samples were obtained using a D8 Bruker x-ray powder diffractometer shown in Figure 3.3 at the chemistry department, American University in Cairo (AUC). The PXRD patterns of the samples were obtained for a 2theta range between 5° and 80° (step increment: 0.03 per 1 sec).

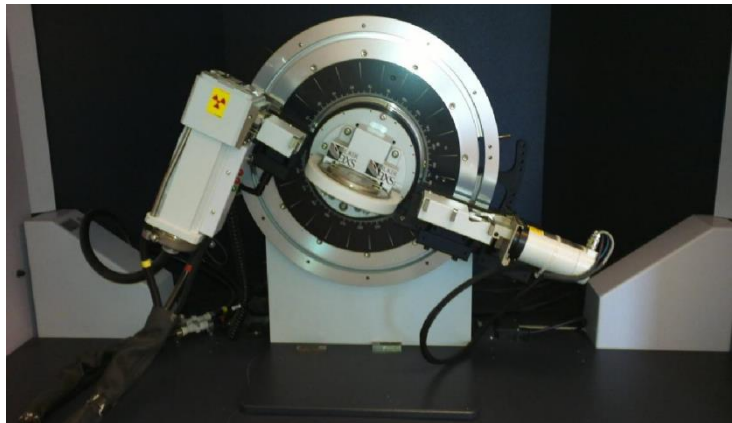


Figure 3.3 Powder X-Ray Diffractometer, at the Chemistry Department, AUC.

### ***3.3.5. Gel Permeation Chromatography (GPC):***

---

About 20 milligrams of each synthesized polymer was sent to the National Research Center to determine their molar mass, molecular weight and poly-dispersity using Agilent 1100 series, Germany, detector; refractive index. 0.01 grams of each sample was dissolved in 2 milliliters of THF, and filtrated using syringe filter 0.45 micron before being placed in the GPC device. The samples were compared to poly-styrene standard; PL-gel particle size (5 $\mu$ m), 3 columns of pore type (100, 104, 105 A $^{\circ}$ ) on series, length 7.5x 300 mm (Mw1000, 4000000).

### ***3.3.6. Thermaogravimetric Analysis (TGA):***

---

The thermal stability profiles of the different polymers were revealed using Thermogravimetric Analysis (TGA Q50, TA Instruments) shown in Figure 3.4 at the Center of Materials Science, Zewail City. Five milligrams of each polymer were placed in the platinum pan and tested under a 60 ml/min purge of nitrogen. The samples were then heated up to 700 $^{\circ}$ C at a rate of 10 $^{\circ}$ C /min.



Figure 3.4 TA Instruments, TGA Q50, Center of Materials Science, Zewail City.

### ***3.3.7. Nitrogen Adsorption Analysis (BET):***

---

Nitrogen adsorption/desorption isotherms were measured using the Micromeritics ASAP 2020 surface area and porosimetry analyser shown in Figure 3.5 at the Center of Materials Science, Zewail City. These isotherms were analyzed in order to obtain both the Brunauer–Emmett–Teller (BET), Langmuir surface area, pore volume and pore size distribution in all the synthesized polymers. 20-50 milligrams of the samples were degassed at 120°C with a rate 1°C/min and 10µmHg pressure with a rate 5mmHg/sec. This was followed by the analysis of the degassed samples using N<sub>2</sub> gas at 77 K (liquid nitrogen).

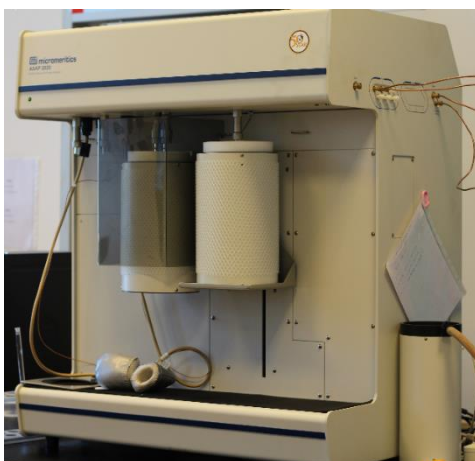


Figure 3.5 Micromeritics ASAP 2020 Surface Area and Porosimetry Analyzer, Center of Materials Science, Zewail City.



### *3.3.8. Carbon Dioxide Adsorption Analysis:*

---

Carbon dioxide isotherms were measured using the Micromeritics ASAP 2020 surface area and Porosimetry analyzer at the Center of Materials Science, Zewail City. However, in these analyses the temperature was controlled by means of a chiller filled with water and ethylene glycol mixture (10% ethylene glycol). The analysis was carried out at three different temperatures, namely 0°C, 10°C and 20°C.

## Chapter 4:

# **Results and Discussion**

## *4. Results and Discussion:*

---

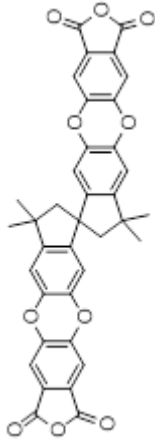
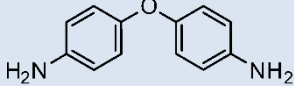
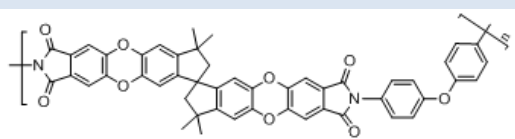
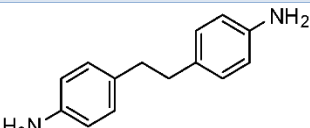
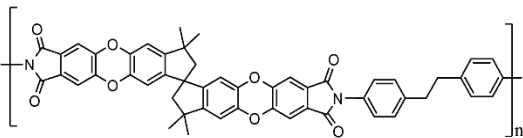
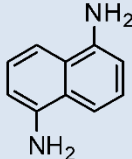
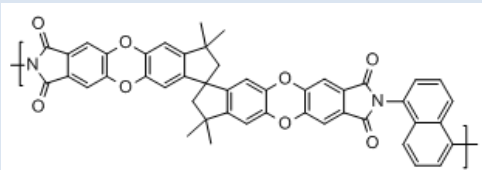
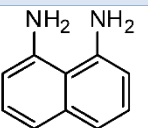
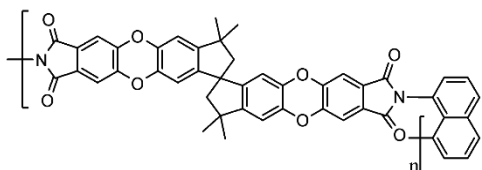
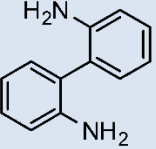
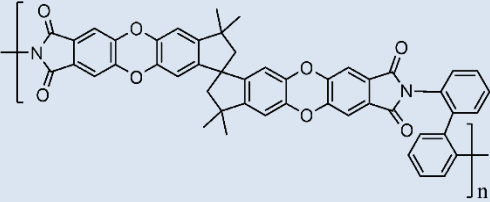
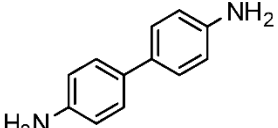
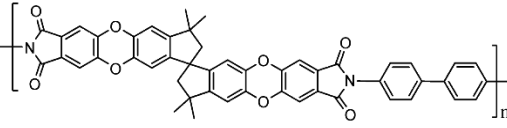
### *4.1. Structural Analysis of the Synthesized PIMs-PIs:*

---

The aim of the synthesis procedures is to prepare different polymers that will possess certain surface area and porosity in order to be used for gas separation and adsorption. Therefore, a complete analysis needed to be done to characterize the synthesized polymeric structures. Different Techniques were used to study the structure of the synthesized polymers such as FTIR, NMR, CHNS, GPC and XRD. First, preparation of a dianhydride monomer was essential as to be able to carry out the poly-condensation polymerization.

Poly-condensation polymerization is the classical method used to synthesize a polymer from dianhydride and aromatic diamine monomers. In this study, different diamine moieties were used to produce six different polymers, of which five are novel structures and the sixth polymer was synthesized to provide a means for comparison with physical data available in the literature. In this study, the polymers have taken the abbreviation PIM-PI and are numbered from 01-06 (the one that has been synthesized previously is given the code name PIM-PI-03) .The difference in the aromatic diamines has been carefully considered to provide major variation in the conformational behavior as to allow to investigate the influence of the polymeric microstructures on the creation of the intrinsic microporosity, chain mobility, gas adsorption, gas permeability and local packing using both physical characterization techniques as well as molecular modeling procedures. As shown in Table 4.1, PIM-PI-01 and PIM-PI-02 have the diamine groups separated either by oxygen or ethylene groups which might result in some flexibility in the polymer chains as will be discussed in chapter 6. However for the PIM-PI-04, 05, and 06 the diamines have fused aromatic rings in different orientations which might result in a certain degree of conformational inflexibility. Therefore, complete chemical characterization were needed to allow understanding the correlation between the polymeric structures and ultimate physical properties.

Table 4.1 The Synthesis of PIM-PIs.

Name	Dianhydride Monomer	Diamine Monomer	Repeat Unit
PIM-PI-01		 4,4'-oxydianiline	
PIM-PI-02		 4,4'-ethylenedianiline	
PIM-PI-03		 1,5-diaminonaphthalene	
PIM-PI-04		 1,8-diaminonaphthalene	
PIM-PI-05		 2,2'-biphenyldiamine	
PIM-PI-06		 Benzidine	

### 4.1.1. Fourier Transform Infrared Spectroscopy (FTIR):

As shown in Figure 4.1, the dianhydride monomer was synthesized from its corresponding acid as a dehydrating agent. FTIR analysis was used to ensure the appropriate conversion of the tetra-carboxylic acid to the dianhydride monomer as shown in Figure 4.2. The dianhydride monomer spectrum shows a complete disappearance of the broad peak of the (O-H) stretching at  $3400\text{ cm}^{-1}$  as was expected. In addition, the shift in the peaks at  $1840$  and  $1760\text{ cm}^{-1}$  account for the formation of the carbonyl (C=O) stretching of the anhydride group.

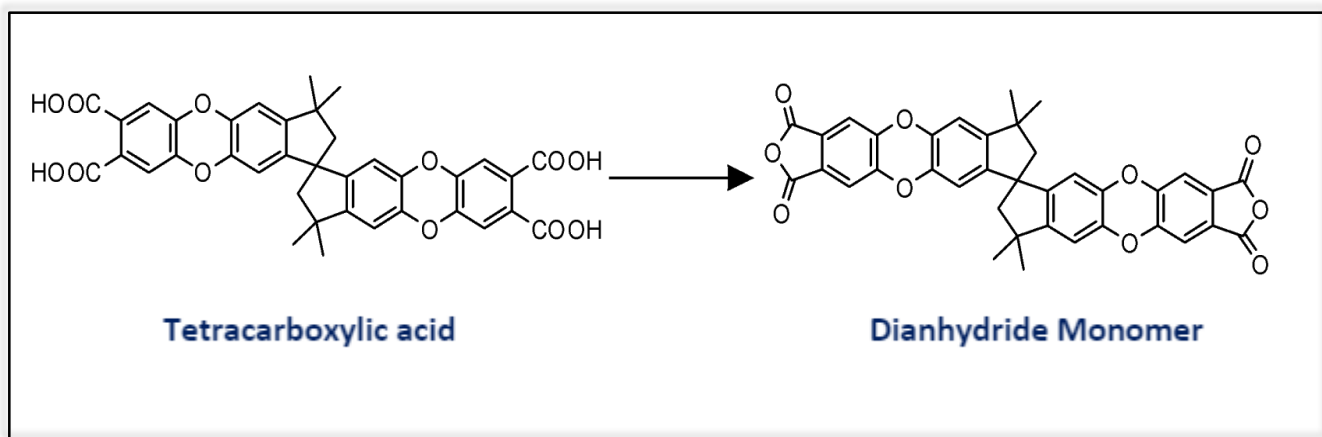


Figure 4.1 The Synthesis of the Dianhydride Monomer.

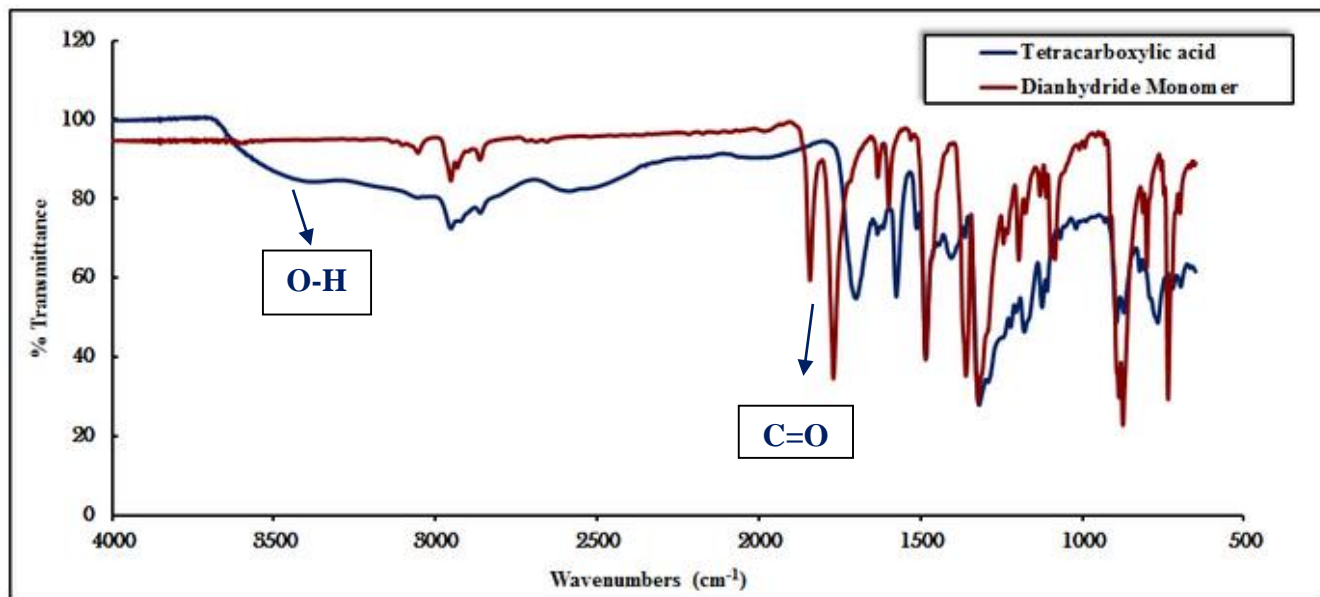


Figure 4.2 The FTIR spectra of tetracarboxylic acid (—) and dianhydride monomer (—).

FTIR was also used to characterize the chemical structure of the PIMs-PIs in comparison to the chemical structure of the dianhydride monomer to assure their appropriate conversion. The method that was followed in order to produce the polyimides is the classical method at which nucleophilic substitution reaction occurs. In this case, the amine attacks one of the carbonyl carbons and displaces the carboxylate group followed by proton transfer. This reaction yield was around 36% for PIM-PI-03 to 86% for PIM-PI-04.

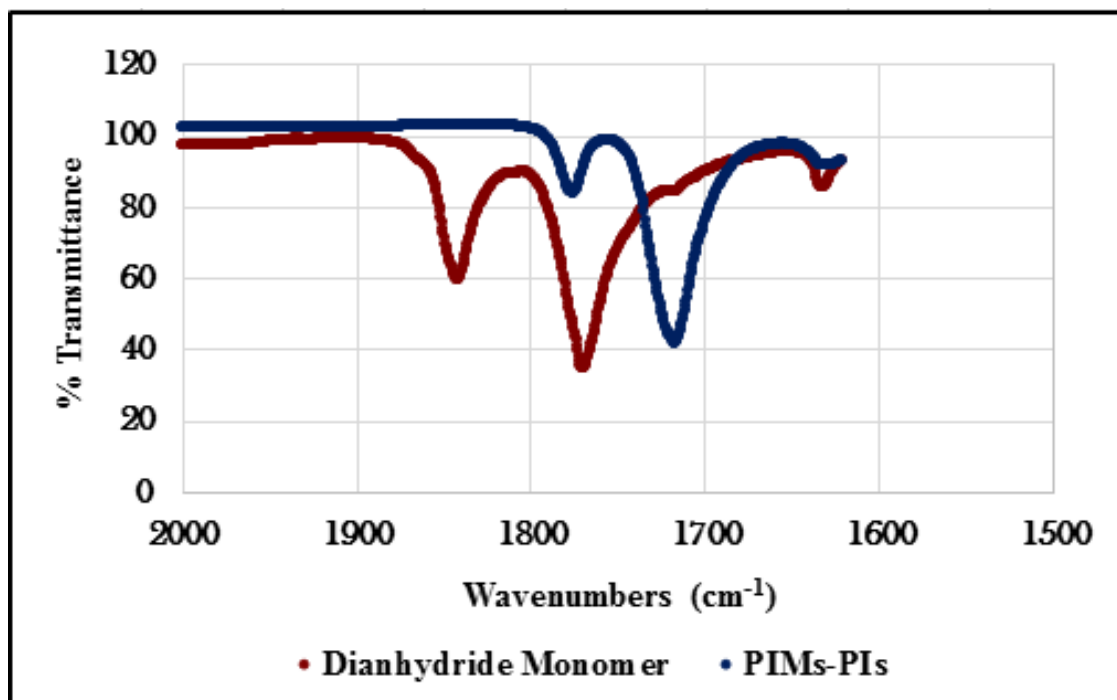


Figure 4.3 The FTIR spectra of the PIMs-PIs (—) and the dianhydride monomer (—).

Confirmation of their synthesis was revealed through FTIR analysis and by comparing the spectra of the six PIMs-PIs with the dianhydride monomer as shown in Figure 4.3. The absence of any peaks in the range of 3000-3500  $\text{cm}^{-1}$  accounts for the formation of tertiary amine ( $\text{R}_3\text{-N}$ ). The shifting in the carbonyl ( $\text{C=O}$ ) peaks from 1840 and 1760  $\text{cm}^{-1}$  to lower wavenumbers 1780 and 1750  $\text{cm}^{-1}$  assures the substitution of the oxygen atom of the anhydride with the nitrogen of the diamines.

#### *4.1.2. Nuclear Magnetic Resonance Spectroscopy (NMR):*

---

Both H-NMR and C-NMR were employed to follow the nucleophilic substitution reaction between the dianhydride and the diamine monomers. In H-NMR, singlets in ranges of 1.33 and 1.39 have been found in all the synthesized polymers. This represents 12 H atoms in the 4 methyl groups and thus confirming the presence of the methyl groups. Moreover, the duplicates in the ranges of 2.19 and 2.35 which represents the 4 H atoms of the 2 methyl groups in the spiro rings also confirms the presence of the spiro center. In addition, the singlets in ranges of 6.39 and 6.73 represent the 4 H atoms in the aromatic rings of the dianhydride monomer. All the peaks ensures that the dianhydride monomer remained unchanged except through the condensation reaction with the diamine monomer which has been presented through the different multiple peaks found from the range 7 to 9 and differs according to the type of diamine used.

Additionally, the C-NMR were employed to fully confirm the obtained structures. Singlet peaks have been observed in ranges of 30, 31, 43, 57, and 59 which represents 2 CH<sub>3</sub>, 2 CH<sub>3</sub>, 2 CH<sub>2</sub>, 2 C and 1 C respectively. These carbons are related to the dianhydride monomer. The reactions of the dianhydride monomer with the diamines have been confirmed through the number of peaks found in the range from 110 to 170. Interestingly, the significant singlet peak appeared in the range of 166 in all the synthesized polymers confirms the unchanged carbonyl groups.

#### *4.1.3. Elemental Analysis (CHNS):*

---

Percentages of the C, H, and N elements were evaluated for each synthesized PIM-PI and compared to those calculated as shown in table 4.2. It was observed that all the values were within the expected range. Only a small reduction in the carbon percentage was observed in all the polymers which might be due to an incomplete combustion. This might also be attributed to the thermal stability obtained from the carbon concentrated rigid structure.

Table 4.2. Comparing the percentages of C, H, N and O calculated (Expected) to those determined (Found) using the Elemental Analyzer (Flash 2000, CHNS/O).

PIM-PI	Carbon %		Hydrogen %		Nitrogen %	
	<i>Expected</i>	<i>Found</i>	<i>Expected</i>	<i>Found</i>	<i>Expected</i>	<i>Found</i>
<b>01</b>	74.34%	72.65%	4.37%	4.15%	3.47%	4.57%
<b>02</b>	76.18%	75.60%	4.79%	4.65%	3.42%	4.20%
<b>03</b>	75.37%	72.71%	4.65%	4.35%	3.59%	3.86%
<b>04</b>	75.28%	69 %	4.34%	3.75%	3.66%	3.9%
<b>05</b>	75.84%	78.87%	4.46%	4.60%	3.54%	3.66%
<b>06</b>	75.84%	75.09%	4.46%	4.51%	3.54%	3.41%

#### ***4.1.4. Gel Permeation Chromatography (GPC):***

---

GPC was used to evaluate the molecular weights of the synthesized polymers. THF solvent was used to solubilize the polymers during the evaluation procedures. However, this could not be achieved with PIM-PI-02 and PIM-PI-06 due to their insolubility in THF. As shown in Table 4.3 different number-average molecular weights (Mn) and weigh average molecular weights (Mw) were obtained depending on the reactivity of the monomers as well as the reaction conditions. PIM-PI-01 possessed the lowest molecular weights, this is due to the presence of electron withdrawing group between the diamine rings. This would lower the basicity of the diamine unit and consequently its reactivity towards the dianhydride monomer, resulting in lower molecular weights. This agrees with what Liaw et.al [30], and Thomas et.al [31], have mentioned. The polydispersity index is also calculated as shown in the table.



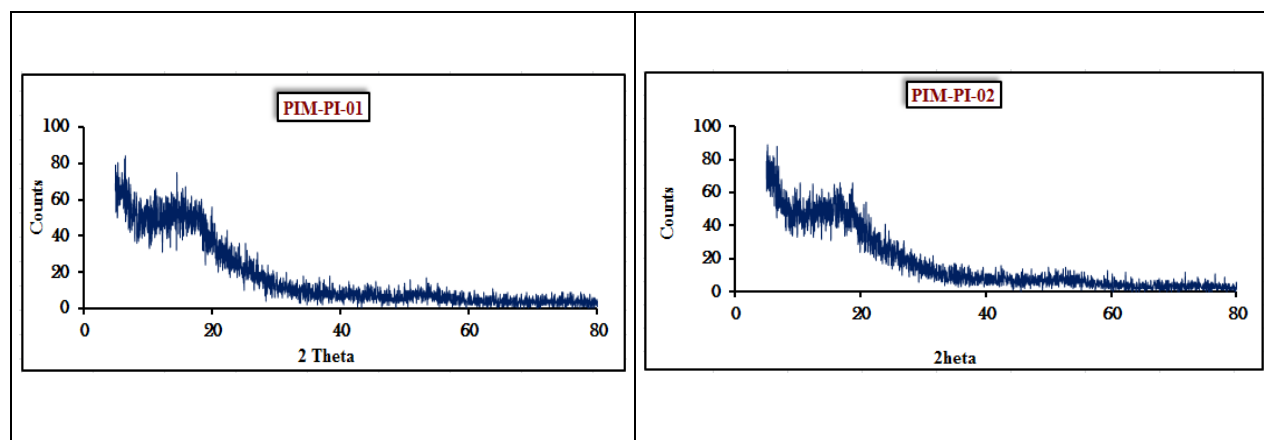
Table 4.3. Gel Permeation Chromatography (GPC) Analysis in tetra-hydro-furan (THF).

PIM-PI	Repeat Unit Formula	Mn g.mol <sup>-1</sup>	Mw g.mol <sup>-1</sup>	Poly-dispersity (PDI) (Mw/Mn)
<b>01</b>	$C_{50}H_{35}N_2O_9$	2495.9	12176	4.8
<b>02</b>	$C_{52}H_{39}N_2O_8$		N/A*	
<b>03</b>	$C_{49}H_{36}N_2O_8$	3726.5	13091	3.5
<b>04</b>	$C_{48}H_{33}N_2O_8$	12006	49386	4.1
<b>05</b>	$C_{50}H_{35}N_2O_8$	3490.2	32574	9.3
<b>06</b>	$C_{50}H_{35}N_2O_8$		N/A*	

\* The material is insoluble in the solvent THF used for the analysis.

#### 4.1.5. Powder X-Ray Diffraction (XRD):

Powder X-ray diffractograms of the polymeric samples proved an amorphous structure to all with no obvious crystallinity except for PIM-PI-04 and PIM-PI-06 where a slight chains ordering could be argued as presented in Figure 4.4.



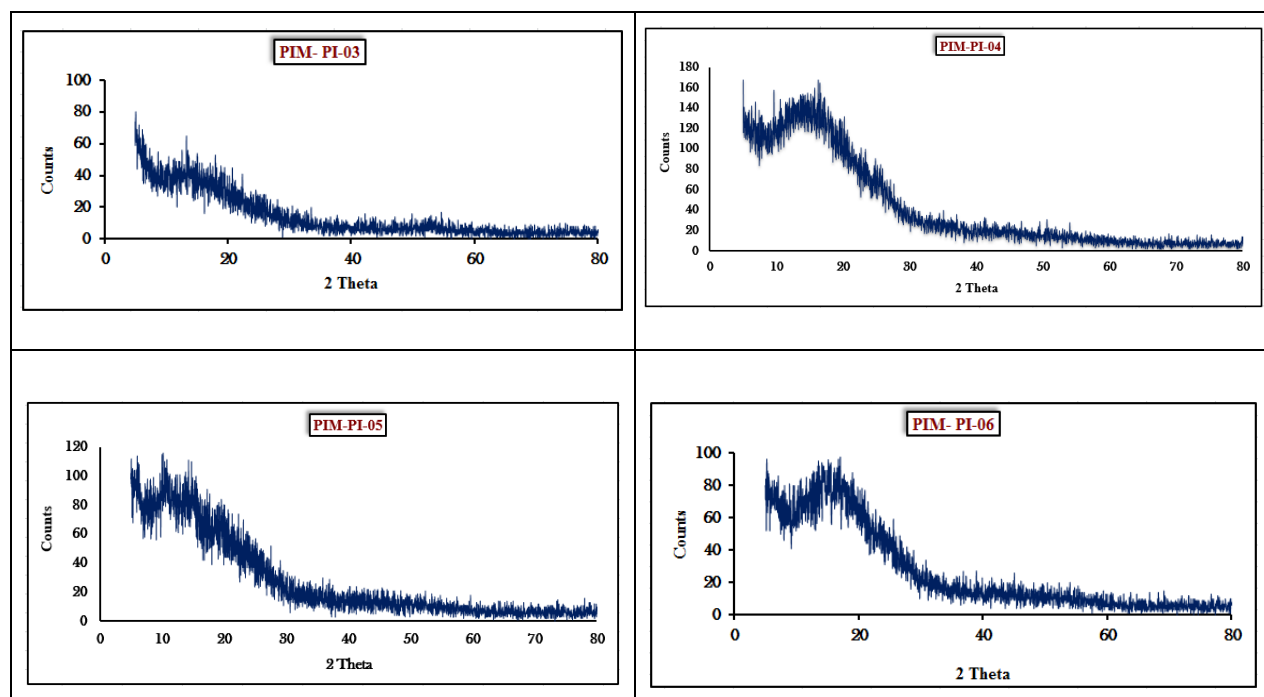


Figure 4.4 Powder X-ray Diffraction analysis for PIM-PIs.

#### ***4.2. Performance Analysis of the Synthesized PIMs-PIs:***

In this section the results for the thermal stability, surface area, porosity and gas adsorption of the synthesized PIM-PIs is presented and discussed. The purpose behind synthesizing the PIM-PIs is to gain a deep understanding their structure-property relationship as to facilitate their development as nanoporous membranes for gas adsorption and separation. Consequently, specific properties related to this application need to be investigated. Adsorption and/or separation of gases under the application of high pressures usually result in considerable temperature increase. Therefore, it is essential to evaluate the thermal stability of the synthesized polymers. Moreover, the hypothesis made by Mckweon that the presence of spiro center hinders the freedom of polymeric chain to rotate and thus resulting in nano-porous structures. The study of the surface areas and porosity of these nanoporous polymers is also essential for the evaluation of the influence of the molecular structures on the conformational behavior of the polymers and its subsequent ability to create nanoporous voids within the polymeric matrix.

### 4.2.1. Thermal Gravimetric Analysis:

Thermogravimetric analysis (TGA) was used to evaluate the thermal stability of the synthesized polymers. All prepared polymers showed high single degradation temperature ranging from 450 to 550°C due to the presence of highly stable imide group. However, PIM-PI-03, PIM-PI-05 and PIM-PI-06 showed an additional weight loss within the range of 100-120°C, Figure 4.5, possibly due to the trapped toluene molecules (B.P. 110°C) used in the synthesis process. The presence of this additional weight loss performed by PIM-PI-03, PIM-PI-05 and PIM-PI-06 could be related to the possessed low pore size as compared to other polymers.

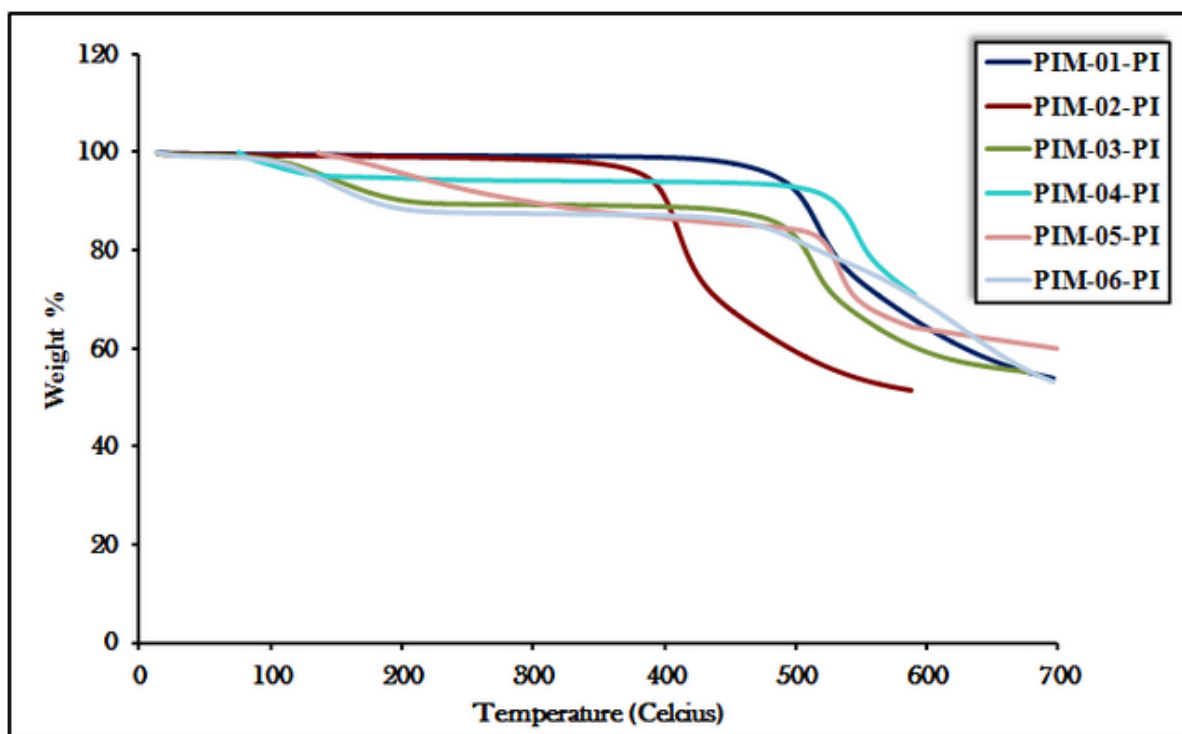


Figure 4.5 Thermal Gravimetric Analysis for PIM-PIs.

As shown in Figure 4.5 PIM-PI-02 possessed the lowest weight loss temperature, however PIM-PI-04 showed the highest weight loss temperature. This might be due to the difference in the diamine units present in each polymer. In case of PIM-PI-02, the diamine was 4, 4'-ethylenediamine, which consists of two phenyl rings separated by the flexible ethylene group whereas the diamine group of PIM-PI-04, was 1, 8'-diaminonaphthalene which contains a

fused ring structure. In general, the apparent thermal stability of the PIMs-PIs series are exhibiting fair values of stability against temperature increase basically due to the presence of imide groups and the skeletal arrangements of the benzene ring.

#### *4.2.2. Nitrogen Adsorption Analysis:*

---

The nitrogen adsorption isotherms obtained at 77 K was used to evaluate the surface area and porosity of the synthesized polymers. They present significant adsorption at low relative pressure, which is an indication for micro-porosity. Moreover, they have shown increasing uptake with increasing relative pressure and the desorption curve lies well above the adsorption curve for all samples leading to significant hysteresis extended to low relative pressure, which might be due to the tortuosity of the pore structure. However, the isotherm showed more characteristics to type IV isotherms, which indicates mesoporosity, Figures 4.6-4.11. This indicates that the polymers might be having both micro-pores and mesopores within its structure depending on the local packing of the polymer molecules.

As shown in Table 4.4 The apparent BET surface areas were determined to be in the range 360- 510 m<sup>2</sup>/g (except for PIM-PI-01 and PIM-PI-02, which were characterized with 61 and 81 m<sup>2</sup>/g respectively) using a multipoint BET calculation, indicating a highly mesoporous polymers. The total pore volume was also determined and calculated from the amount of nitrogen adsorbed at a relative pressure  $p/p^{\circ} = 0.98$  and was found to be in the range of 0.4-0.59 cc/g (except for PIM-PI-01 and PIM-PI-06, which were found to possess total pore volume 0.08 and 0.23 cc/g respectively).

Table 4.4 The BET Surface Areas and Pore Volume of PIM-PIs.

PIM-PI	BET Surface Area (m <sup>2</sup> /g)	Pore Volume (cm <sup>3</sup> /g)
<i>PIM-PI-01</i>	61	0.08
<i>PIM-PI-02</i>	81	0.23
<i>PIM-PI-03</i>	362	0.40
<i>PIM-PI-04</i>	508	0.59
<i>PIM-PI-05</i>	506	0.57
<i>PIM-PI-06</i>	450	0.47

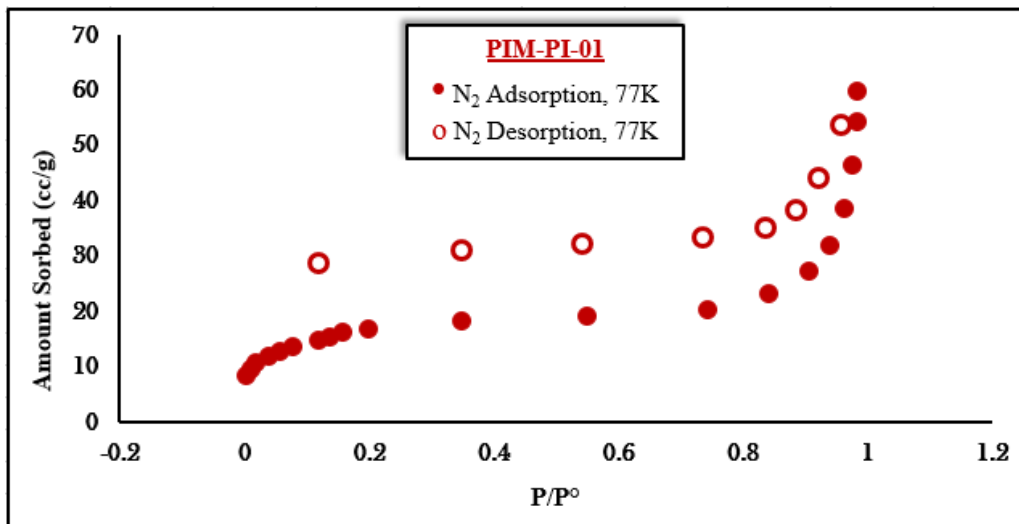


Figure 4.6 The N<sub>2</sub> isotherm for PIM-PI-01.

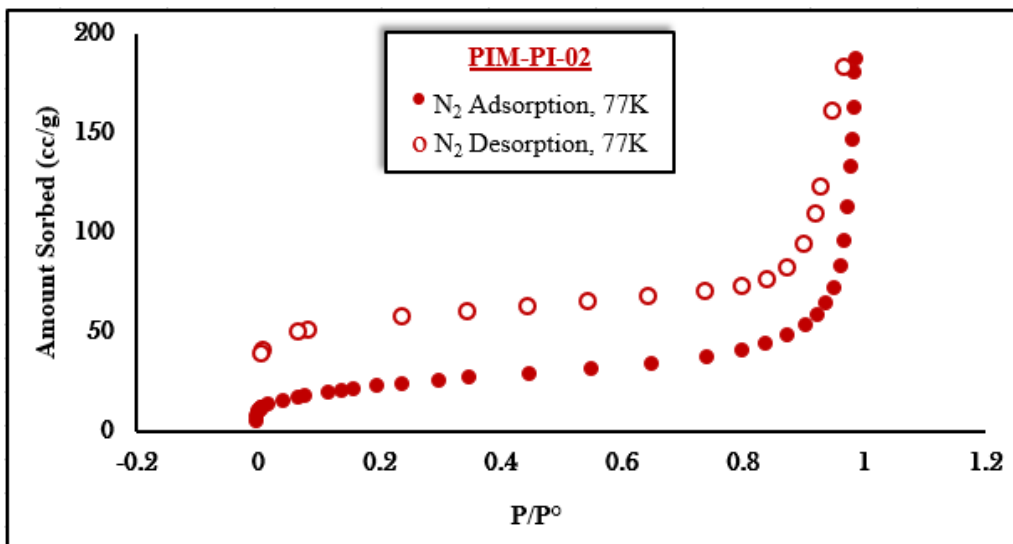


Figure 4.7 The  $N_2$  isotherm for PIM-PI-02.

The above data contradict the hypothesis made by Mckweon recently that the presence of a spiro center in a rigid backbone is the main reason for the porosity observed in these high porous polymers. This is since both PIM-PI-01 and PIM-PI-02 have spiro centers but possess very low surface area and pore volume as compared to the other polymers. The high porosity was not only dependent on the spiro containing monomer but also on the structure of the diamine group. Both PIM-PIs consists of flexible diamine groups, namely, 4, 4'-oxydianiline and 4, 4'-ethylenedianiline respectively. Those flexible structures resulted in less rigid backbone, and less ability of the polymer chains to pack space efficiently which resulted in polymers with limited porosity. In contrast, to the diamines Mckweon and Ghanem [28,85] used mostly fused rings structures or rings with bulky side chains which was one of the main reasons for obtaining high porous polymers.

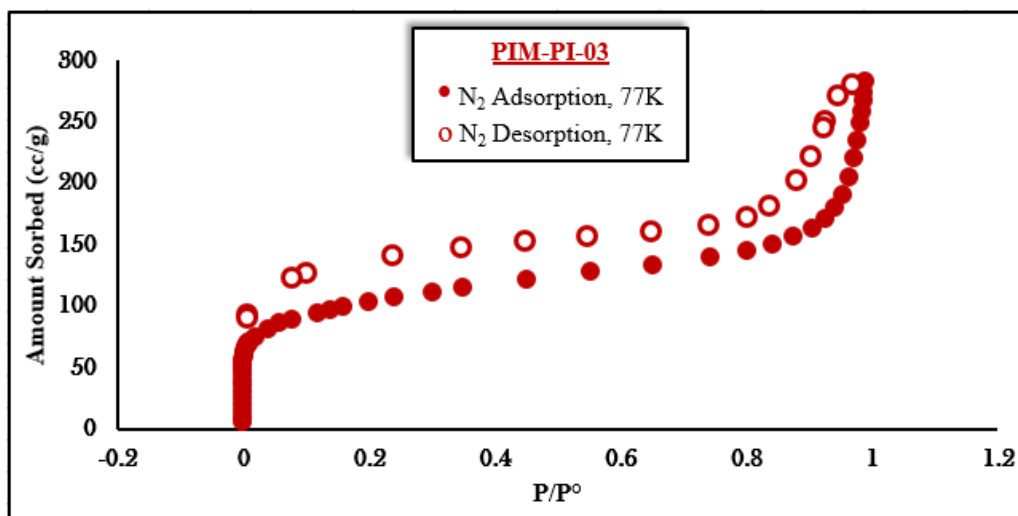


Figure 4.6 The N<sub>2</sub> isotherm for PIM-PI-03.

On the other hand, PIM-PI-04, 05 and 06 showed high surface area and porosity, in Figure 4.9, 4.10 and 4.11. This confirms that the diamine monomer plays a fundamental role in the porosity formed within the synthesized polymers. They were synthesized from the spiro center monomer and 1, 8-diaminonaphthalene, 2, 2'-biphenyldiamine and benzidine, respectively. As it is observed they are either composed of fused rings or rigid rings. Those rigid diamine structures resulted in hindering the free rotation of the polymer backbone and diminishing the ability of these chains to pack space efficiently leading to the formation of these micro- and nanopores within the polymeric matrix.

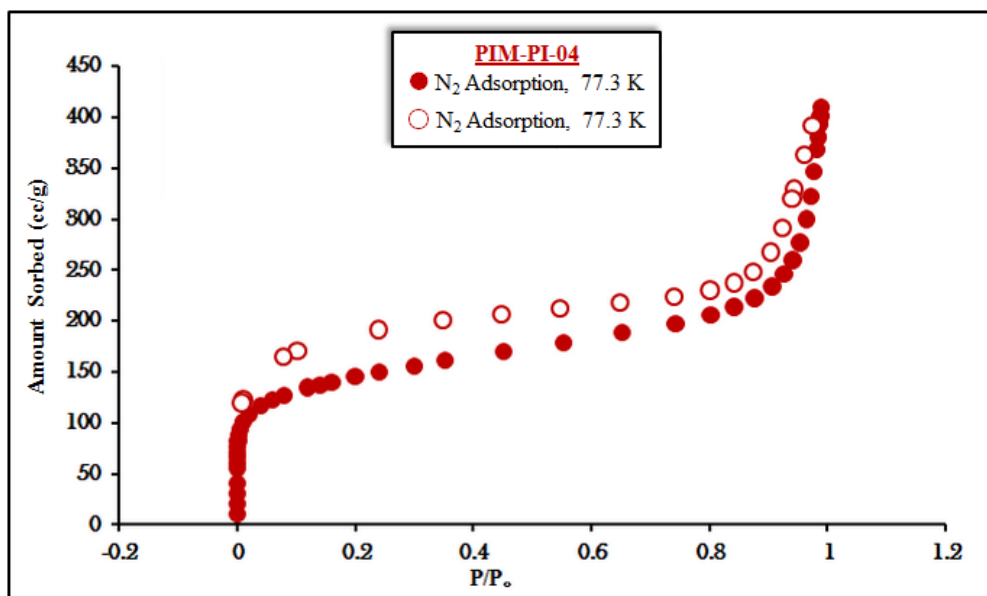


Figure 4.9 The N<sub>2</sub> isotherm for PIM-PI-04.

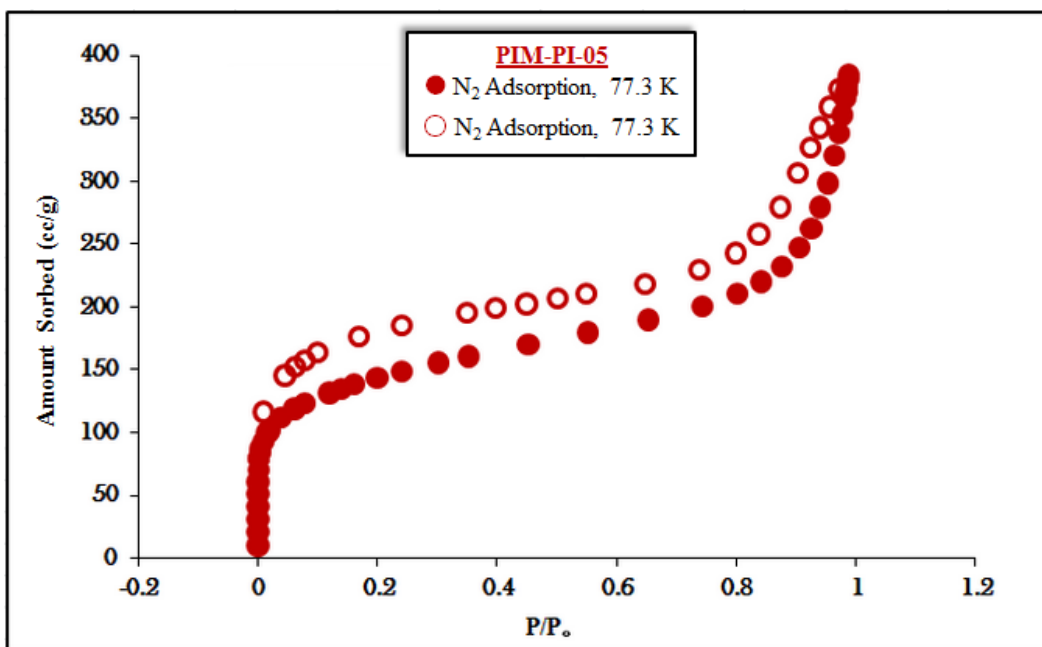


Figure 4.10 The N<sub>2</sub> isotherm for PIM-PI-05.



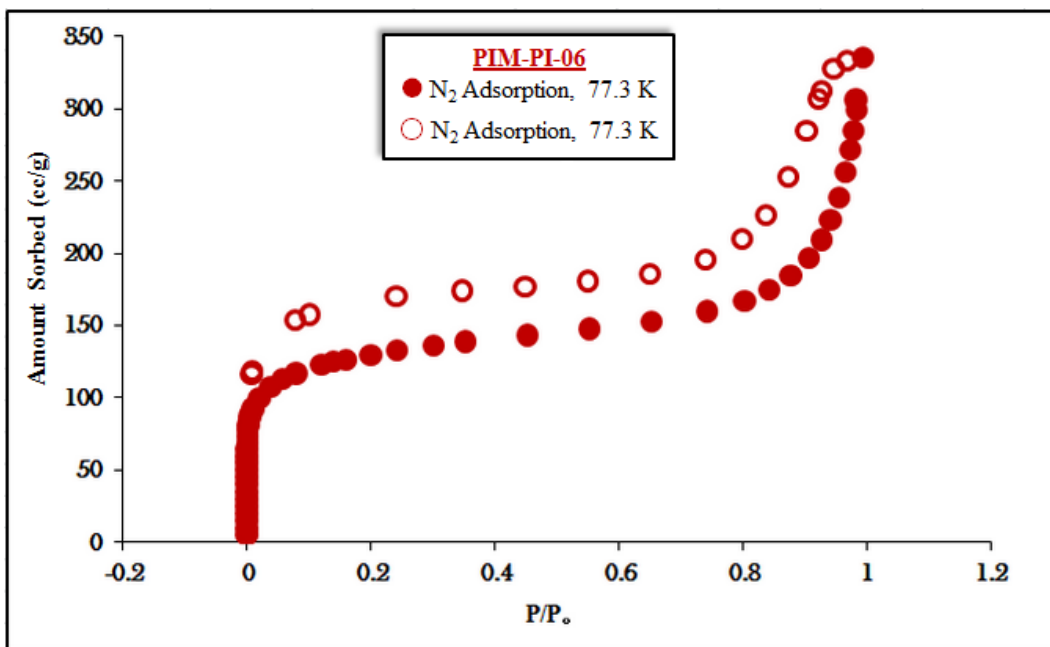
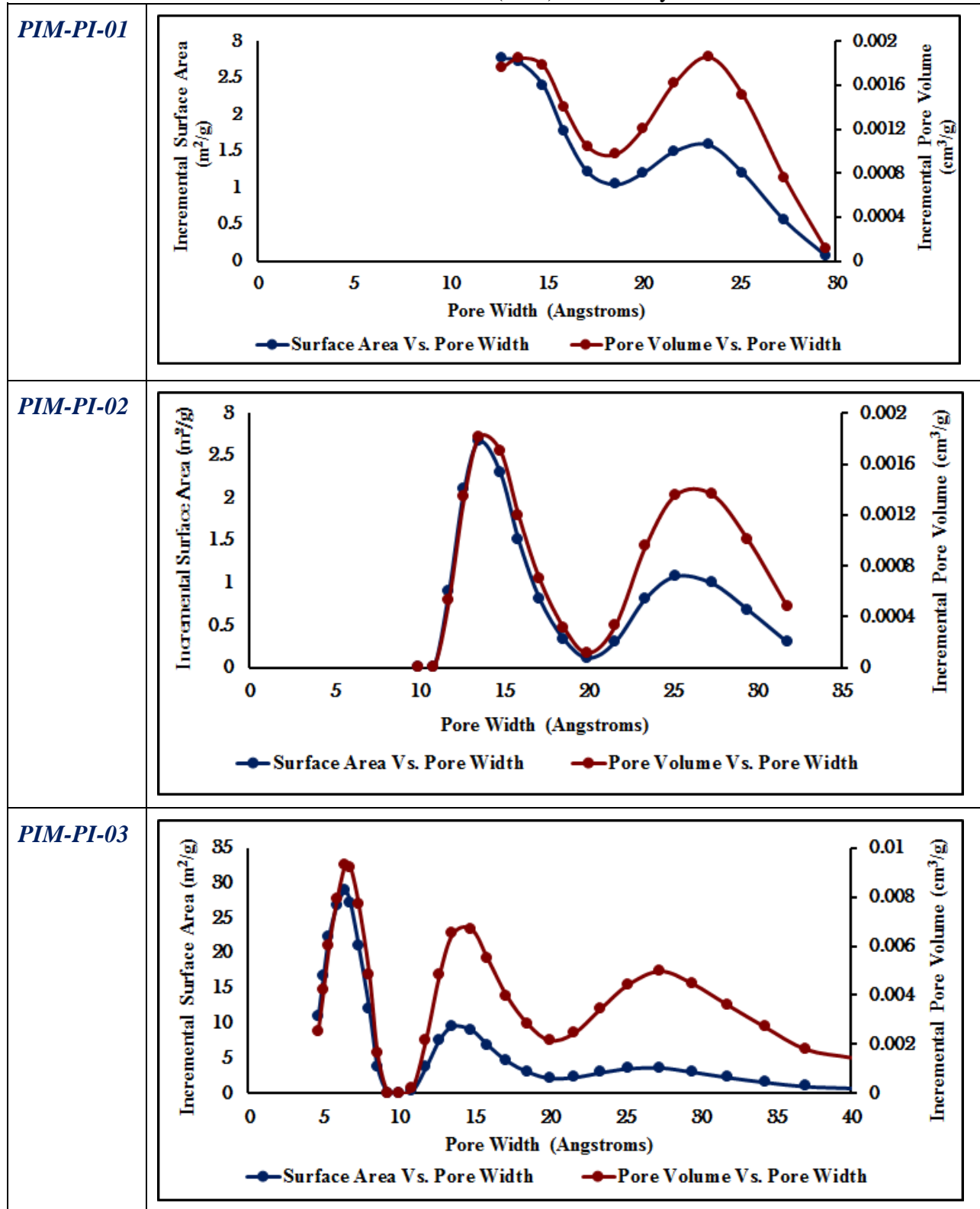


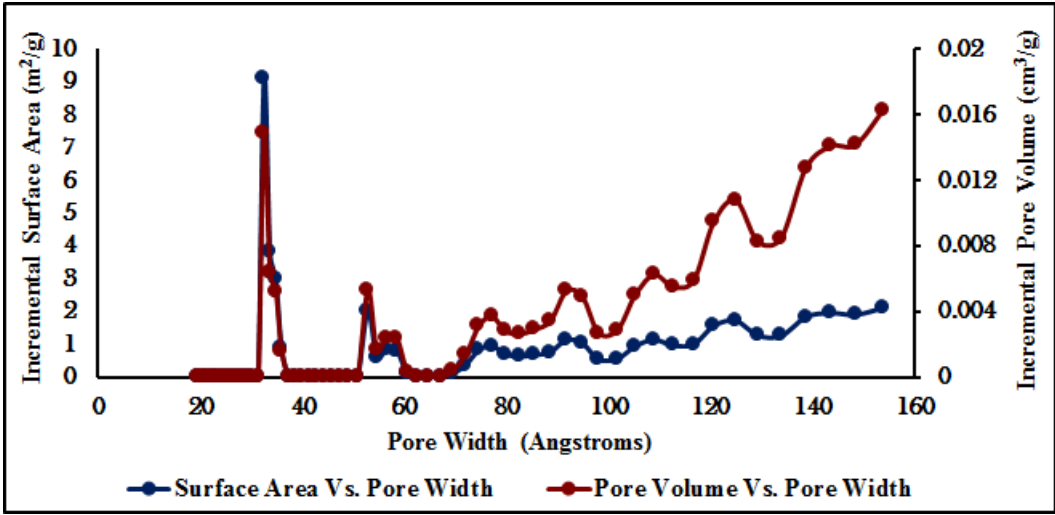
Figure 4.11 The N<sub>2</sub> isotherm for PIM-PI-06.

Pore size distribution (PSD) is a physicochemical property that determines the distribution of pore volume in relation to pore size. It shows the pore volume available to molecules of a certain size. By comparing those charts with the ones showing the distribution of pore surface area versus pore size, the pore sizes present in each synthesized PIM-PI could thus be evaluated. It was observed that the pore sizes in the synthesized polymers range from 0.5 to 20 nanometers, which subsequently confirms that the polymers possessed both meso-porous and microporous structures as shown in Table 4.5.

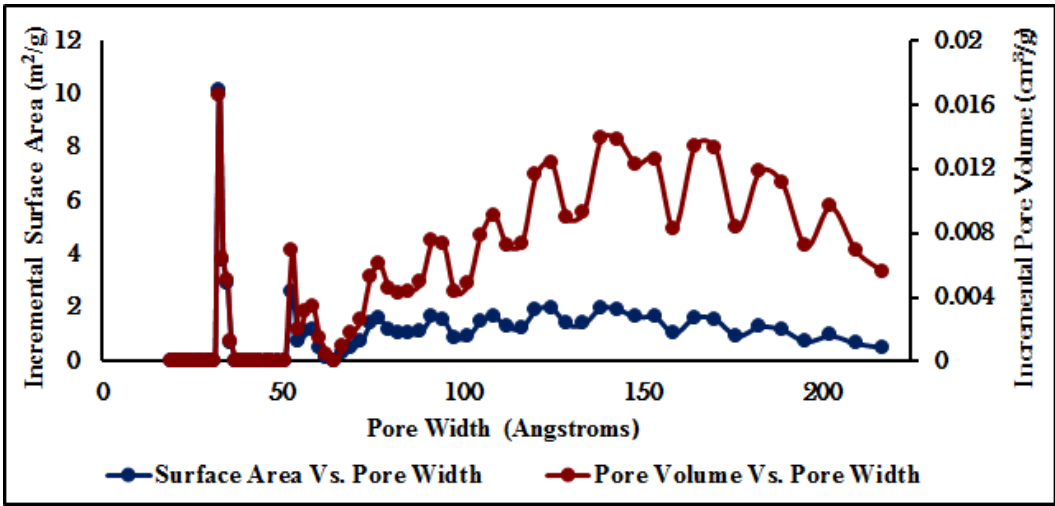
Table 4.5 The Pore Size Distribution (PSD) For The Synthesized PIM-PIs.



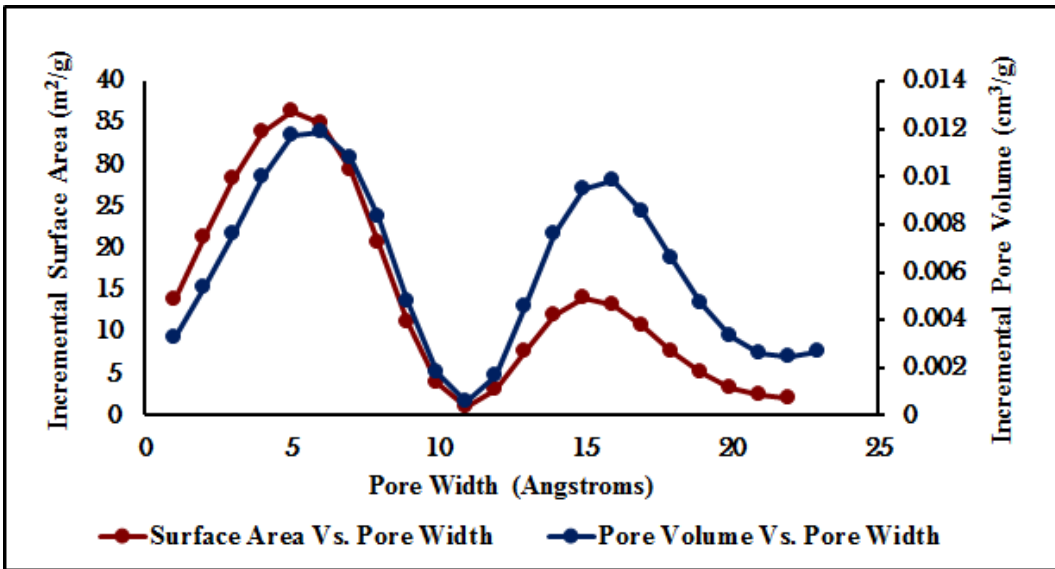
PIM-PI-04



PIM-PI-05



PIM-PI-06



### 4.2.3. Carbon Dioxide Adsorption Analysis:

Carbon dioxide adsorption isotherms obtained at the three different temperatures, 273°, 283° and 293° K for all the synthesized polymers are shown in Figures 4.12-4.17. In case of PIM-PI-01 and PIM-PI-05 the 278 K temperature was used instead of 273 K due to an instrumental error. Those isotherms are determined to evaluate the heat of adsorption of the synthesized polymers.

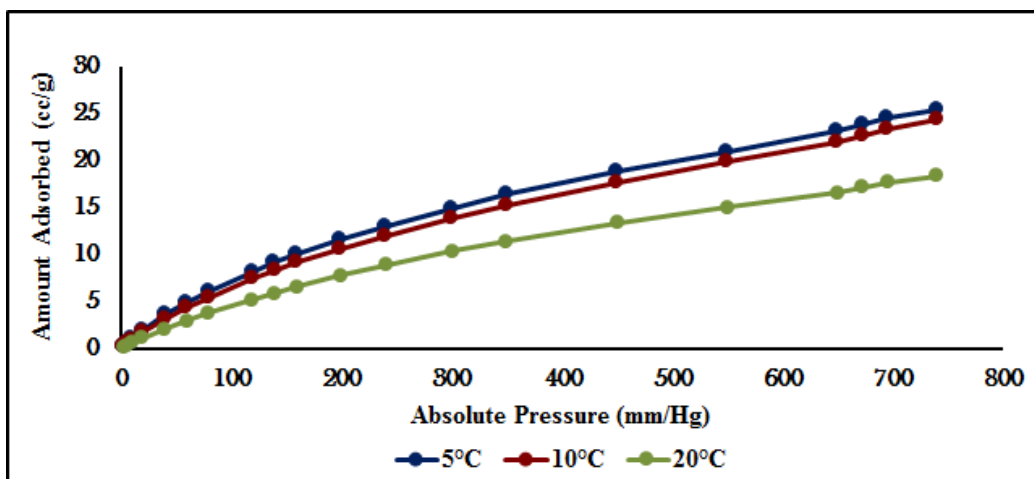


Figure 4.12 CO<sub>2</sub> Adsorption for PIM-PI-01.

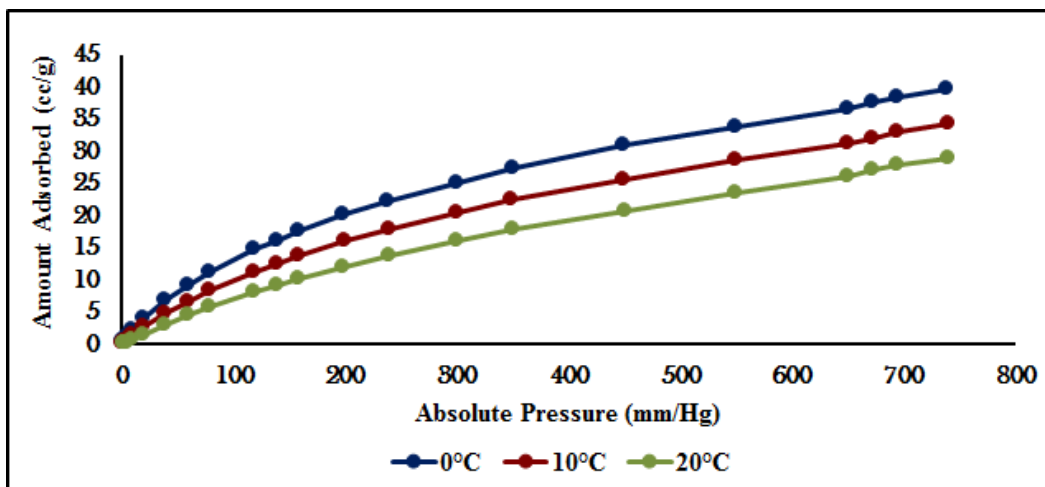


Figure 4.13 CO<sub>2</sub> Adsorption for PIM-PI-02.

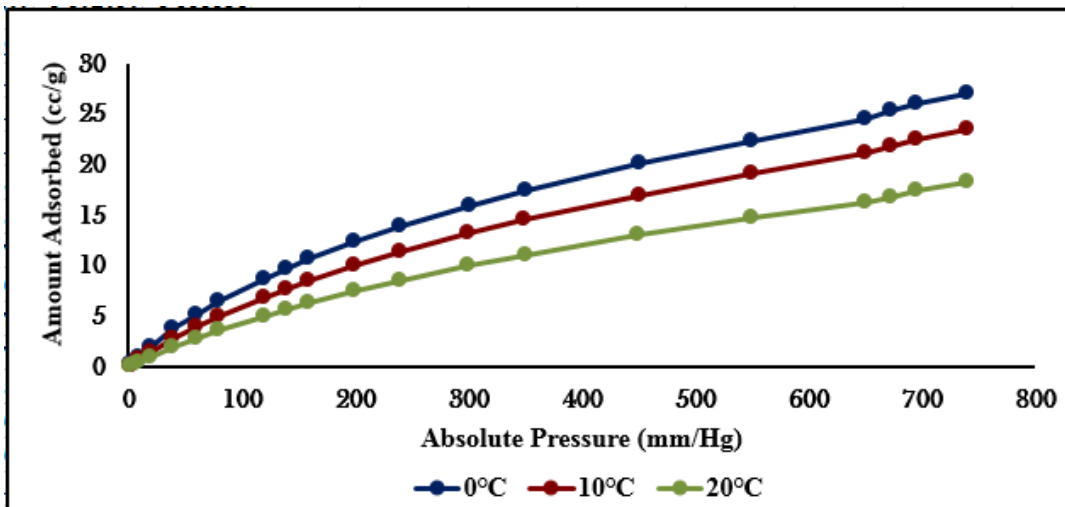


Figure 4.14 CO<sub>2</sub> Adsorption for PIM-PI-03.

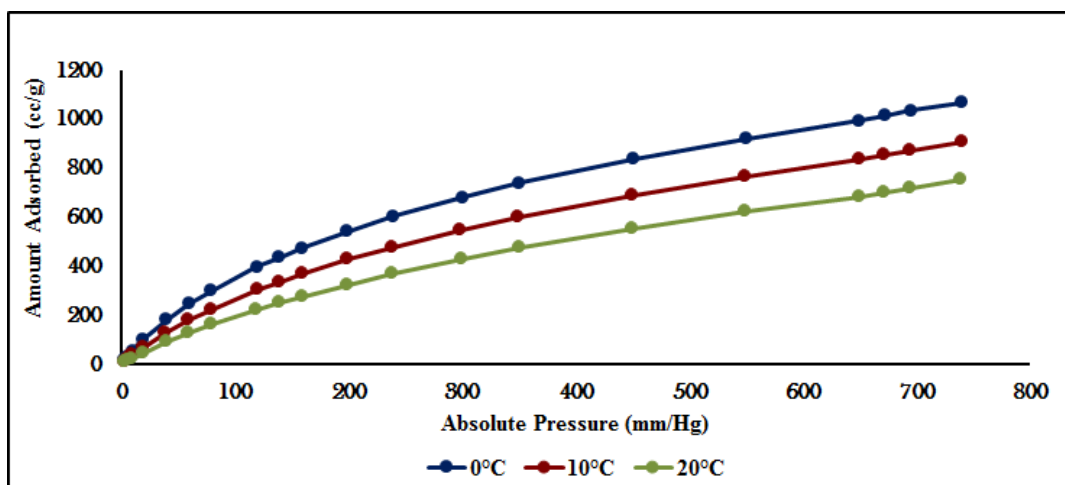


Figure 4.15 CO<sub>2</sub> Adsorption for PIM-PI-04.

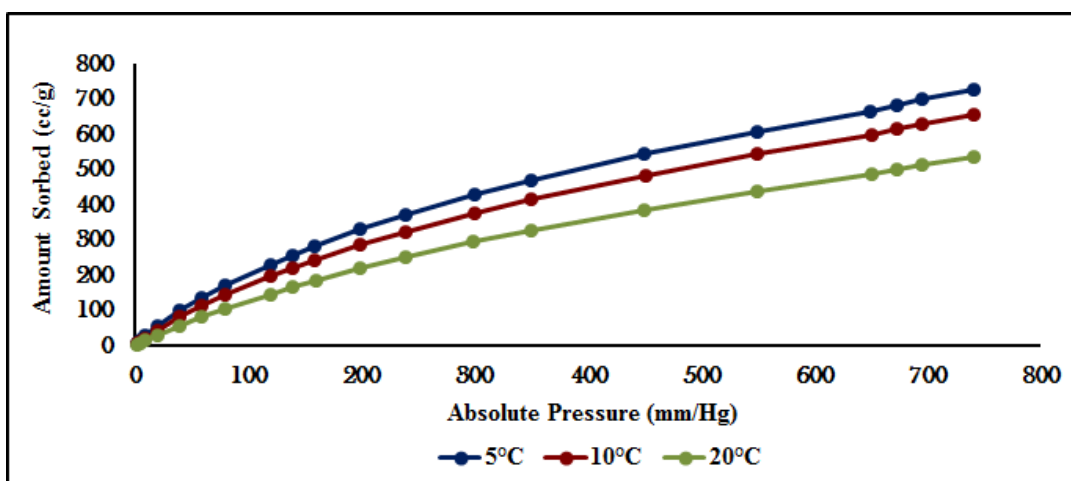


Figure 4.16 CO<sub>2</sub> Adsorption for PIM-PI-05.

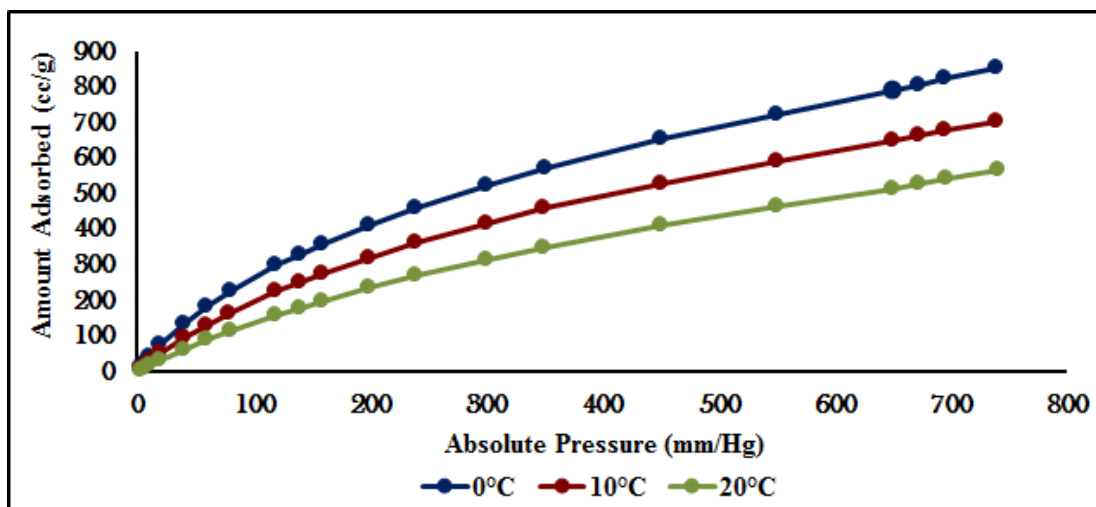


Figure 4.17 CO<sub>2</sub> Adsorption for PIM-PI-06.

As expected it was observed in all the isotherms that the increase in temperature or pressure resulted in the increase of the adsorbed amount of CO<sub>2</sub>. The same holds also for as by increasing the surface area of the polymers. PIM-PI-04, was found to acquire the highest surface area, 508 m<sup>2</sup>/g, and accordingly adsorbs the highest CO<sub>2</sub>, 1200 cc/g. However PIM-PI-01 which had a surface area of 61 m<sup>2</sup>/g surface area, showed adsorbed amount of maximum value around 25 cc/g.

The heat of adsorption for the synthesized polymers was evaluated and compared to each other as shown in Figures 4.18 and 4.19. They were all characterized by high heat of adsorption values within the ranges 25 to 35 kJ/mol. This indicates that the pore sizes within the polymers are very small causing a certain type of interaction to occur between the polymeric pore walls and the adsorbate leading to a release of energy in the form of heat. This is quite interesting since the greater the amount of released heat the more stable the polymer/gas mixture will be and the greater the efficiency of the polymer as a CO<sub>2</sub> capture and storage systems. PIM-PI-04 is obviously an excellent candidate as a CO<sub>2</sub> Storage Substance.

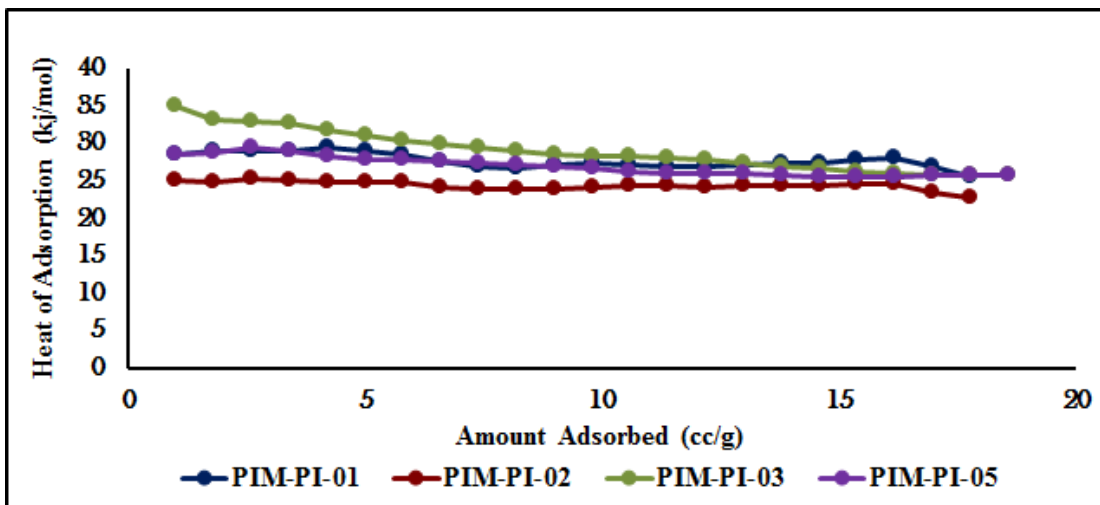


Figure 4.18 Heat of Adsorption for PIM-PI-01, PIM-PI-02, PIM-PI-03 and PIM-PI-05.

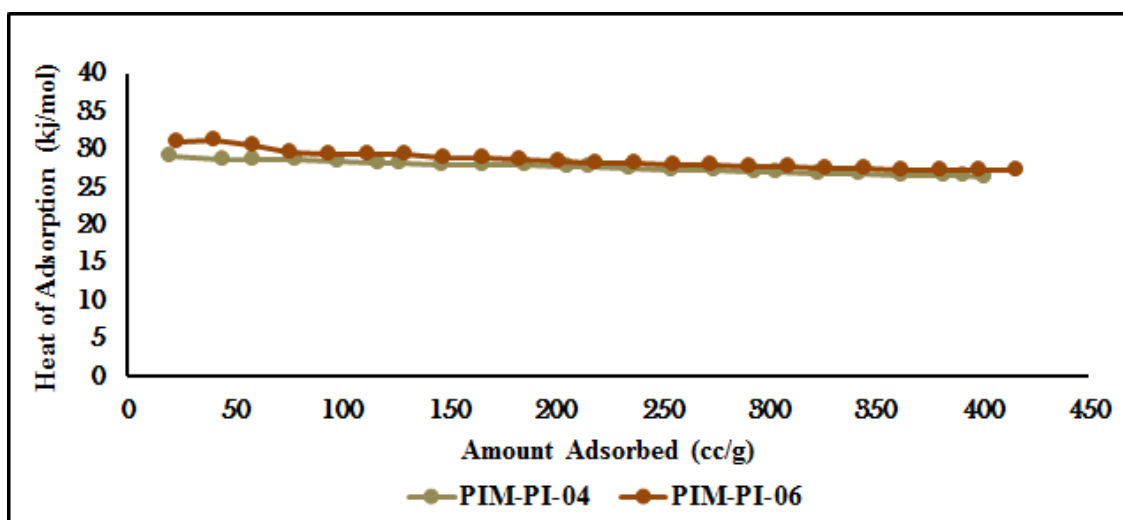


Figure 4.19 Heat of Adsorption for PIM-PI-04 and PIM-PI-6.

## Chapter 5:

# **Molecular Simulation of Polymers of Intrinsic Micro-Porosity Based on Polyimides Structures**



## *5. Molecular Simulation of Polymers of Intrinsic Micro-Porosity Based on Polyimides Structures:*

---

This chapter presents the methodology used to molecularly simulate three of the synthesized PIM-PIs; PIM-PI-04, 05 and 06. Those polymers have shown the highest surface area and pore volume when characterized experimentally as shown in chapter six. Results of Fractional-Free Volume (FFV), Connolly surface area to total volume ratio ( $S/V_T$ ) are compared to those found in literature to validate the utilized protocol. This will subsequently help in simulating the polymeric structures for the prediction of mean-square displacement and diffusion coefficients.

### *5.2. Modeling and Simulation Protocol:*

---

Molecular dynamics simulation modules of Materials Studio® simulation package available from Accelrys, Inc., UK was used to construct and investigate molecular models of three of the synthesized PIM-PIs; namely, PIM-PI-04, PIM-PI-05, and PIM-PI-06. This study was aimed to investigate the influence of different diamines groups on: (i) the mean-square displacement; (ii) the self-diffusion coefficients; (iii) the Connolly surface area, (iv) the surface area to volume ratio and (v) the radial distribution functions in relation to the local packing of the polymeric segments.

#### *5.2.1. Molecular dynamics simulation protocols:*

---

The MS amorphous cell module was used to construct the simulation amorphous cells. Each cell contains four PIM-PI chains of each type with each chain composed of five repeat units. As shown in Figure 5.1 five penetrate molecules of each gas under study ( $\text{CO}_2$  and  $\text{H}_2$ ) were introduced into the amorphous cell to simulate the diffusion of the gas molecules through the polymer segments. The simulation cells were cubic having densities 1.2 g/cc. The cells were all constructed using COMPASS forcefield assigned charges and Ewald electrostatic summation method. After the construction was completed, the simulation cell was minimized using the MS Discover module with atom-based electrostatic summation method till complete convergence [99]. Once the simulation cells were minimized, they were all subjected to molecular dynamics runs using NVT ensemble for 100 ps with 1fs time step at the temperature of 298 K. Final

structure trajectory was saved every 100 steps with total 100000 steps. During the simulation, the temperature was controlled using Brendson thermostat. The final snapshot was saved and then used as the starting coordinates for the molecular dynamics runs using the same parameters for 1000000 steps with 1fs time step. Each trajectory was constructed twice for reproducibility and in case of wide variation of the simulated data, a third run was conducted. Each run took about five days of continuous computer calculations for completion.

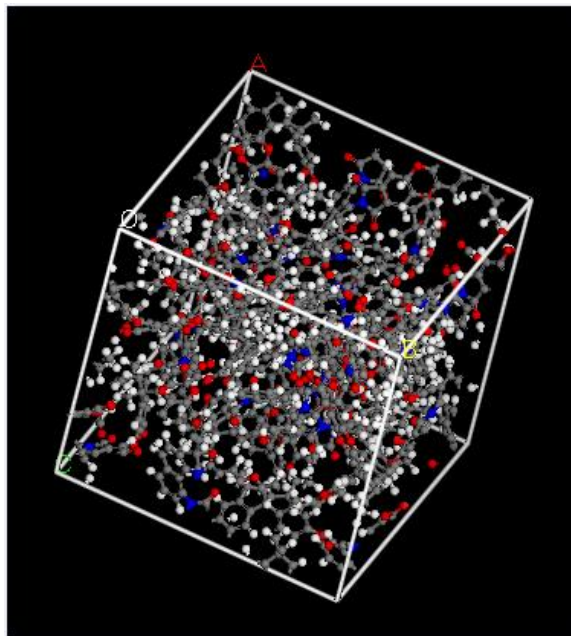


*Figure 5.1* The Simulation Cells Containing both PIM-PI-04 and CO<sub>2</sub> gas.

### *5.2.2. Evaluation of the Fractional-Free Volume and Connolly Surface Area to Volume Ratio:*

---

In order to evaluate the free-volume in bulk simulated molecular models, the hard probe method was used [100]. In this method, the periodic box was divided into 100 x 100 x 100 cubic subcells. All the atoms were assumed to be hard spheres with radii equal to 88% of the full van der Waals radii. Each subcell was then scanned to screen out the occupied whenever more than half of the subcell size lay within any hard sphere. After checking occupancy, a probe, which is also assumed to be a hard sphere, was introduced at the center of an unoccupied subshell. Each unoccupied subcell was determined to be “inaccessible” if more than half of any occupied subcell size lay within the spherical probe. The inaccessible subcells were classified as occupied subcells as well. According to Kim and Mattice [101], connectivity is formed when two

unoccupied subcells having connectivity were assigned to the same void. The total unoccupied volume of the cell divided by the total volume of the cell is thus defined as the fractional free-volume of that cell.

Connolly surface area [102] is the contact surface created when a spherical probe (presenting the solvent) is rolled over the van der Waals surface of the models. The data are presented as the Connolly surface area to volume ratio ( $S/V_T$ ).

### *5.2.3. Determination of the mean-square displacement and the self-diffusion coefficients:*

---

The diffusion coefficients of the gases were calculated by selecting the gas and evaluating its mean-square displacements. The self-diffusion coefficients were assessed through selecting the PIM-PIs chains and evaluating their mean-square displacements. The self-diffusion coefficients of the PIM-PIs and the diffusion coefficients ( $D_0$ ) of the gases was calculated using Einstein relation:

$$D_0 = \frac{1}{6N} \lim_{t \rightarrow \infty} \frac{d}{dt} \sum_{i=1}^N \langle [r_i(t) - r_i(0)]^2 \rangle \quad (\text{Eqn5.1})$$

where  $r_i$  is the position of atom  $i$  and  $N$  is the number of atoms in one chain.

### *5.3. Assessment of the NanoPorosity of the Simulated PIM-PIs:*

---

In this section, an account of the modelling and simulation results is given in order to assess the nano-porous characteristics of the simulated polymers. Some of the obtained results are compared to available data for previously synthesized and/or simulated PIM-PIs to validate the modelling protocol. Once validated the protocol could be further used to predict new characteristic pertaining to the nano-porosity of the simulated polymers.

### *5.3.1. Evaluation of the Fractional free-volume (FFV) and the Connolly surface area to volume ( $S/V_T$ ) ratio:*

---

Figure 5.2 (a) is a schematic representation of a simulated molecular cell of a PIM-PI-04 showing the extent of the Connolly surface area and the resulting polymeric nanopores. It is quite interesting to observe the difference in the extent of the free volume of this nanoporous polymer as compared to that of nonporous polyamide, Figure 5.2 (b).

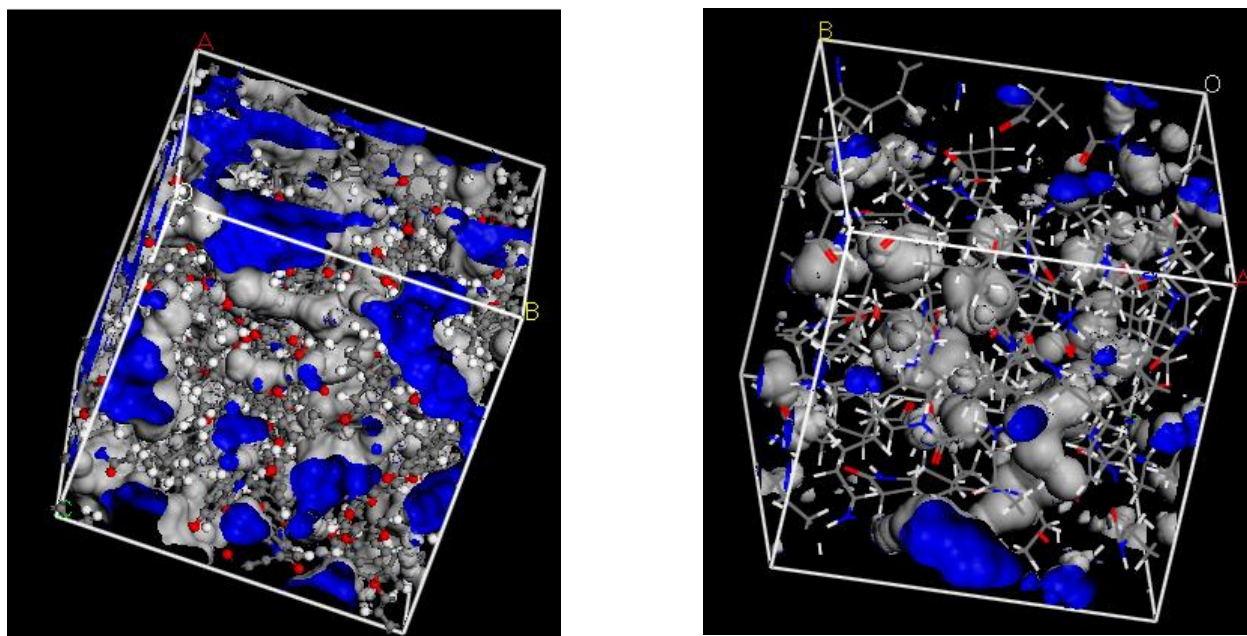


*Figure 5.2.* The extent of Connolly Surface area in (a) porous PIM-PI-04, (b) non-porous Polyamide.

Table 5.1 lists various nanoporous characteristics for the three simulated polymeric structures. It is obvious from the table that both the simulated fractional free volume and Connolly surface area to total volume ratio is in close agreement to those listed in the literature for nano-porous polymers of similar structures either simulated ( $\sim 0.23$  FFV and  $\sim 0.30$   $S/V_T$ ) [96] or determined experimentally ( $\sim 0.22$  FFV) [85].

Table 5.1 List for Total Volume ( $V_T$ ), Free-Volume ( $V_o$ ), Fractional Free-Volume (FFV) and Connolly Surface Area to Total Volume Ratio ( $S/V_T$ )

PIM-PI	$V_T (nm^3)$	$V_o (nm^3)$	FFV	$S/V_T$
<i>PIM-PI-04</i>	<b>210.93</b>	<b>55.74</b>	<b>0.26</b>	<b>0.32</b>
<i>PIM-PI-05</i>	<b>215.10</b>	<b>52.59</b>	<b>0.24</b>	<b>0.32</b>
<i>PIM-PI-06</i>	<b>26.17</b>	<b>10.2</b>	<b>0.39</b>	<b>3.3</b>

This is quite interesting since it validates the used simulation protocol in this study to elaborate further investigation of the diffusivity of gases of interest through these nano-porous polymers.

### ***5.3.2. Evaluation of the Diffusion Coefficients:***

---

Diffusion coefficients of the polymeric chains and the penetrate gas molecules were estimated through the evaluation of the mean square displacement obtained from the simulation and using Einstein equation (Eqn. 5.1). Figure 5.3 shows the mean square displacement of both the polymer segments of PIM-PI-04 and the penetrate CO<sub>2</sub> gas molecules. It is obvious from the figure that the mean square displacement of the polymer segments are of much lower values as compared to those of the penetrate gas molecules resulting in much lower diffusion coefficient for the polymer than that of the gas molecules. This was also observed with PIM-PI-05 as shown in Figures 5.4. This is naturally due to the inherent stiffness and the high molecular weight of the polymer chains thus restricting its mobility. It could be observed from the mean square displacement behavior of the CO<sub>2</sub> gas molecules that the gas diffuses within the time range at two different rates. This is possible since the gas diffuses through the pores with higher diffusion rate followed by its diffusion through the dense polymer molecules with much lower diffusion rate. A close inspection in the molecular structure may provide a reasoning for such observation. CO<sub>2</sub> is a non-polar linear molecule with both C=O bonds polar in nature. The two oxygen atoms of the CO<sub>2</sub> molecule carry negative charges while the carbon atom of the same molecule carries a positive charge arising from the difference in the electronegativity between these atoms. Through the course of the diffusion of CO<sub>2</sub> molecule through the polymer chains, intermolecular columbic interactions are formed between the charged atoms of the polymeric and CO<sub>2</sub> molecules. This

has the potential of slowing the diffusion of the CO<sub>2</sub> molecule as a result of this “sticky diffusion” in addition to the greater size of the CO<sub>2</sub> molecule over that of H<sub>2</sub>.

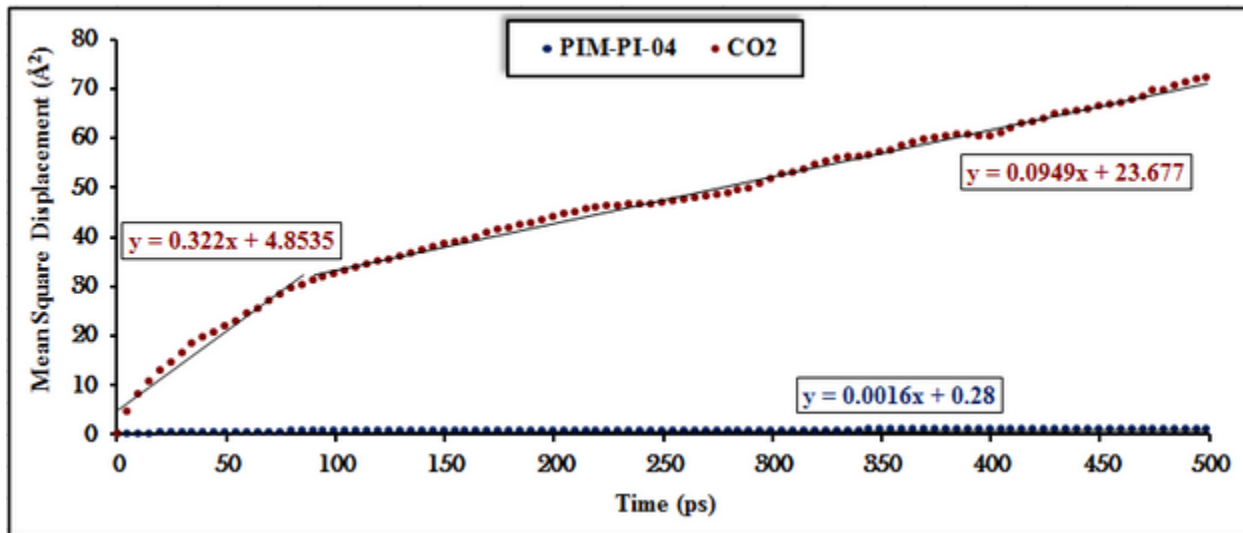


Figure 5.3 Mean Square Displacement of PIM-PI-04 with CO<sub>2</sub>.

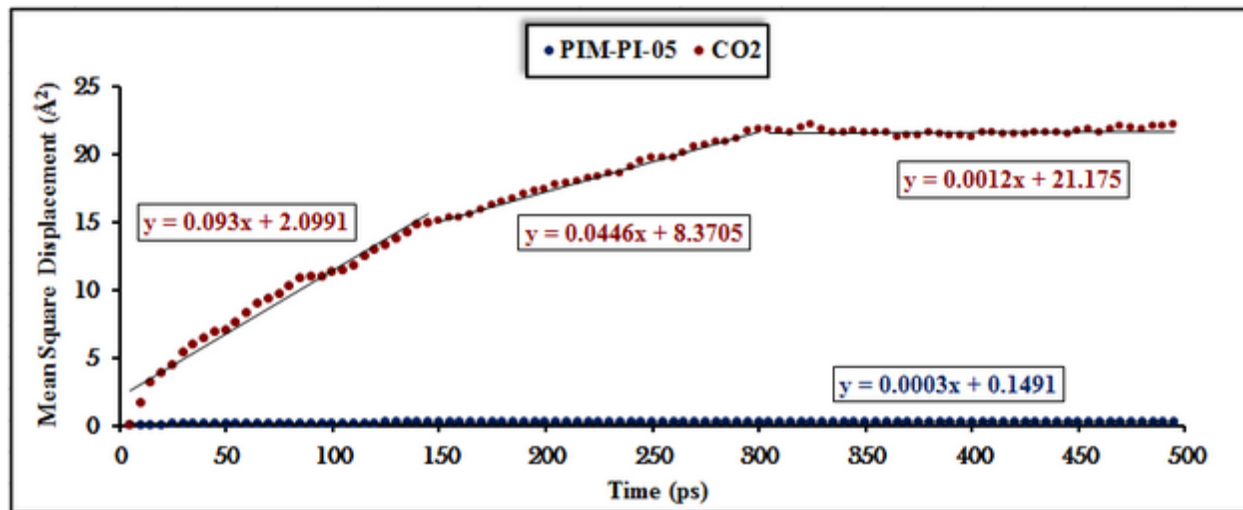


Figure 5.4. Mean Square Displacement of PIM-PI-05 with CO<sub>2</sub>.

Interestingly, this behavior for the CO<sub>2</sub> gas molecules is not observed for the H<sub>2</sub> gas molecules. It is worth mentioning here that the diffusion coefficient of H<sub>2</sub> molecules through the polymer is 100 times greater than that of the CO<sub>2</sub> molecules Figures 5.5 and 5.6.

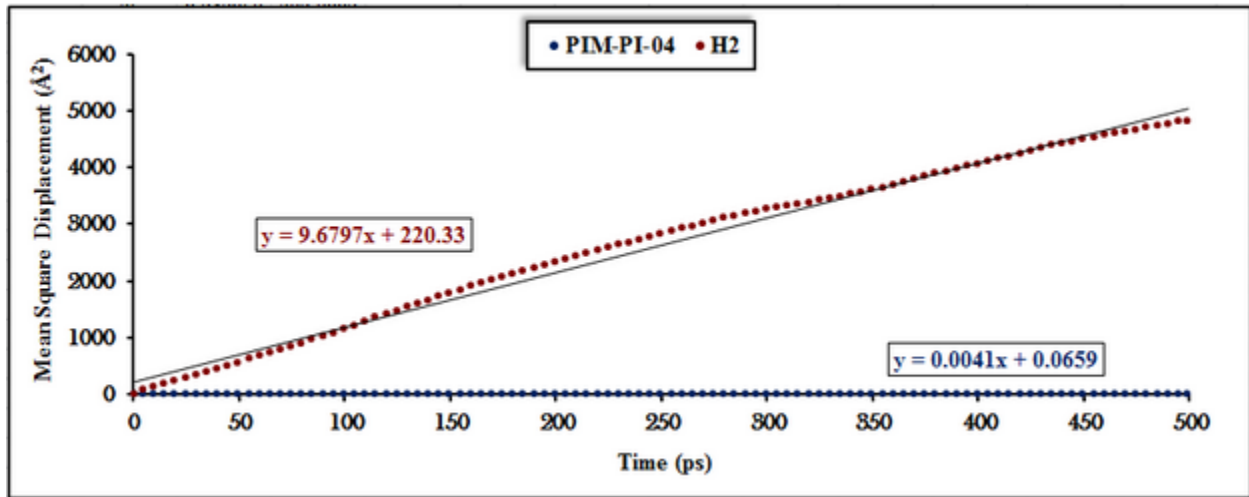


Figure 5.5. Mean Square Displacement of PIM-PI-04 with H<sub>2</sub>.

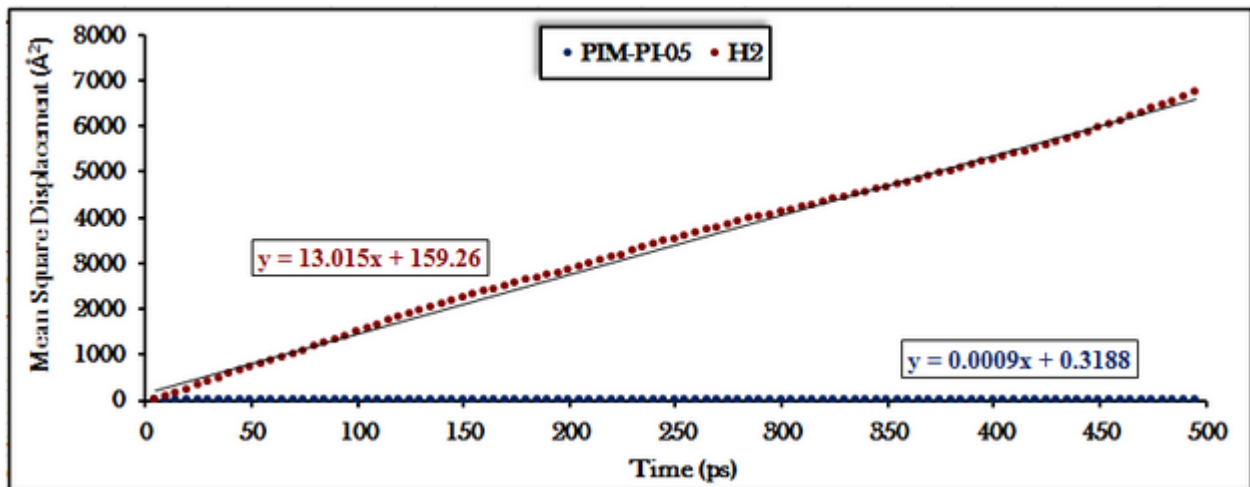


Figure 5.6. Mean Square Displacement of PIM-PI-05 with H<sub>2</sub>.

This can only be explained by assuming that the large nanopores are interconnected by the much smaller micropores forming nanochannels through the polymeric matrix. Due to the smaller size of the H<sub>2</sub> molecules, they can easily diffuse through these narrow channels giving rise to a single diffusion rate as observed in Figures 5.5 and 5.6 and a diffusion rates that are 100 times greater than that of CO<sub>2</sub>, Table 5.2. In case of CO<sub>2</sub> molecules, their larger size prevent them from diffusing through these narrow channels and forcing them to diffuse at one instance through the nanopores and in another instance through the polymeric matrix thus slowing down



tremendously and resulting in the observed multi-rate diffusion. This is very interesting as it provides the basis as well as the molecular interpretation for the size-exclusion phenomenon of these nanoporous polymers for natural and industrial gas separations.

Table 5.2 Self-Diffusion Coefficients (D) of PIM-PI-04, 05 and 06 and Diffusion Coefficients of CO<sub>2</sub> (D (CO<sub>2</sub>)) and H<sub>2</sub> (D (H<sub>2</sub>)) gases.

**Diffusion Coefficient, D \* 10<sup>7</sup> (cm<sup>2</sup>/s)**

<b>PIM-PI</b>	<b>D (Polymer)</b>		<b>D (CO<sub>2</sub>)</b>			<b>D (H<sub>2</sub>)</b>	
	<b>CO<sub>2</sub>*</b>	<b>H<sub>2</sub>*</b>	<b>1<sup>st</sup> rate</b>	<b>2<sup>nd</sup> rate</b>	<b>3<sup>rd</sup> rate</b>	<b>1<sup>st</sup> rate</b>	<b>2<sup>nd</sup> rate</b>
<b>PIM-PI-04</b>	<b>0.27</b>	<b>0.68</b>	<b>54</b>	<b>16</b>	<b>-----</b>	<b>1610</b>	<b>-----</b>
<b>PIM-PI-05</b>	<b>0.05</b>	<b>0.15</b>	<b>15</b>	<b>7.4</b>	<b>0.20</b>	<b>2170</b>	<b>-----</b>
<b>PIM-PI-06</b>	<b>1.8</b>	<b>2.5</b>	<b>132</b>	<b>64</b>	<b>84.9</b>	<b>5751</b>	<b>3878</b>

\* Diffusion Coefficients of the polymer segments in the presence of the indicated gas molecules.

\*\* Diffusion of CO<sub>2</sub> molecules may occur in two or more intervals with different diffusion rates.

It was, however, observed that the self-diffusion coefficients of the polymer segments vary in the presence of penetrate gas molecules. Similar behavior for the diffusion coefficients may also be observed for the other polymers, Figures 5.7 and 5.8.

PIM-PI-06 has shown, however, an interesting feature with H<sub>2</sub> molecules at which it possessed two different rates of diffusion. The fast starting rate is due to its diffusion through the pores with the slower rate for its diffusion through the polymeric matrix. This might be an indication that the pores present in PIM-PI-06 is not interconnected pores or that the narrow channels are quite small to allow the H<sub>2</sub> molecules pass through. Therefore, the H<sub>2</sub> molecules are forced to diffuse through the polymeric matrix.



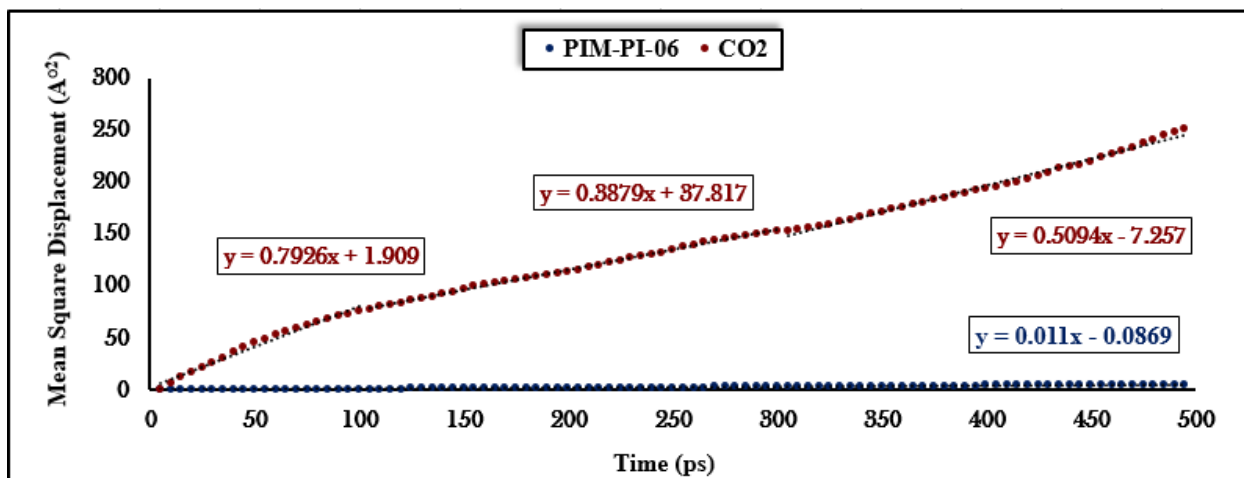


Figure 5.7 Mean Square Displacement of PIM-PI-06 with CO<sub>2</sub>.

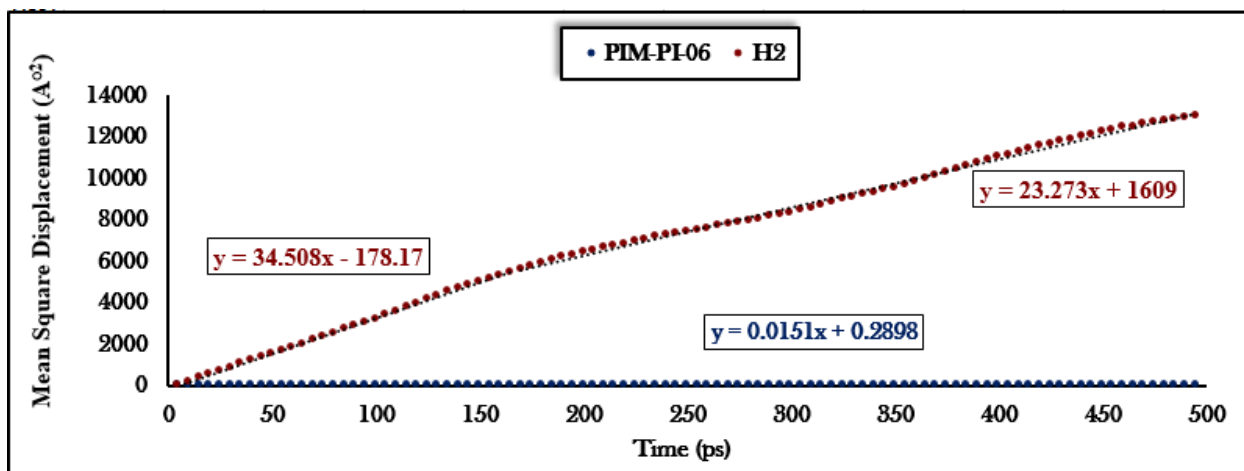


Figure 5.8 Mean Square Displacement of PIM-PI-06 with H<sub>2</sub>.

Furthermore, a closer look at the chemical formulae of the simulated polymers, Section 4.2., reveals the unusual arrangement of the polymeric backbone of PIM-PI-04 as evident by the polymeric molecular model shown in Figure 5.9 in comparison to the other polymers. This peculiar arrangement obviously influenced the molecular packing of the polymeric chains resulting in the variation of the diffusion rate of the non-polar hydrogen molecules, Table 5.1. Interestingly this variation is reversed in the case of CO<sub>2</sub> molecules with the diffusion coefficient through PIM-PI-04 is at least twice as much that through PIM-PI-05.

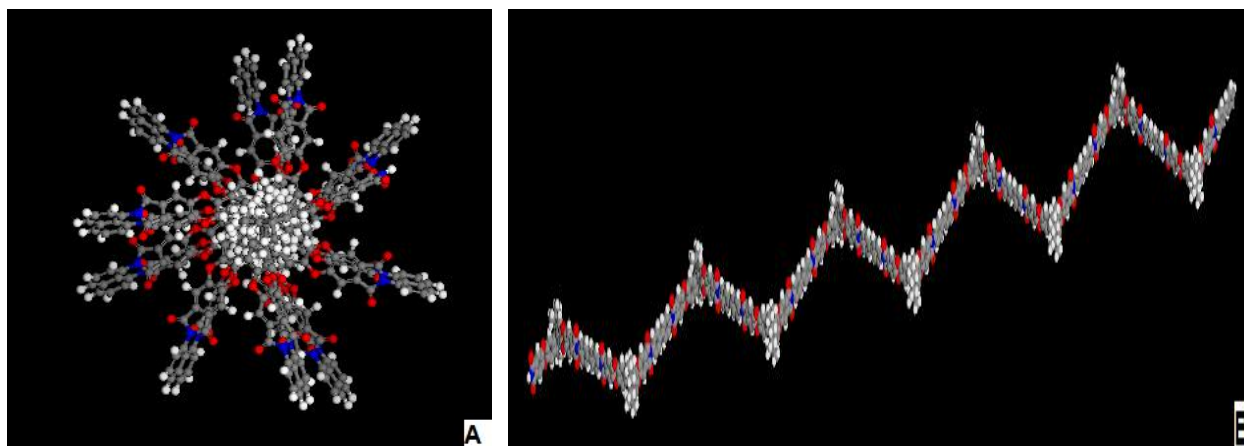


Figure 5.9 The molecular simulation model for (a) PIM-PI-04 and (b) PIM-PI-05.

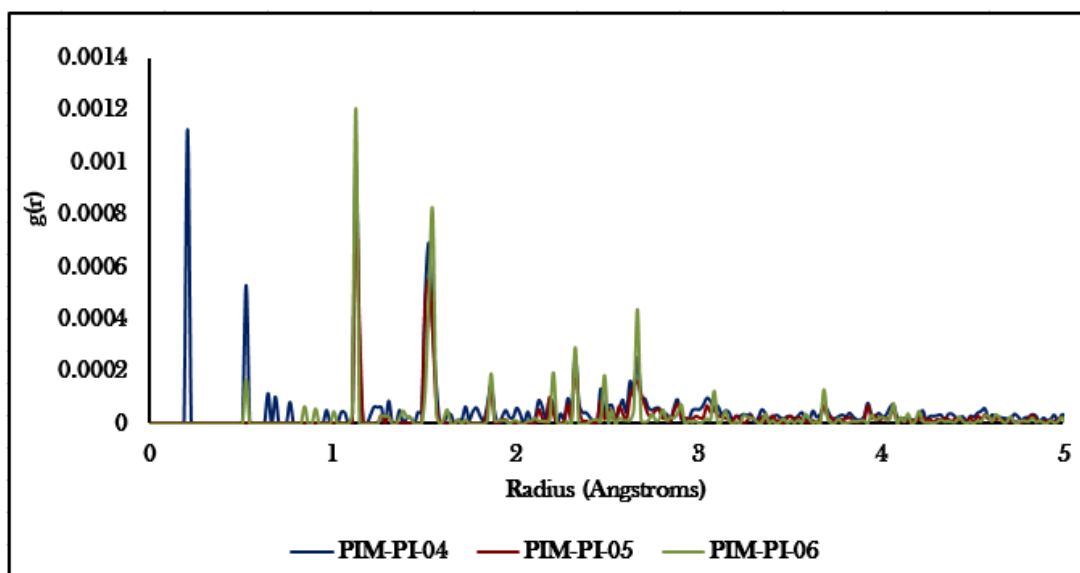


Figure 5.10 Radial Distribution Function of PIM-PI-04, 05, and 06.

To illustrate this point further, the radial distribution functions in direct relation to the local packing of the polymeric segments of the three simulated polymers are shown in Figures 5.10. It is interesting to observe from Figure 5.8 that the PIM-PI-04 is closely packed compared to the other polymers as evident by the presence of major peaks at the small spatial distances. As illustrated in Figure 5.9 PIM-PI-04 packs in a star-shaped architecture whereas PIM-PI-05, for example, packs in a zigzag-like architecture. The dense packing in PIM-PI-04 results in the reduction of the diffusion rate of the non-polar  $H_2$  molecules through the polymer, whereas the

open architecture in PIM-PI-05 and PIM-PI-06 facilitates the diffusion of the non-polar H<sub>2</sub> molecule, Table 5.1. In case of CO<sub>2</sub> diffusion and due to the presence of intermolecular interactions between the charged CO<sub>2</sub> atoms and the charged polymeric atoms, the close packing of PIM-PI-04, in fact, facilitates the diffusion of the CO<sub>2</sub> molecules. This indicates that the permeability of the uncharged H<sub>2</sub> molecules through the nano-porous polymers depends mainly on the diffusivity part of the permeability, whereas the permeability of the charged CO<sub>2</sub> gas through the nano-porous polymers depends mainly on the solubility part of the permeability.

## Chapter 6:

# **Conclusion and Future Perspectives**

## *6. Conclusion and Future Perspectives:*

---

### *6.2. Conclusion:*

---

This study aims at investigating the influence of different diamine units on the final structure of polymers of intrinsic microporosity (PIM) based on polyimides (PI) structures. Six different (PIM-PI) polymers were synthesized, of which five polymers were novel polymers to be reported for the first time in literature. The sixth polymer is only a repetition of an already synthesized polymer to validate the modelling study. Those polymers were prepared in order to investigate their porosity and subsequent influence on the diffusion rates of both carbon dioxide and hydrogen gases. This study was conducted through experimental and theoretical methodologies. Experimentally, the high surface area and porosity of the synthesized polymers were observed using ASAP 2020. It was found that PIM-PI-04 acquires the largest surface area and pore volume, while PIM-PI-01 possessed the lowest surface area and pore volume. It was also observed that the porosity of the polymers was not only dependent on the monomer containing contortion site as Mckweon claimed in his studies, but also on the structure and orientation of the diamine groups, which played significant role in the formation of the porosity of the polymers and subsequently their observed high surface areas. TGA studies proved that all prepared polymers were thermally stable up to 450°C, which is within the same range found in literature with polymers similar to those synthesized. Consequently, the experimental part proved the presence of porous, thermally stable polymers that can be used further in the separation and storage of gases.

The theoretical part of this study meant to investigate the packing structures of the three polymers with highest surface area. Additionally, the study of the diffusion of the CO<sub>2</sub> and H<sub>2</sub> gases through the pores and the polymeric segments, to relate the influence of the chemical structure and the packing of these polymers. For example PIM-PI-04 possessed as Star-like architecture however PIM-PI-05 had a Zigzag like shape. It was observed in all the simulated polymers that the self-diffusion of the polymers were greatly influenced by the type of introduced gas. The H<sub>2</sub> gas molecules possessed higher diffusion rates than that of CO<sub>2</sub> gas molecules. It was also observed that the CO<sub>2</sub> gas molecules diffuses with different rates

depending on whether they are in the pores or the polymer segments. It was concluded that the permeability of the uncharged H<sub>2</sub> molecules through the nano-porous polymers depends mainly on the diffusivity part of the permeability, whereas the permeability of the charged CO<sub>2</sub> gas through the nanoporous polymers depends mainly on the solubility part of the permeability. The H<sub>2</sub> gas molecules did not show this behavior in general possibly due to the interconnection of the nanopores by micropores forming narrow channels through which the small H<sub>2</sub> molecules may diffuse. The great difference in the observed diffusion rates of the H<sub>2</sub> and CO<sub>2</sub> gas molecules makes those polymers much required for the separation of H<sub>2</sub>/CO<sub>2</sub> gas mixtures based on size exclusion principle.

### *6.3. Future Perspectives:*

---

The interesting properties observed for the synthesized polymers make them great candidates for the preparation of polymeric membranes for separation of natural and industrial gas mixtures based on size exclusion principle. Since, polyimide membranes are glassy in nature, which hinders greatly their application in industrial settings, they may be prepared on another flexible polymeric support. They can be also synthesized as fibers and being cross-linked with more flexible polymers and be tested for various gas mixtures of interest to the industry.

## References:

---

- [1] Xu, G., Liang, F., Yang, Y., Hu, Y., Zhang, K., Liu, W. “An improved CO<sub>2</sub> separation and purification system based on cryogenic separation and distillation theory,” *Energies*, vol. 7, pp. 3484–3502, 2014.
- [2] Burt, S., Baxter, A., & Baxter, L. “Cryogenic CO<sub>2</sub> Capture to Control Climate Change Emissions,” *Clear. Conference*, 2009.
- [3] Wong, S., & Bioletti, R. “Carbon dioxide separation technologies,” *Alberta Research Council*, 2002.
- [4] Bullinger, H. “Fossil energy” *Technology Guide*, pp. 330–333, 2009.
- [5] McKeown, N.B., Budd, P.M., & Book, D. “Microporous polymers as potential hydrogen storage materials,” *Macromolecular Rapid Communications*, vol. 28, pp. 995–1002, 2007.
- [6] Ohta, T. (Ed.). (n.d.). "Energy Carriers and Conversion Systems with Emphasis on Hydrogen". In *Energy Carriers and Conversion Systems*, vol. 1, pp. 382. UNESCO.
- [7] McCracken, M.C., "Climatic effects of atmospheric carbon dioxide". New York: Science, pp. 873–874, 1983.
- [8] Sundblad, E., Biel, A., Garling, T. “Intention to change activities that reduce carbon dioxide emissions related to worry about global climate change consequences,” *European Review of Applied Psychology*, vol. 64, no. 1, pp. 13–17, 2012.
- [9] Khuram, M., Aditi, M., Abulhassan, A., Kajari, K., & Saibal, G. “Cryogenic carbon dioxide separation from natural gas: a review based on conventional and novel emerging technologies,” *Reviews in Chemical Engineering*, vol. 30, no. 5, pp. 453–477, 2014.
- [10] Rapier, R. “Global Carbon Dioxide Emissions — Facts and Figures,” 2012. [Online]. Available: <http://www.energytrendsinsider.com/2012/07/02/global-carbon-dioxide-emissions-facts-and-figures/>.
- [11] Davis, B.J. “Hydrogen Fuel,” 2010. .
- [12] Edward, I.F., Kuznetsov, P.P., David, V.L. “Hydrogen Energy,” *Philosophical Trans. R. Soc. A Math. Phys. Eng. Sci.*, vol. 365, no. 1853, pp. 1043–1056.
- [13] Ghosh, M.A., Prelas, T.K. "Hydrogen Energy". pp. 455–629, 2011.
- [14] Williams, L.O., "Hydrogen Power: An introduction to hydrogen energy and its applications" 2013.

- [15] “Worldwide challenges.” [Online]. Available: [http://adecosolar.com/?page\\_id=421](http://adecosolar.com/?page_id=421).
- [16] Ravanchi, M.T., Sahebdehfar, S., & Zangeneh, F.T. “Carbon dioxide sequestration in petrochemical industries with the aim of reduction in greenhouse gas emissions,” *Front. Chem. Eng. China*, vol. 5, no. 2, pp. 173–178, 2011.
- [17] Wilcox, J. *Carbon Capture*. New York: Springer, 2012.
- [18] Dawson, R., Cooper, A.I., & Adams, D.J. “Nanoporous organic polymer networks,” *Prog. Polym. Sci.*, vol. 37, no. 4, pp. 530–563, 2012.
- [19] Maly, K.E. “Assembly of nanoporous organic materials from molecular building blocks,” *Mater. Chem.*, vol. 19, pp. 1781 – 1787, 2009.
- [20] Inglezakis, M., *Handbook of Natural Zeolites*. Bentham Science, 2012.
- [21] McKeown, N.B., Budd, P.M., Msayib, K.J., Ghanem, B.S., Kingston, H.J., Tattershall, C.E., Makhseed, S., Reynolds, K.J., & Fritsch, D. “Polymers of intrinsic microporosity (PIMs): Bridging the void between microporous and polymeric materials,” *Chem. - A Eur. J.*, vol. 11, pp. 2610–2620, 2005.
- [22] Namasivayam, c., & Kavitha, D. “Removal of Congo Red from water by adsorption onto activated carbon prepared from coir pith, an agricultural solid waste,” *Dye. Pigment.*, vol. 54, pp. 47–58, 2002.
- [23] Malik, P.K. “Use of activated carbons prepared from sawdust and rice-husk for adsorption of acid dyes: A case study of acid yellow 36,” *Dye. Pigment.*, vol. 56, pp. 239–249, 2003.
- [24] Budd, P. M., Makhseed, S. M., Ghanem, B. S., Msayib, K. J., Tattershall, C. E., & McKeown, N.B. “Microporous polymeric materials,” *Mater. Today*, vol. 7, no. 4, pp. 40 – 46, 2004.
- [25] Ritter, N., Antonietti, M., Thomas, A., Senkovska, I., Kaskel, S., & Weber, J. “Binaphthalene-based, soluble polyimides: the limits of intrinsic microporosity,” *Macromolecules*, vol. 42, no. 21, pp. 8017–8020, 2009.
- [26] Staiger, C. L., Pas, S. J., Hill, A. J., & Cornelius, C.J. “Gas separation, free volume distribution, and physical aging of a highly microporous spirobisindane polymer,” *Chem. Mater.*, vol. 20, no. 8, pp. 2606–2608, 2008.
- [27] Makhseed, S., Ibrahim, F., & Samuel, J. “Phthalimide based polymers of intrinsic microporosity,” *Polym. (United Kingdom)*, vol. 53, no. 14, pp. 2964–2972, 2012.
- [28] McKeown, N.B., “Polymers of intrinsic microporosity,” *Materials Science.*, vol. 2012, 2012.



- [29] McKeown, N.B., & Budd, P.M. “Exploitation of intrinsic microporosity in polymer-based materials,” *Macromolecules*, vol. 43, pp. 5163–5176, 2010.
- [30] Liaw, D.J., Wang, K.L., Huang, Y.C., Lee, K.R., Lai, J.Y., & Ha, C.S. “Advanced polyimide materials: Syntheses, physical properties and applications,” *Prog. Polym. Sci.*, vol. 37, no. 7, pp. 907–974, 2012.
- [31] Thomas, S., & Visakh, P.M., *Polyimides: Synthesis properties, characterization and applications*. Hoboken, NJ, USA: John Wiley & Sons, Inc., pp. 211–288.
- [32] Ghosh, A., Sen, S.K., Dasgupta, B., Banerjee, S., & Voit, B. “Synthesis, characterization and gas transport properties of new poly(imide siloxane) copolymers from 4,4'-(4,4'-isopropylidenediphenoxy)bis(phthalic anhydride),” *J. Memb. Sci.*, vol. 364, no. 1–2, pp. 211–218, 2010.
- [33] Voksen, W., *Advances in Polymer Science*, Newyork:Springer, vol. 117, p. 111, 1994.
- [34] Ding, M. “Isomeric polyimides,” *Prog. Polym. Sci.*, vol. 32, pp. 623–668, 2007.
- [35] Sridhar, S., Bee, S., Suresh, K.B. “Membrane-based Gas Separation: Principle, Applications and Future Potential,” pp. 1–25.
- [36] Shiotani, A., & Kohda, M. “Preparation of polyimides derived from biphenyltetracarboxylic dianhydrides and aromatic diamines bearing alkylene spacers,” *J. Appl. Polym. Sci.*, vol. 74, pp. 2404–2413, 1999.
- [37] Kostina, J., Bondarenko, G., Gringolts, M., Rodionov, A., Rusakova, O., Alentiev, A., Yakimanskii, A., Bogdanova, Y., & Gerasimov, V. “Influence of residual solvent on physical and chemical properties of amorphous glassy polymer films,” *Polym. Int.*, vol. 62, no. April, pp. 1566–1574, 2013.
- [38] Garson, “Diffusion Theory,” *Policy*, pp. 16–28, 2006.
- [39] “CO<sub>2</sub> capture/separation technologies.” [Online]. Available: [http://www.co2crc.com.au/aboutccs/cap\\_membranes.html](http://www.co2crc.com.au/aboutccs/cap_membranes.html).
- [40] Collins, M., & Ramirez, W. “Transport through polymeric membranes,” *J. Phys. Chem.*, pp. 5–12, 1979.
- [41] Schuth, F., Sing, K., Weitkamp, J., Ed., *Handbook of Porous Solids*. Berlin: Wiley-VCH, 2002.
- [42] Eddaoudi, M., Kim, J., Rosi, N., Vodak, D., Wachter, J., O’Keefe, M., “Systematic design of pore size and functionality in isorecticular MOFs and their application in methane storage,” *Science*, vol. 295, no. 5554, pp. 469–472, 2002.

- [43] Kim, J., Chen, B., Reineke, T.M., Li, H., Eddaoudi, M., Moler, D.B., O’Keeffe, M., & Yaghi, O.M. “Assembly of metal-organic frameworks from large organic and inorganic secondary building units: New examples and simplifying principles for complex structures,” *J. Am. Chem. Soc.*, vol. 123, no. 2, pp. 8239–8247, 2001.
- [44] Bligh, E.G. “Citation Classics,” *J. biol. Chem*, no. 35, p. 1978, 1978.
- [45] Chen, Q., Wang, J., Yang, F., Zhou, D., Bian, N., Zhang, X., Yan, C., & Han, B. “Tetraphenylethylene-based fluorescent porous organic polymers: preparation, gas sorption properties and photoluminescence properties,” *J. Mater. Chem.*, vol. 21, p. 13554, 2011.
- [46] Tsyurupa, V.A., & Davankov, M.P. “Hypercrosslinked polymers: basic principle of preparing the new class of polymeric materials,” *React. Funct. Polym.*, vol. 53, pp. 193–203, 2002.
- [47] Davankov, M.P., Rogozhin, V.A., & Tsyurupa, S.V. “A Method of Obtaining Macronet Copolymers of Styrene,” 3,729,457, 1970.
- [48] Tsyurupa, V.A., Davankov, M.P. “Porous structure of hypercrosslinked polystyrene: State-of-the-art mini-review,” *React. Funct. Polym.*, vol. 66, no. 7, pp. 768–779, 2006.
- [49] Germain, J., Frechet, J. M. J., Svec, F. “Hypercrosslinked polyanilines with nanoporous structure and high surface area: potential adsorbents for hydrogen storage,” *J. Mater. Chem.*, vol. 17, no. 47, pp. 4989–4997, 2007.
- [50] Germain, J., Frechet, J. M. J., Svec, F. “Nanoporous, hypercrosslinked polypyrroles: effect of crosslinking moiety on pore size and selective gas adsorption,” *Chem. Commun.*, no. 12, pp. 1526–1528, 2009.
- [51] Germain, J., Svec, F., Frechet, J.M. “Preparation of Size-Selective Nanoporous Polymer Networks of Aromatic Rings: Potential Adsorbents for Hydrogen Storage,” *Chem. Mater.*, vol. 20, no. 22, pp. 7069–7076, 2008.
- [52] Germain, J., Svec, F., Frechet, J.M. “Nanoporous Polymers for Hydrogen Storage,” *Small*, vol. 5, no. 10, pp. 1098–1111, 2009.
- [53] Masuda, T., Isobe, E., Higashimura, T., Takada, K. “Poly[1-(trimethylsilyl)-1-propyne]: a new high polymer synthesized with transition-metal catalysts and characterized by extremely high gas permeability,” *J. Am. Chem. Soc.*, vol. 105, no. 25, pp. 7473–7474, 1983.
- [54] McKeown, N.B. *Phthalocyanine Materials: Synthesis, Structure, and Function*. Cambridge, p. 193, 1998.

- [55] Makhseed, S., McKeown, N.B. “Novel spiro-polymers with enhanced solubility,” *Chem. Commun.*, no. 3, pp. 255–256, 1999.
- [56] McKeown, N.B., Makhseed, S., Budd, P.M. “Phthalocyanine-based nanoporous network polymers,” *Chem. Commun.*, no. 23, pp. 2780–2781, 2002.
- [57] McKeown, N.B., Makhseed, S. “Organic microporous materials derived from porphyrinic macrocycles,” PCT WO 2003/000774, 2002.
- [58] Hashem, M., Bezzu, B.M. Kariuki, C.G., McKeown, N.B. “Enhancing the rigidity of a network polymer of intrinsic microporosity by the combined use of phthalocyanine and triptycene components,” *Polym. Chem.*, vol. 2, no. 10, pp. 2190–2192, 2011.
- [59] Makhseed, S., Al-Kharafi, F., Samuel, J., Ateya, B. “Catalytic oxidation of sulphide ions using a novel microporous cobalt phthalocyanine network polymer in aqueous solution,” *Catal. Commun.*, vol. 10, no. 9, pp. 1284–1287, 2009.
- [60] MacKintosh, H.J., Budd, P.M., McKeown, N.B. “Catalysis by microporous phthalocyanine and porphyrin network polymers,” *J. Mater. Chem.*, vol. 18, no. 5, pp. 573–578, 2008.
- [61] McKeown, N.B., Gahnem, B., Msayib, K.J. “Towards polymer-based hydrogen storage materials: engineering ultramicroporous cavities within polymers of intrinsic microporosity,” *Angew. Chemie*, vol. 45, no. 11, pp. 1804–1807, 2006.
- [62] Budd, P.M., Butler, A., Selbie, J., “The potential of organic polymer-based hydrogen storage materials,” *Phys. Chem. Chem. Phys.*, vol. 9, no. 15, pp. 1802–1808, 2007.
- [63] McKeown, N. B., Budd, P. M., Book, D., “Microporous polymers as potential hydrogen storage materials,” *Macromol. Rapid Commun.*, vol. 28, no. 9, pp. 995–1002, 2007.
- [64] Makhseed, S., Samuel, J., “Hydrogen adsorption in microporous organic framework polymer,” *Chem. Commun.*, no. 36, pp. 4342–4344, 2008.
- [65] Makhseed, S., Samuel J., Bumajdad A., Hassan, M., “Synthesis and characterization of fluoropolymers with intrinsic microporosity and their hydrogen adsorption studies,” *J. Appl. Polym. Sci.*, vol. 109, no. 4, pp. 2591–2597, 2008.
- [66] Budd, P. M., McKeown, N.B. Fritsch, D., “Free volume and intrinsic microporosity in polymers,” *J. Mater. Chem.*, vol. 15, no. 20, pp. 1977–1986, 2005.
- [67] McKeown, N. B., Budd, P.M., “Polymers of intrinsic microporosity (PIMs): organic materials for membrane separations, heterogeneous catalysis and hydrogen storage,” *Chem. Soc. Rev.*, vol. 35, no. 8, pp. 675–683, 2006.

- [68] Budd, P.M. Ghanem, B.S. Makhseed, S., Mckeown, N.B., “Polymers of intrinsic microporosity (PIMs): robust, solution-processable, organic nanoporous materials,” *Chem. Commun.*, no. 2, pp. 230–231, 2004.
- [69] Budd, P.M., Elabas, E.S., Ghanem B.S., Makhseed, S., & McKeown, N.B. “solution-processed, organophilic membrane derived from a polymer of intrinsic microporosity,” no. 5, pp. 2002–2005, 2004.
- [70] Du, N., Robertson, G.P., Pinnau, I., & Guiver, M.D. “Polymers of intrinsic microporosity derived from novel disulfone-based monomers,” *Macromolecules*, vol. 42, pp. 6023–6030, 2009.
- [71] Carta, M., Msayib, K.J., Budd, P.M., & McKeown, N.B., “Novel Spirobisindanes for use as Microporosity,” *Org. Lett.*, vol. 10, no. 17, p. 2641, 2008.
- [72] Budd, P. M., McKeown, N. B. , Ghanem, B. S., Msayib, K. J., Fritsch, D., Starannikova, L., Belov, N., ...& Shantarovich, V. “Gas permeation parameters and other physicochemical properties of a polymer of intrinsic microporosity: Polybenzodioxane PIM-1,” *J. Memb. Sci.*, vol. 325, pp. 851–860, 2008.
- [73] C. G. Bezzu, M. Carta, A. Tonkins, J. C. Jansen, P. Bernardo, F. Bazzarelli, and N. B. McKeown, “A spirobifluorene-based polymer of intrinsic microporosity with improved performance for gas separation,” *Adv. Mater.*, vol. 24, pp. 5930–5933, 2012.
- [74] M. D. G. N. Du, G.P. Robertson, J. Song, I. Pinnau, “High-Performance carboxylated polymers of intrinsic microporosity (PIMs) with tunable gas transport properties,” *Macromolecules*, vol. 42, pp. 6038–6043, 2009.
- [75] J. C. J. C.R. Mason, L. Maynard-Atem, N.M. Al-Harbi, P.M. Budd, P. Bernardo, F. Bazzarelli, G. Clarizia, “Polymer of intrinsic microporosity incorporating thioamide functionality: Preparation and gas transport properties,” *Macromolecules*, vol. 44, pp. 6471–6479, 2011.
- [76] M. D. G. N. Du, H.B. Park, G.P. Robertson, M.M. Dal-Cin, T. Visser, L. Scoles, “Polymer nanosieve membranes for CO<sub>2</sub>-capture applications,” *Nat. Mater.*, vol. 10, pp. 372–375, 2011.
- [77] W. F. Bailey, “Ladder Polymers,” *The Encyclopaedia of Polymer Science and Engineering*. John Wiley & Sons, p. 158, 1993.
- [78] D. H. M. Heuchel, D. Fritsch, P.M. Budd, N.B. McKeown, “Atomistic packing model and free volume distribution of a polymer with intrinsic microporosity (PIM-1),” *J. Memb. Sci.*, vol. 318, pp. 84–99, 2008.
- [79] F. F. T. Emmler, K. Heinrich, D. Fritsch, P.M. Budd, N. Chaukura, D. Ehlers, K. Ratzke, “Free volume investigation of polymers of intrinsic microporosity (PIMs): PIM-1 and

- PIM1 copolymers incorporating ethanoanthracene units,” *Macromolecules*, vol. 43, pp. 6075–6084, 2010.
- [80] I. P. J. Song, N. Du, Y. Dai, G. P. Robertson, M. D. Guiver, S. Thomson, “Linear High Molecular Weight Ladder Polymers by Optimized Polycondensation of Tetrahydroxytetramethylspirobisindane,” pp. 7411–7417, 2008.
- [81] T. Segments, “Polymers of Intrinsic Microporosity with Dinaphthyl and Thianthrene Segments,” pp. 8580–8587, 2010.
- [82] Carta, M.M., Msayib, K.J., & Mckweon, N.B., “Novel Polymers of intrinsic microporosity derived from novel disulfone-based monomers,” *Tetrahedron Lett.*, vol. 50, no. 43, pp. 5954–5954, 2009.
- [83] Fritsch, M.D., Bengtson, G., & Carta, C. “Synthesis and Gas Permeation Properties of Spirobischromane-Based Polymers of Intrinsic Microporosity,” *Macromol. Chem. Phys.*, vol. 212, no. 11, pp. 1137–1146, 2011.
- [84] Ghanem, S., Mckeown, N.B., & Budd, P.M. “High-Performance Membranes from Polyimides with Intrinsic Microporosity,” pp. 2766–2771, 2008.
- [85] Ghanem, B. S., Mckeown, N. B., Budd, P. M., Al-harbi, N. M, Fritsch, D., Heinrich, K., Starannikova, L., Tokarev, A., & Yampolskii, Y. “Synthesis , Characterization , and Gas Permeation Properties of a Novel Group of Polymers with Intrinsic Microporosity : PIM-Polyimides,” vol. 2, pp. 7881–7888, 2009.
- [86] Weber, J., Su, Q., Antonietti, M., & Thomas, A. “Exploring polymers of intrinsic microporosity - Microporous, soluble polyamide and polyimide,” *Macromol. Rapid Commun.*, vol. 28, pp. 1871–1876, 2007.
- [87] Ma, X., Swaidan, R., Belmabkhout, Y., Zhu, Y., Litwiller, E., Jouiad, M., Pinnau, I., & Han, Y., “Synthesis and gas transport properties of hydroxyl-functionalized polyimides with intrinsic microporosity,” *Macromolecules*, vol. 45, pp. 3841–3849, 2012.
- [88] Shamsipur, H., Dawood, M., Budd, P. M., Bernardo, P. , Clarizia, G., & Jansen, J. C. “Thermally Rearrangeable PIM-Polyimides for Gas Separation Membranes,” *Macromolecules*, vol. 47, pp. 5595–5606, 2014.
- [89] Carta, M.M., Msayib, K.J., & Mckweon, N.B., “Novel Polymers of intrinsic microporosity (PIMs) derived from 1,1-spiro-bis(1,2,3,4-tetrahydronaphthalene)-based monomers,” *Tetrahedron Lett.*, vol. 50, no. 43, pp. 5954–5957, 2009.
- [90] Yampolskii, Y. “Polymeric gas separation membranes,” *Macromolecules*, vol. 45, pp. 3298–3311, 2012.

- [91] Nagaia, P. K., Masudab, T. Nakagawac, T. , Freemana, I. “Poly[1-(trimethylsilyl)-1-propyne] and related polymers: synthesis, properties and functions,” *Prog. Polym. Sci.*, vol. 26, no. 5, pp. 721–798, 2001.
- [92] Robeson, L. M. “Correlation of separation factor versus permeability for polymeric membranes,” *J. Memb. Sci.*, vol. 62, no. 2, pp. 165–185, 1991.
- [93] Schlapbach, A. Z. L. “Hydrogen-storage materials for mobile applications,” *Nature*, vol. 414, pp. 353–358, 2001.
- [94] McKeown N. B., Budd, P. M. “Polymers of intrinsic microporosity (PIMs): organic materials for membrane separations, heterogeneous catalysis and hydrogen storage,” *Chem. Soc. Rev.*, vol. 35, pp. 675–683, 2006.
- [95] Rogan, M. Y. , Starannikova, L.V., Ryzhikh, Y., & Yampolskii, P. Bernardo, F. “Synthesis and gas permeation properties of novel spirobisindane-based polyimides of intrinsic microporosity,” *Polym. Chem.*, vol. 4, no. 13, pp. 3813–3820, 2013.
- [96] Madkour, T. M. “Molecular Dynamics Investigation into the High Permeability and High Selectivity of Nano-Porous Polyimide Membranes for the ‘Green’ Separation of Natural Gas,” *e-Journal Surf. Sci. Nanotechnol.*, vol. 10, no. March, pp. 63–68, 2012.
- [97] Larsen, G. S., Lin, P., Hart, K. E., & Colina, C. M. “Molecular Simulations of PIM-1-like Polymers of Intrinsic Microporosity,” no. Md, pp. 6944–6951, 2011.
- [98] Wohrle, D., Eskes, M., Shigehara, K., and Yamada, A. “Synthesi,” *Synthesis (Stuttg.)*, vol. 195, 1993.
- [99] Madkour, T. M., & Mark, J.M. “Simulations on crystallization in stereoblock poly ( propylene ). Idealized structures showing the effects of atactic block length,” *Macromol. Theory Simulations*, vol. 77, pp. 69–77, 1998.
- [100] Rigby, R. J. “Molecular dynamics simulation of polymer liquid and glass. 4. Free-volume distribution,” *Macromolecules*, vol. 23, no. 26, pp. 5312–5319, 1990.
- [101] Won-Kook Kim, W. L. M “A fully atomistic model of an amorphous polybenzoxazine at bulk density,” *Comput. Theor. Polym. Sci.*, vol. 8, no. 3–4, pp. 353–361, 1998.
- [102] Connolly, M. L. “Analytical molecular surface calculation,” *J. Appl. Crystallogr.*, vol. 16, pp. 548–558, 1983.